



UNIVERSITÀ DEGLI STUDI DI VERONA

DIPARTIMENTO DI INFORMATICA

DOTTORATO DI RICERCA IN
NANOSCIENZE E TECNOLOGIE AVANZATE

Con il contributo di
European Union Horizon 2020 Framework Programme for
Research and Innovation under grant agreement no 665091.

CICLO/ANNO: 32° Ciclo (2016)

TITOLO DELLA TESI DI DOTTORATO

**A framework for surface metrology on
Cultural Heritage objects based on
scanning conoscopic holography**

S.S.D. FIS/07

Coordinatore: Prof. Adolfo Speghini

Firma _____

Tutor: Prof.ssa Claudia Daffara

Firma _____

Dottorando: Dott. Giacomo Marchioro

Firma _____

Quest'opera è stata rilasciata con licenza Creative Commons Attribuzione – non commerciale Non opere derivate 3.0 Italia . Per leggere una copia della licenza visita il sito web: <http://creativecommons.org/licenses/by-nc-nd/3.0/it/>



Attribuzione Devi riconoscere una menzione di paternità adeguata, fornire un link alla licenza e indicare se sono state effettuate delle modifiche. Puoi fare ciò in qualsiasi maniera ragionevole possibile, ma non con modalità tali da suggerire che il licenziante avalli te o il tuo utilizzo del materiale.



NonCommerciale Non puoi usare il materiale per scopi commerciali.



Non opere derivate —Se remixi, trasformi il materiale o ti basi su di esso, non puoi distribuire il materiale così modificato.

A framework for surface metrology on Cultural Heritage objects based on scanning conoscopic holography – Giacomo Marchioro

Tesi di Dottorato

Verona, 25 Giugno 2021

ISBN 9788869251672

SOMMARIO

L'applicazione della metrologia di superficie e dell'analisi dimensionale allo studio dei beni culturali può rivelare importanti informazioni sull'oggetto e favorire l'integrazione di molteplici tecniche diagnostiche. Tuttavia, l'applicazione di queste discipline ai Beni Culturali richiede particolari requisiti e attenzioni. In questa tesi, presento i risultati dell'implementazione di diversi sistemi di misurazione della superficie basati sul principio della conoscopia olografica. I sensori conoscopici sono strumenti capaci di misurare distanze con precisione micrometrica a scale diverse, accoppiati a slitte micrometriche possono essere utilizzati per acquisire scansioni areali dell'oggetto in esame. Per facilitare la loro applicazione alle opere d'arte ho sviluppato un *framework* per applicare la metrologia di superficie ai beni culturali. Il framework copre diversi aspetti del processo di analisi ed utilizzo dei dati e comprende la creazione di raccolte di campioni, le strategie per la scansione dell'oggetto, l'archiviazione e l'analisi dei dati ed eventualmente l'incertezza legata alla misura. Il *framework* mira a rendere più accessibile l'implementazione della metrologia di superficie e dei sistemi di scansione dell'analisi dimensionale per l'analisi dei beni culturali. I risultati raccolti su una varietà di materiali artistici (metalli, dipinti su tavola, tela, carta, pergamena e dipinti murali) mostrano come questi sistemi possano essere utilizzati per monitorare gli effetti delle procedure di pulitura, la stabilità dimensionale delle opere d'arte ed il loro invecchiamento.

ABSTRACT

The application of surface metrology and dimensional analysis to the study of artworks can reveal important information on the object and aid the integration of multiple techniques. However, the application of these disciplines to Cultural Heritage objects necessitates particular care and requirements. In this dissertation, I present the results of the implementation of different systems, based on Conoscopic Holography range finders, for measuring the surface. Conoscopic holography range finders are viable instruments for measuring distances with micrometer accuracy at different scales, coupled with micrometric stages they can be used for acquiring areal scans of the object under investigation. To ease their application to artworks I built a framework for applying surface metrology to Cultural Heritage objects. The framework covers different aspects of the research workflow comprising the creation of samples collections, the strategies for scanning the object, the storing and the analysis of the data and eventually the uncertainty linked to the measurement. This framework aims to make more accessible the implementation of surface metrology and dimensional analysis scanning systems tailored to the analysis of Cultural Heritage objects. The results collected on a variety of artworks materials (metals, panels painting, canvas, paper, parchment and mural paintings) show how these systems can be used for monitoring the effects of cleaning procedures, the dimensional stability of the artworks and their ageing.

Preface

In this thesis, I have summarized the work I carried out at the OpDATECH laboratory of the University of Verona led by Prof. Claudia Daffara for implementing a scanning mechanical systems based on Conoscopic Holography and tried to develop solutions that could address some problems faced during the various projects where the system was used. I studied most of the topics written in this thesis during the European Project Scan4Reco (Multimodal Scanning of Cultural Heritage Assets for their multilayered digitization and preventive conservation via spatiotemporal 4D Reconstruction and 3D Printing, grant agreement No. 665091) coordinated by Dr Dimitrios Tzovaras from the Centre for Research & Technology, Hellas (CERTH) with the main objective to develop a novel portable, integrated and modular solution for customized automatic digitization and analysis of cultural heritage objects (CHOs), even *in situ*. The project (ended in 2018) was structured in mainly three phases: 1) create and analyze artificially aged reference material coupons of bronze, silvers and egg-tempera 2) investigate the degradation mechanism and possible ageing models and 3) build a mechanical positioning system that allowed to investigate an artwork with different analytical techniques (e.g. Raman, FT-IR etc. etc.) referenced over a 3D model of the object.






The knowledge gained during the first two phases has been eventually used by a decision support system and a simulation environment for helping the restorer and the conservation scientist to preserve the artwork.

A larger version of the mechanical system, that integrates the microprofilometer module developed in our lab for scanning the surfaces with sub-milimeter resolution, was developed in the Ormylia Art Diagnosis Centre by the team led by Dr.Ing.Georgios Karagiannis while a commercial solution is under development by AVASHA AG. CERTH implemented ageing simulation and ROS system and software for the multi-modal acquisition driving the system.

Disclaimer: The views and opinions expressed in this dissertation are those of the author and do not necessarily reflect the opinions of the consortium.

External data

Different tools have been used to share open data and products of the research for easing the replicability of the experiments. Most of the research is shared on Zenodo¹. However, for sharing specific file formats I took advantage of other web-based hosting services. Kaggle data sets² for .csv files. GrabCAD³ for CAD files and Github⁴ for the code. During this dissertation, some special boxes with icons are used to indicate that some external content relevant to the section is hosted in one of the web-based hosting services listed above. The external content is categorized as follows:

	The data set box indicates that a data set collected during the research project is accessible online with a short description and a link to access it.
	This box indicates that is available some 3D models in .FCStd or .step of the custom pieces of the instruments designed for implementing the systems used in the research project.
	This box indicates that is available an Arduino project for implementing a system used in the thesis. Arduino is an open-source framework for programming microcontrollers using a C++ dialect.
	The Python box is used for linking to external software libraries developed by the author using Python programming language ^a . Libraries from third parties are cited in the bibliography. <hr/> ^a https://www.python.org/
	This box indicates that is available an interactive jupyter notebook for showing the data processing or for didactic purposes that uses Python for implementing the concepts and procedure explained in the section.

For allowing to reproduce some of the experiments presented in this dissertation I have used Jupyter notebooks (highlighted by the aforementioned box or contained in the Kaggle data set). These Jupyter notebooks contain Python code

¹<https://zenodo.org/>

²<https://www.kaggle.com/giacomomarchioro/datasets>

³<https://grabcad.com/giacomo.marchioro-1/models>

⁴<https://github.com/giacomomarchioro>

that can be run offline once the notebook has been downloaded and the needed software is installed. Otherwise, for easing the accessibility to the code I linked some of these notebooks to a cloud service provided by Google Inc. for running the code directly in the cloud by means of a browser. The reader can access the resource by clicking on the url contained in the Jupyter box. Which has the following structure:

```
https://colab.research.google.com/github/giacomomarchioro/phdthesis...
```

Google Colab cloud service GitHub file path

For retrieving the original file without the interactive functionality of Google Co-Lab, the reader must copy only the *GitHub file path* and concatenate it at the end of the hosting service GitHub:

```
https://www.github.com/giacomomarchioro/phdthesis...
```

GitHub hosting service GitHub file path

This dissertation has been created using \LaTeX markup language the source-code and some of the additional content is hosted at the following website <https://github.com/giacomomarchioro/phdthesis>. All the images can be found in the same repository and can be reused.

Why Python has been chosen?

I choose to use Python programming language because it is a free and open-source programming language with established scientific libraries. The simple syntax allows also non-computer scientists to use and understand the code and its functioning. Python is the most popular programming language in 2019 according to IEEE spectrum[28] and the third according to TIOBE index [24] and hence the code produced can be used and maintained by a wider audience of scientists and engineers.

Websites in the bibliography

The websites cited in the bibliography that are referring to resources that might change during the time, link to a snapshot of the website in a web archive (Wayback Machine). This ensures that the reader and the author are referring to the same version. If the reader wants to consult the latest version of the website (that might be updated or deleted) the first part of the link must be removed. For instance, if the reader wants to consult the latest version of this cited website:

```
https://web.archive.org/web/20190828085342/http://getty.edu/
```

Web archive reference Original url

Only the `Original url` part must be used.

Acknowledgements

This project has been funded by Horizon 2020 European Union funding programme. I would like to thank my supervisor Prof. Claudia Daffara for the support, encouragement and the opportunity to work on various interesting topics.

I am deeply grateful to my reviewers Prof. Roger M. Groves of the Delft University of Technology and Prof. Haida Liang of Nottingham Trent University for the corrections and suggestions which I have tried to implement to the best of my ability.

I would like also to thank Nicola Gaburro who has been a peerless labmate and among other things the developer of the graphical user interface for controlling the microprofilometer.

Contents

1	Introduction	1
1.1	Structure of the work and definition of the terms	1
1.1.1	Structure of the dissertation	1
1.1.2	Related work	2
1.1.3	Classification of the modalities and definition of the terms . . .	2
1.2	Dimensional and surface metrology	3
1.2.1	An overview of the main techniques used in dimensional and surface metrology	3
1.3	Comparison of the performance of commercial systems	6
1.3.1	Dimensional and surface metrology for a complete surface analysis	8
1.3.2	The problem of surface and dimensional metrology applied to Cultural Heritage objects	10
1.4	ISO benefits and costs	12
1.4.1	The choice of the standards	13
1.5	Discrete representations of the surface	14
1.6	Summary	17
2	Automating the creation of flat samples collections	19
2.1	The workflow for creating the samples collection	21
2.2	The tool for creating the samples collection	22
2.3	Conventions and suggestions	25
2.4	Description of the modified SVG file format	25
2.5	Reading and querying the SVG	28
2.6	An example of the manufacturing process of the samples collection .	29
2.7	Summary	30
3	Scanning strategies	33
3.1	Introduction	33
3.1.1	Choosing the right positioning system	34
3.2	Scanning analysis	35
3.2.1	Factors influencing the sampled area in dynamic acquisitions .	36
3.2.2	Triggering synchronization and data transfer from the sensor .	38
3.3	Scanning patterns for single-spot acquisition	39
3.3.1	The definition of the scanning patterns	41
3.3.2	Misalignments due to dynamic scans	41
3.3.3	Point, profile and areal measurement	43
3.4	Conoscopic holography principles and applications	43

3.4.1	Conoscopic holography rangefinders	44
3.4.2	Disambiguation of the terms	45
3.4.3	The physical principle of conoscopic interference pattern . . .	45
3.4.4	Rangefinders based on shearing interferometry with Savart plates and Wollaston prisms	45
3.4.5	Conoscopic holography rangefinder with quarter-wave plate .	46
3.4.6	Linear conoscopic rangefinders: ConoProbes	46
3.5	Design and implementation of scanning conoscopic holography sys- tems	48
3.5.1	Requirements for implementing an optimal scanning cono- scopic holography set-up	49
3.5.2	The solutions proposed.	50
3.6	Summary	51
4	Data analysis	53
4.1	Storing the data	53
4.1.1	Level of processing	53
4.1.2	Unprocessed data	54
4.1.3	Processed data	54
4.2	The signal of the surface	55
4.3	The processing workflow	56
4.4	The tool developed for analyzing the data: “micropro”	58
4.5	Matrix reconstruction, quality control, and masking	59
4.6	Improving the quality fusing multiple scans	61
4.7	Fitting	62
4.7.1	Short introduction to the least-square fitting for surface metrol- ogy	62
4.7.2	Analysis, levelling, form removal and rotation	64
4.8	Digital filtering	67
4.9	Surface subdivision	68
4.9.1	Varying sampling length or area approach	69
4.9.2	Irregular sampling area	71
4.10	Calculation of metrological field parameters	73
4.10.1	Introduction to the ISO conventions	73
4.10.2	Profile parameters	73
4.10.3	Areal field parameters	74
4.11	Areal features parameters	75
4.11.1	Hierarchical Peak-Valley Analysis (HPVA)	75
4.12	Summary	82
5	The surface representations	85
5.1	Introduction	85
5.1.1	The problem of the surface definition	86
5.1.2	The coastline mapping problems	87
5.2	Uncertainties in determining the interface	87
5.2.1	Materials properties critical for the acquisition	88

5.2.2	Assessing the influences of transparent windows in front of the sensor	88
5.2.3	Assessing the performance using half-transparent step metric test objects	90
5.2.4	A possible interpretation of the artifacts	91
5.2.5	Assessing the performance on certified reference standard . . .	93
5.2.6	Comparison of Conoscopic Holography measurement with Acoustic Microscopy	95
5.2.7	Towards a quantitative interpretation of the difference between the scans.	99
5.3	Variation of the interface due to external forces	100
5.3.1	Reference materials	101
5.3.2	Monitoring the effects of relative humidity change on the dimensional stability of hygroscopic artworks.	102
5.4	The coastline paradox	107
5.4.1	Richardson effect and fractal dimension	110
5.5	Summary	111
6	Case study	113
6.1	Introduction	113
6.2	Monitoring aging process in metals and pictorial layers.	113
6.2.1	Aim and description of the study	113
6.2.2	Materials and methods	116
6.2.3	Acquisition times	116
6.2.4	Data analysis	116
6.2.5	Discussions and conclusion	119
6.3	Analysis of Peasaro Madonna	120
6.3.1	Aim and description of the study	120
6.3.2	Timeline and report of the measurements	120
6.3.3	Data analysis	122
6.3.4	Discussions and conclusion	125
6.4	Testing tarnished silver cleaning	125
6.4.1	Aim and description of the study	125
6.4.2	Methods	126
6.4.3	Data analysis	126
6.4.4	Discussions and conclusion	129
6.5	Assessing the removal of limewash layers	131
6.5.1	Aim and description of the study	131
6.5.2	Methods	131
6.5.3	Data analysis	132
6.5.4	Discussions and conclusion	134
6.6	End-user feedback	135
6.7	Summary	135
	Conclusion	141

List of Tables

2.1	Common standardized dimensions that can be used for easing the process of creating samples collection.	20
3.1	References to some scanning systems developed for the diagnostic of Cultural Heritage	34
3.2	Specification of the ConoProbe systems (lens and probe) used during the project.	48
3.3	Specification of the linear stages by PhysikInstrumente selected for creating the system.	49
4.1	Quality parameters suggested by the manufacturer, for achieving acceptable and optimal measurement.	60
5.1	Comparison of the computed metrological parameters and the parameters measured using the different conoscopic probes.	95
6.1	Some of the processes that induce morphological variations of the surface.	114
6.2	Average scan times for each sample typology.	116

List of Figures

1.1	Schematic of the principles of surface metrology techniques	4
1.2	The spatial sampling against the height accuracy of the claimed performance of metrology instruments.	7
1.3	The maximum working range against the height accuracy of the claimed performance of metrology instruments.	8
1.4	Work-flow for the analysis of a collection of samples.	11
1.5	The number of ISO standard per year published by the TC 213.	12
1.6	A representation of a stack of 2D-array of distances.	16
2.1	The procedure for creating and analyzing samples collection with the tool created during the project.	21

2.2	The output file containing all the information regarding the samples and the sample holder.	24
2.3	Creation of the samples collection using a laser cutter and plastic masks.	29
2.4	The creation of a samples collection with samples cut from a poplar panel.	30
3.1	The sampled area represented by a super ellipse.	37
3.2	Some of the different scanning patterns that can be used for scanning an area.	39
3.3	Snake pattern scans during dynamic acquisition scans.	42
3.4	Different set-ups related to conoscopy.	44
3.5	Schematic of a simple conoscopic holography set-up	46
3.6	A reconstruction of a possible schematic of a linear conoscopic holography range finder (ConoProbe).	47
3.7	Drawing of a side view of a ConoProbe.	47
3.8	The scanning systems developed during the project.	50
4.1	Decomposition into shape, waviness and roughness of an amphora fragment.	55
4.2	Flow diagram of the metrology surface data-analysis workflow	57
4.3	Example of distance map retrieved using the conoscopic holography scanning system.	59
4.4	Improvement of the surface reconstruction fusing multiple acquisition of a Russina icon.	61
4.5	Comparison of the procedure for removing the tilting of a profile using subtraction and rotation	65
4.6	The effects of subtraction (left plot) and rotation (right plot) on the computation of some metrological parameters (P_{sm} , P_q , P_a , P_t , P_{sk} , P_{ku}) computed on a synthetic sinusoidal profile ($A=2$, $\lambda=6$).	66
4.7	The relative error computed at different angles against the values with the profile parallel to the direction of scanning.	66
4.8	Subdivision of the profile parts re-adapted as shown in [14]. Run-up and Over travel are the offset of the measurement.	68
4.9	Exemplification of the result of the varying sampling area algorithm.	70
4.10	Roughness parameter S_q computed after subdividing a filtered sample surface into squared sampling areas.	71
4.11	Application of SLIC algorithm and computing of the roughness for the sampling areas enclosed in each super pixel.	72
4.12	The creation of a synthetic profile used in figure 4.13 summing three different signals.	76
4.13	Application of the HPVA for a generic profile.	77
4.14	A scan of a portion of wooden panel prepared using gypsum acquired with the ConoProbe-3 lens 75 mm after levelling.	78
4.15	The first three horizontal and vertical levels of the valleys levels retrieved using HPVA computed on the scan shown in figure 4.14. . . .	80

4.16	The distribution of the spacing between the valleys of the first three horizontal and vertical levels retrieved using HPVA computed on the scan shown in figure 4.14.	81
5.1	Profile of a tilted aluminium breadboard acquired through a polystyrene window.	89
5.2	Drawing of the step-height transparent object made using microscope slides.	90
5.3	Conoscopic scan of the step-height transparent object made using microscope slides.	91
5.4	Interaction of the light with transparent layers and windows.	92
5.5	Acquisition of the reference specimen 526X by Rubert & Co Ltd. using a ConoProbe-3HD	93
5.6	Photograph of patinated bronze mock-up.	96
5.7	Comparison of the two techniques used for scanning a patinated bronze.	97
5.8	The egg tempera patch number 15 of the data set and the ROI investigated with the two techniques.	97
5.9	Comparison between the conoscopic holography and the acoustic microscopy scan on a egg tempera patch.	98
5.10	Calculation of Sq parameter over square patch subdivisions of acoustic and conoscopic holography scans of a bronze sample.	99
5.11	Displacement analysis of a piece of parchment at 25 °C inducing sudden variation of RH (circle marks).	103
5.12	Conoscopic holography scan of lambskin parchment samples at different relative humidity levels.	104
5.13	Profiles measured along the curvature of an icon exposed at different relative humidity levels.	105
5.14	The series of profiles collected following the curvature of the icon transitioning from 15 % to 50 % RH.	106
5.15	Procedure used by Richardson on a generic surface profile.	108
5.16	Log-log plot of the total length of different portion of the Great Britain against the probing distance.	109
5.17	Application of the algorithm proposed by Richardson on the coastline of Britain	110
6.1	3D rendering of a egg tempera patch after the aging process.	117
6.2	Height difference from the reference plane of the egg tempera sample (6) after three aging steps.	117
6.3	Height difference from the reference plane of the egg tempera sample (11) after three aging steps.	118
6.4	Height difference from the reference plane of the egg tempera sample (30) after three aging steps.	118
6.5	3D rendering of conoscopic holography scan of the wrinkling on the Pala Pesaro.	119
6.6	3D reconstruction of the set-up and the environment during the acquisitions.	120

6.7	A ROI of the initial measurement performed on the painting.	121
6.9	The acquisition of the cleaned area before and after the cleaning process.	122
6.8	The peaks found using HPVA on a region of the Pesaro Madonna.	123
6.10	The difference between the levelled scan after the cleaning and the levelled scan before the cleaning.	124
6.11	Part of the silver sample reconstructed using the data from the conoscopic holography scan and a texture obtained fusing multiple photos taken with a Nikon D810.	126
6.12	Conoscopic Holography heights difference map of two areas of the sampled cleaned using different methods.	127
6.13	Subdivision of the sample B1, after levelling, in squared patches with side 750 μm and computation of Sq parameter for each patch.	128
6.14	Boxplot of the Sq values recorded on each sample after the leveling and subdivision of the area in patch with a side 750 μm . For each pair of box, on the left side the cleaned area on the right the reference uncleaned area.	128
6.15	AFM scan of a portion of the cleaned sample C1 tilted of 45 degrees and AFM scan of the cleaned sample D1 tilted of 45 degrees.	129
6.16	Averaged Sq roughness computed on cleaned and uncleaned patches on five scan for each patch.	130
6.17	Mock-up of the smalt-blue mural painting samples with limewash layer and cleaning tests.	131
6.18	3D rendering of a part of the conoscopic holography acquisition of the mural painting mock-up samples.	133
6.19	The analysis of Sp, Sv, Sz, Sq, Sa variation after applying the limewash and the consecutive removal using a) a scalpel on wet substrate and b) a precision engraver.	134

List of Equations

1.1	1-dimensional array of distances.	14
1.2	2-dimensional array of distances.	14
1.3	Generic profile of heights.	15
1.4	List of n-tuple.	16
3.1	Calculation of the exposure length during linear motion.	36
3.2	Superellipse centered at the origin.	36
3.3	Superellipse with displacement along exposure length components.	37
3.4	Calculation of the total sampled area of single-spot in dynamic acquisition mode.	37
3.5	Calculation of the exposure length during uniform acceleration.	40

3.6	Calculation of the minimum acceleration to reach the linear motion before the end of the scanning offset.	40
4.1	Least squares fitting for a line.	63
4.2	Least squares fitting for a plane.	63
4.3	Second order polynomial least squares fitting for a surface.	63
4.4	Usage of Boolean masks in least squares fit process.	64
4.5	Rotation matrix for a profile.	64
4.6	Gaussian filter.	68
4.7	Integral calculation of the roughness parameter R_q	73
4.8	Discrete calculation of the roughness parameter R_q	74
4.10	Continuous calculation of the roughness parameter S_q	74
4.11	Discrete calculation of the roughness parameter S_q	74
4.12	Generic profile of heights variations.	75
4.13	Formalization of the algorithm for recording the heights of the peaks of the first level of the hierarchical peak analysis.	76
4.14	Formalization of the algorithm for recording the peaks location of the first level of the hierarchical peak analysis.	76
4.15	Formalization of the algorithm for computing the spacing between adjacent peaks.	77
4.16	Formalization of the algorithm for computing the height difference between adjacent peaks.	77
5.2	Snell–Descartes law.	91
5.3	Snell–Descartes law for the ordinary ray.	91
5.4	Snell–Descartes law for the extraordinary ray.	92
5.5	Equation of a generic sinusoidal profile with given P_t and R_{Sm}	94
6.1	Definition of the S_p parameter.	132
6.2	Definition of the S_v parameter.	132
6.3	Definition of the S_z parameter.	134

Listings

2.1	Example of creating a samples collection programatically using SVGsamplescollection Python module.	22
2.2	Example of creating a samples collection programatically using SVGsamplescollection Python module.	25
2.3	The definition of the collection borders and the description of the steps.	26
2.4	The group containing the samples positions.	27
2.5	The group section containing the information regarding the samples.	27
2.6	Example of querying a samples collection programatically using SVGsamplescollection Python module.	28

*... e sol fa questo per non perdere la bellezza del mondo,
la quale consiste nella superficie de' corpi sí accidentali come
naturali, i quali si riflettono nell'occhio umano.*

Leonardo da Vinci, Trattato della pittura

1

Introduction

This introduction focuses on the acquisition of the concepts from different disciplines in defining the general terms and approach of the dissertation and the guidelines followed aiming to use in the field of Cultural Heritage an appropriate lexicon and terminology.

1.1 Structure of the work and definition of the terms

1.1.1 Structure of the dissertation

After this introduction, the work will be structured as follows. The second chapter deals with the implementation of a file format for describing and creating flat samples collections that can be at the same time human and machine-readable. The third chapter explains the main concepts and strategies for creating a scanning system and a review of conoscopic holography rangefinders applications. The fourth chapter deals with the data analysis showing: a new workflow for surface metrology analysis using masked-arrays, a tool developed during the project for performing surface metrology and its validation against reference standards. Eventually, are shown some algorithms that I developed for studying the surface subdivided into sampling areas with different extents and the test of some algorithms for the automatic segmentation of heterogeneous surface and for exploratory data analysis extracting the hierarchy of peaks and valleys of the surface. The fifth chapter investigates the uncertainty linked with the acquisition showing experimental results on the variation of the surface due to external factors (relative humidity, temperature) on hygroscopic materials. The uncertainties linked with the presence of transparent materials are studied creating metric test objects using microscope slides. Taking into account the uncertainties the last chapter reports a series of case study on artworks and artworks materials using the concepts and the tools explained previously.

1.1.2 Related work

The need of integrating different analytical techniques and creating an open workflow for maintaining and analysing the data is recognised by the Cultural Heritage community [72]. The important role of the development and testing of 3D microprofilometric set-up has been the subject of a European project [168]. Mona Hess in her PhD dissertation [67] created a metric test object for Cultural Heritage acquisition and evaluated many aspects of the fruition of 3D reconstruction of artworks. The development of scanning conoscopic holography system for the application to artworks began with the work carried out at the Italian National Institute of Optics [50] and by Spagnolo[166]. While in depth analysis of conoscopic holography principle can be found in [163, 66] a lot of research on the systems was carried out by the University of Olviedo [106, 8, 151]. The need for the creation of reference samples collection is still actual. The American Library of Congress in 2019 announced that the Preservation Research and Testing Division (PRTD) launch a new infrastructure initiative call: the Center for Library Analytical Scientific Samples Digital (CLASS-D)[34] is a transformative methodology that links multiple analyses to one sample or object, and potentially multiple samples in a project to previous longitudinal research studies.

1.1.3 Classification of the modalities and definition of the terms

I investigated the usage of the different modalities and terms used for describing non-invasive analysis in an attempt to uniform the treating of the description of complex analytical systems and workflow. In this dissertation I have used the convention that when the information is collected on a single spot e.g. using a handheld spectrometer I refer to this analysis as a **single-spot analysis**. We can hence repeat a single-spot analysis making a random or reasoned sampling of the surface to be investigated, and register or reference the value to other points, an image or a 3D model previously acquired. Alternatively we can repeat the analysis following a specific pattern with the aid of a positioning system or other mechanical systems. In the latter case, I call this process **scanning**. Often the term **mapping** is used (e.g. spectroscopic mapping), I prefer to use this term for indicating the process of associating (or mapping) to a certain signal or position a value rather to the acquisition itself. From the practical point of view, we define the scanning techniques as any technique where the probe, part of the probe or the object is moved in a specific pattern to analyse a larger area and produce a scan. These systems may acquire simultaneously a line of signals (**line scan**) or a single spot. Eventually, **imaging techniques** are able to acquire information regarding multiple spots simultaneously. The border between imaging and scanning techniques is often blurred. From one side, scanning techniques produce images and hence are often included into the imaging class. On the other side, some imaging techniques are actually scanning across the scene and not acquiring all the signals simultaneously. This is the case of sensors that are using *rolling shutters* instead of *global shutters*. A series of concepts linked to the scanning analysis will be explained in the following chapters. It is important to notice that these categories are valid regardless of the type of properties that are measured, thus imaging or scanning techniques can be

used to retrieve spectral data as well as data regarding the dimensions. What could be particularly interesting are the implications of measuring the object acquiring an image or scanning an object when the time delay between the first and the last measurement of the scan can reach several hours.

1.2 Dimensional and surface metrology

The analysis of the 3D geometry of an object can be divided into two main fields: **dimensional metrology** and **surface metrology** (or roughness analysis). Dimensional metrology studies how to measure distances and hence focuses on the physical shape of the objects[48]. It treats methods for measuring distances between elements of an object or calculates shapes that best fit the object. Surface metrology [186] focuses on methods for measuring statistically the distribution of heights or features on the profile or the area under investigation. The two fields are often separated because of different instrument requirements and the representation of the surface may differ. For dimensional metrology, it is required to measure volumes at a larger scale while for surface metrology a sub-micrometer resolution is preferable. In this dissertation, I use a custom conoscopic holography set-up for carrying out both, dimensional metrology and surface metrology. These two disciplines are widely developed in engineering but not very widespread in the analysis of Cultural Heritage objects.

1.2.1 An overview of the main techniques used in dimensional and surface metrology

Several techniques have been developed during the last century for measuring accurately the surface of an object and its dimensions. Figure 1.1 shows a simplified schematic of the main systems and principles used for retrieving the distances.

Stylus profilometers are the gold standard for roughness analyses [167, p.177]. Usually, a piezoelectric stage scan the surface using a stylus with a tip with a radius ranging on average from 0.2 to 10 μm [21] but a small diamond tip can achieve lateral resolution up to 20 nm. The transducer (which is often a linear variable differential transformer[142]) senses the movements of the probe producing a digital representation of the profile. A similar principle is used by the **Atomic Force Microscope (AFM)** in this case the tip has radii ranging from 4 to 50 nm and it is attached at the end of a small cantilever. A laser irradiates the cantilever and a detector captures the reflected light. Depending on the position of the reflected light on the detector the height of the point is recorded. Unlike the stylus profilometer—that works always in *full-contact mode* with the tip “dragged” on the surface—the AFM can operate also in *tapping mode* and in *non-contact mode*. In the first case, the cantilever oscillates close to its resonance frequency, in this way the tip will touch the surface at regular intervals for a short period of time. In the second case, with the non-contact mode, the tip is still oscillating but does not touch the surface. The variation on the amplitude of the oscillations due to the van der Waals forces are used by a feed-back loop for maintaining the distance from the

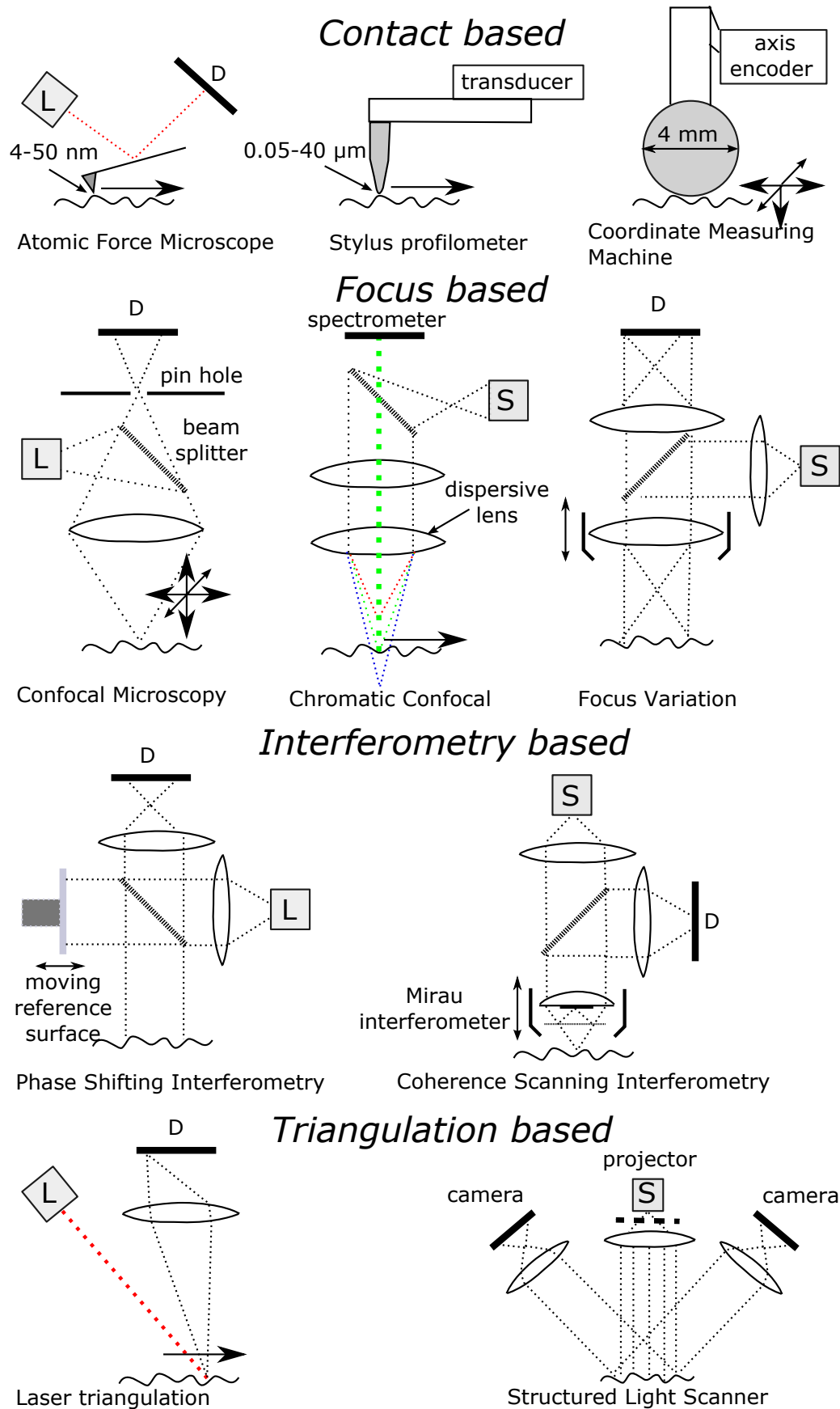


Figure 1.1: A schematic of the principles of some of the most common techniques used for surface metrology and dimensional analyses.

surface to the tip constant. A piezo-electric stage keeps the tip at a constant distance while the system records the distance travelled by the piezo-electric stage for reconstructing the topography of the surface. The approach of measuring the distance travelled by a linear stage until is constrained by the boundary of the surface is used also by the **coordinate measuring machine (CMM)**. In this case the probe has usually a radius of 4 mm hence these instruments can be used only for dimensional metrology. However, modern linear stages can achieve an accuracy of the measurement on the order of micrometers, combined with the fact that this approach allows virtually to measure objects of any size and dimension[157] they are one of the main tools used nowadays for dimensional metrology.

Optical techniques for measuring surface roughness and performing dimensional metrology take advantage of several optical phenomena. A review of the techniques can be found in literature [13, 109], here I briefly introduce the most used techniques and their core concepts. In figure 1.1 I divided the non-contact techniques in three groups. Many techniques take advantage of the variation of the signal at different focal planes. **Confocal microscopy** can retrieve high-resolution 3D topography scanning the object in the three dimensions and limiting the radiation collected to the point at focus. A simpler solution can be designed based only on the difference of intensity registered when the surface is moved away from the focus point. **Chromatic confocal** instead uses a dispersive lens so that the focus of the radiation varies depending on the wavelength. A spectrometer measures the wavelength of the back-scattered radiation for determining the corresponding distance using a look-up-table retrieved from the calibration phase. This approach can be extended for measuring simultaneously a line of points. Lately, measurements of areas can be also performed using techniques based on **focus variation**. In this technique, the lens is moved perpendicular to the surface and the in-focus areas of the image are mapped for each scanning step. It is hence possible to associate at a particular height the in-focus regions of the image, thus reconstructing the topography from the stack of images.

To achieve higher resolutions interferometric techniques are employed. In **phase shifting interferometry (PSI)** the interferogram is produced by the interference of the light reflected by the sample and the light reflected by a reference surface which is moved while performing the analysis. Using this technique a resolution below the nanometer can be achieved, however the maximum height step is determined by the wavelength of the laser light used, thus the applications are often limited to very flat surfaces. To overcome the working range limitations of PSI, **coherence scanning interferometry (CSI)** can be an option. CSI calculates the distance taking into account also the strength of the interference signal for each pixel of the detector. There are many different configurations, one of the most common uses a Miraou interferometer to create the fringe pattern as shown in figure 1.1, this technique is usually called **white light interferometry (WLI)**. Also techniques normally used for retrieving the topography of materials such as **optical coherence tomography (OCT)** could be included in the same class of techniques, in fact Fourier domain OCT systems have been proved to be effective in performing profilometry and roughness analysis[107].

If nanometer resolutions are not necessary for the application, cheaper and

more portable techniques can be developed using the triangulation principle. Projecting a line or a pattern onto a surface and recording an image of the pattern with a camera slightly tilted allows retrieving the topography measuring the position and the distortions of the light patterns. **Laser triangulation** sensors are very common in industry automation but can measure simultaneously only a single line. Fringe pattern recording systems (best known as **Structured light scanner**) projecting a known and variable pattern on the surface are able to acquire an area of the surface keeping the device in a stationary position.

Many structured light devices with a double camera take advantage of principles based on **photogrammetry**, this approach can be exploited also using a single camera capturing many images of the object from various orientations (**Structure from Motion (SfM)**). Due to its simplicity, it is a very common tool used in Cultural Heritage science and archaeology [4]. In the context of archaeology, also devices based on the measurement of time of flight (ToF) of electromagnetic radiation or ultrasounds must be mentioned. In the first case, **terrestrial laser scanners (TLS)** measure the time needed by a laser impulse to be reflected and collected by the detector. Knowing the speed of light the distance can be thus retrieved. TLS have a very large working range and accuracy on the order of centimetres and are thus normally used only for surveying buddings or archaeological sites[141]. Eventually, cheaper alternatives based on coded light depth and depth from stereo (e.g. Intel RealSense[®]) or ToF (e.g. Microsoft Kinect[®]) are now available on the market and commonly known as **depth cameras** and have been applied also to Cultural Heritage objects[27].

1.3 Comparison of the performance of commercial systems

To have an insight into the current panorama of available instruments I compiled a data set based on the specifications of instrument configurations provided by the instruments manufacturers. A configuration in this case is an arrangement of the systems with a particular accessory (often lens). The data set contains the major figures of merits of the performance for many configurations available on the market based on the principles explained in section 1.2.1. Besides, the configurations based on the aforementioned principles the data set includes also the specification of the conoscopic holography probes that were used for the systems developed during this thesis, and that will be treated in detail in chapter 3. The comparison using the specification provided by the manufacturer is not always accurate due to the fact that different manufacturers calculate the figure of merits using different methods. Moreover, is always very hard to condense the performance in a single number, for instance, the accuracy or the repeatability of many instruments depend on several factors comprising the position of the surface on the working range of the instrument (the offset from the optimal distance), the material properties and the environment. However, the data can give an approximate bench-marking of the conoscopic probes that are available on the market. In this analysis, I focus on three main figures of merit: spatial sampling, working range and height

1.3. Comparison of the performance of commercial systems

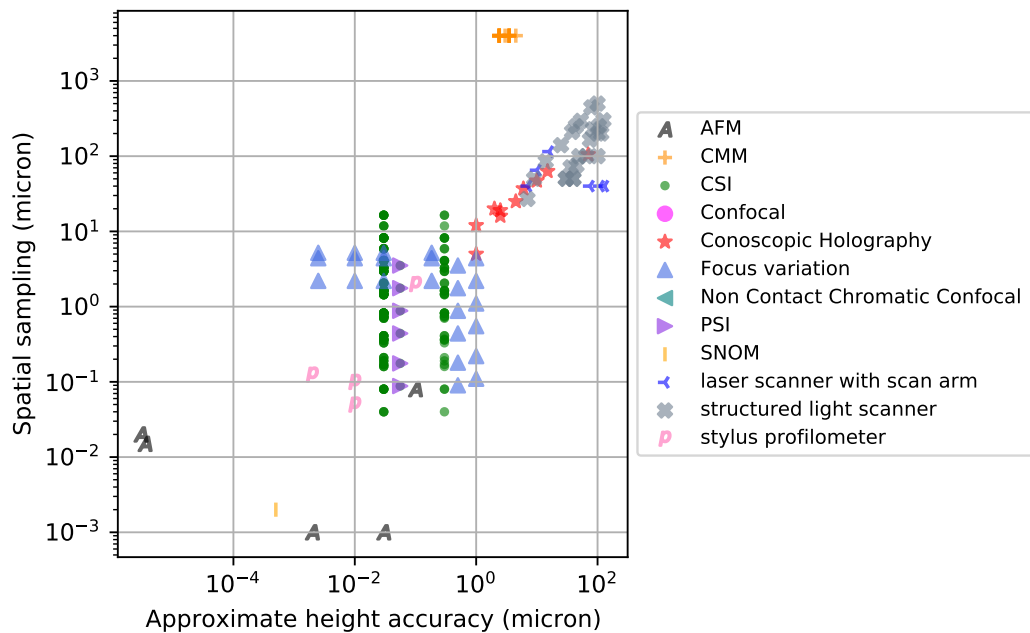
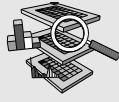


Figure 1.2: The spatial sampling against the height accuracy of the claimed performance of metrology instruments. Note that the axis is logarithmic and the bottom left corner represents higher performance.

accuracy. The spatial sampling is the minimum distance between two consecutive points, in this case, it give us an idea of the smallest surface feature width that could be detected with the technique. The working range is here defined as the maximum step height measurable without re-positioning the object. Finally, the accuracy is an estimate of the average error of the acquired surface from the real surface.



systemsfor3dsurface measurements.csv contains a list of 381 systems configurations based on the principles explained in section 1.2.1. The data can be accessed at <https://www.kaggle.com/giacomomarchioro/systemsfor3dsurfacemeasurements>. The plot here presented can be generated using the kernel <https://www.kaggle.com/giacomomarchioro/kernel20bd88d37e>.

From figure 1.2 we can observe that the contact profilometers listed in the data set are still the most performing instruments in terms of spatial sampling and height accuracy (in this case we have to be aware that the accuracy of AFM is not easy to determine correctly due to many artifacts that can occur during the measurement). Two main clusters appear from the scatter plot: the first containing the interferometric and focus based techniques, the second containing the techniques that use the triangulation/photogrammetric principles. Conoscopic holography probes have intermediate performance. They can reach spatial sampling and accu-

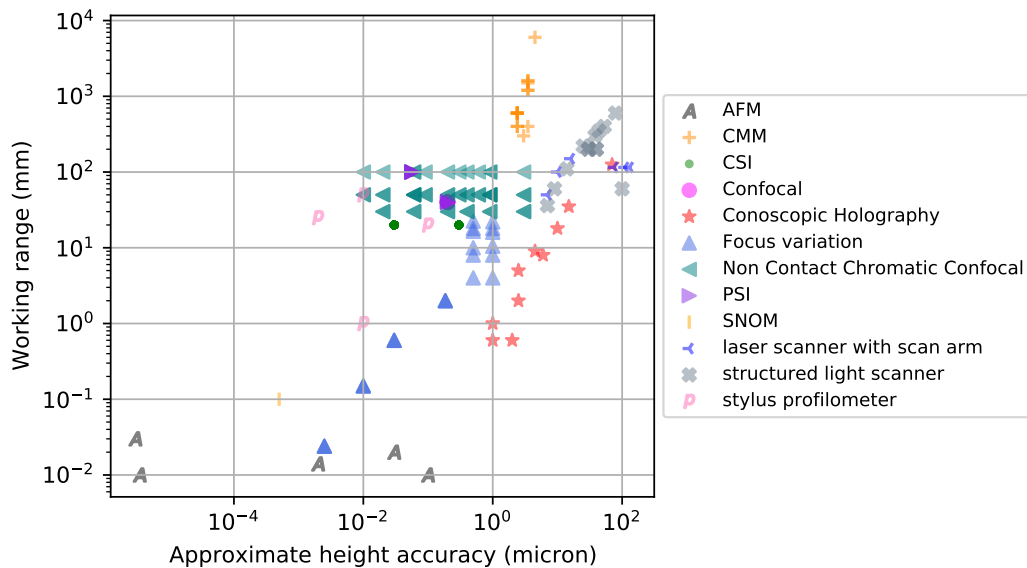


Figure 1.3: The maximum working range against the height accuracy of the claimed performance of metrology instruments. Note that the axis is logarithmic and, in this case, the top left corner represents higher performance.

racy similar to the less performing metrology instruments of the first group. However, regarding the working range and accuracy trade-off they can cover a wider portion of the performance plot of figure 1.3, thus they can be used for collecting with the same instrument (changing the configuration) acquisitions at different scales. Moreover, the surface topography acquired using other techniques can be more easily registered to the same three-dimensional model. Hence results of the techniques based on triangulation/stereo principles can be potentially fused with the results of the conoscopic holography set-ups. In the same manner, nanometer resolution topography map can be registered on the acquisitions collected with the conoscopic holography systems.

1.3.1 Dimensional and surface metrology for a complete surface analysis

With good reason the reader may wonder what are the benefits of applying surface and dimensional metrology to Cultural Heritage objects. The first reason is that the information contained in the surface topography could tell us details about the material and its conservation history including characterization of the surface finishing, curvature of the object structure of the warp-yarn of the paintings[51], canvas imprint, engravings and inscriptions[52]. These features are linked with the surface morphology of the artwork and a complete characterization requires surface metrology techniques. Indeed, this is true also when we are the ones that are modifying the artwork surface: during the restoration or the cleaning of the object[183, 25, 124] or for monitoring the drying process of varnishes[107]. Monitoring the surface before and after the intervention with an accurate topography map could be beneficial for understanding the effects of our actions on the stub-

ble roughness and on the more evident shape of the artwork. The texture and the shape of the object play a key role in the appearance and hence in its aesthetics[154]. Roughness is also linked with other phenomena that affect the stability and the aging of the artwork materials, for instance, pieces of evidence [140] show a correlation with the corrosion resistance of metals.

When the sample is not homogeneous, sampling only a limited number of spots with other analytical techniques on the surface of the object can be misleading or hide position-dependent correlations crucial for the understanding of the materials and their deterioration[60]¹. In this case, associating the measurement to its precise location is mandatory. This process can be done in post processing using different software techniques for registering² the acquisition, or during the acquisition itself, hence implementing the hardware necessary to carry on the acquisition in the area selected. For registering single-spot analysis in a meaningful and accessible way, both techniques require however a model of the object, or at least a detailed representation, and this step has to be performed often with other techniques before the acquisition of the single-spot analyses to be referenced. The surface and dimensional metrology is hence the starting point for the implementation of more advanced techniques and an understanding of the uncertainties and limits associated with the model is necessary for avoiding any bias on the latter analysis. If we acquire a 3D model using a scanning system or a robotic arm that operates by scanning the whole surface of the object using a mechanical positioning system we could take advantage of the same positioning system and the data collected by the scanning device for precisely positioning other techniques or analytical instruments that need to be in the proximity of the object. Once we have coupled several instruments to the mechanical positioning system we can obtain what in this dissertation I call a **multi-modal system**. I define a multi-modal system as a system that allows to use different analytical techniques using the same positioning system hence allowing a fine registration of the data³.

However, creating a system should not be limited to assembling together different instruments but also to fusing the data in an integrated representation of different physico-chemical aspects of the same object and the environment that surrounds it. Data fusion can be applied to register spatial information at different scales[145] or geometrical and dimensional information with spectral information[51, 63, 62]. Many times this should include also monitoring the environ-

¹In this regard, I found meaningful an anecdote that a restorer told me some years ago. While restoring a wooden statue, the restorer found beneath the pictorial layers a gilding. Sampling in other areas of the statue, she found the same gilding. Because it is well known that, in some circumstances, gilded statues were covered with pictorial layers for avoiding thefts, she decided to remove the pictorial layer for revealing the original gilding. Unfortunately, the gilding was well preserved only in the area where she sampled, and the pictorial layers were added instead for aesthetic reasons.

²the term registering in this context means referencing the data over a model representing a greater part of the object

³multi-technique seems more appropriate when using completely different techniques instead of multi-modal that seems to refer to modalities. AFM microscope for instance could be called multi-modal systems because with the same system they can operate with different modalities (e.g. tapping, non-contact, full-contact etc. etc.). For a system that uses two completely different physical-principles such as a combined XRF and Raman spectrometer[139] the term multi-technique system could seem more appropriate.

mental conditions, even though in this case rather than a spatial registration we perform a temporal synchronization. In fact, when measuring features at micron or nano-scale, vibrations, or a slight variation of the temperature and humidity, can affect the performance, the position of the instrument and the object morphology and properties as will be discussed in this dissertation. Hence it is crucial to develop also quality controls after the data has been acquired, to assess the accuracy of the measurement. Eventually, a data-fusion process should be performed to allow using and exchanging data collected not only between the researchers who performed the analysis but also by the researchers who may be interested in the data-set. To carry out this step is necessary an understanding of the underlying data-structure and effective documentation of the data and all the processing applied to it for correcting and registering the acquisitions. This last passage can be critical, due to the time required for fusing all the data and meta-data relative to the samples.

The complete experimental workflow for the analysis of artworks and materials samples collection can be summarized in figure 1.4 where to every step is assigned an estimation of the **reproducibility** in this case acceptance of “the ability to be reproduced or copied” is more suited for the single steps and the production of documented data set. The analyses are often repeated after intervals of time and in different regions of the sample. Eventually, alteration of the samples due to natural aging or to treatments applied to the sample should be taken into account. In many cases, more than one technique is used to fully characterize the sample. The process is inevitably time consuming, especially if the sample must be sent to different facilities to be analyzed.

1.3.2 The problem of surface and dimensional metrology applied to Cultural Heritage objects

Surface metrology was developed in the field of mechanical engineering and parts manufacturing. In particular, most of the applications are developed for addressing issues related to the automotive, aerospace and semiconductors industry. Applying the same tools to artworks is not straightforward. Here I divided the requirements into two categories: hardware and software requirements.

From the perspective of the hardware there are mainly two requirements. The first requirement is the non-invasiveness of the technique used. Stylus profilers, which are the gold standard in surface metrology, cannot be used without the risk of damaging the surface, leaving traces of the stylus path, as highlighted by different studies [99, 108, 138] [168, sec. 5.9]. The second hardware requirement is the portability of the instrument for performing the analysis on site directly on the artwork. Many interferometric techniques (e.g. white light interferometry, confocal microscopy) are hence not easily applicable (for getting an idea on the portability of the instruments see for instance the weight tabulated on the online data set *systemsfor3Dsurface measurements.csv* of section 1.3).

Regarding the software requirements, we have to consider the robustness of the algorithms in analyzing heterogeneous materials. Industrial applications of surface metrology analyze usually machined metal pieces that are uniform and

1.3. Comparison of the performance of commercial systems

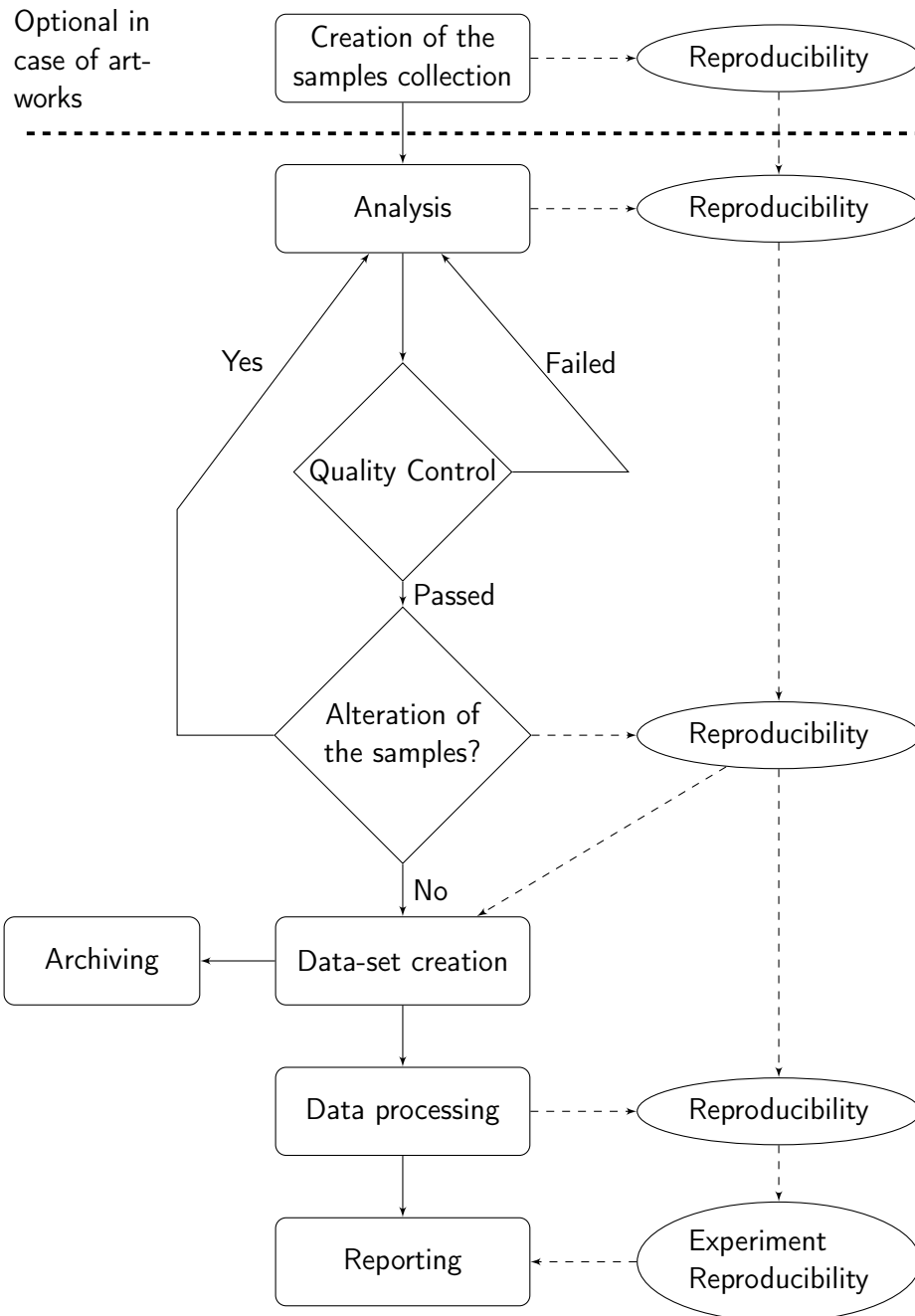


Figure 1.4: Work-flow for the analysis of a collection of samples. To every step is associated a replicability of the procedure.

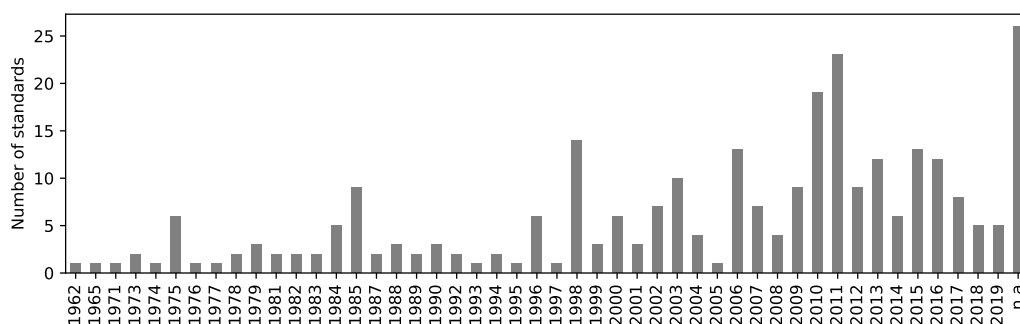


Figure 1.5: The number of ISO standard per year published by the TC 213.

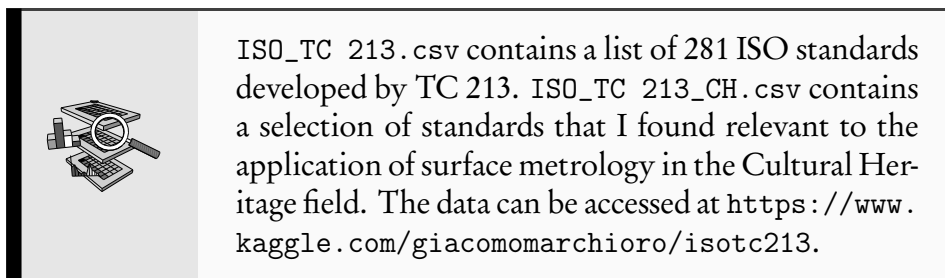
with an expected pattern and materials to characterize. The artwork is often a unique composite object aged and restored during several centuries. The user that performs surface metrology on artworks must be cautious when applying directly the standard methods on the unknown surface. Many standards and conventions developed in surface metrology arise from empirical knowledge gained by analyzing metal parts (for instance, the cut-off filtering parameters derived from the automotive industry) [186, p.10]. This empirical knowledge was gained analyzing millions of similar parts produced in the factories. While the conservation scientist is often analyzing unique products of the creativity of the artist. Hence, there is firstly a need to fill in the lack of tools for exploratory data analysis of complex and unknown surfaces. Aside from analyzing directly artwork is thus propaedeutic to study also the artwork's materials individually under controlled conditions. Using this methodology we can try to infer, with the proper precautions, the origin of the signals measured on the surface. Finally, the need to develop methods to quantify and possibly correct the uncertainties deriving from the analysis of heterogeneous materials (Chapter 5). This process must be repeated for each artwork and surface, hence a considerable amount of automatizing is needed to make it feasible.

The data collected and elaborated by different operators with different instruments on unique objects will necessitate considerable efforts to be comparable. A solid standardization might be necessary for avoiding biases and ambiguities in the collection and analysis of the data. It might be reasonable to adopt the standardization already used by the industry, proposed by the ISO.

1.4 The usage of international standards from ISO: benefits and costs

The complexity of the metrological chain from the measurements to the data elaboration often led to a lack of reproducibility of the procedure [113, 111, 23]. For this reason, institutions and industries spent a lot of efforts in defining standardized way to measure, elaborate and certify the data collected. This work has been carried out in parallel by different national standardization organizations such as the American Society of Mechanical Engineers (ASME) or organizations linked

to specific industrial field as the German Verband der Automobilindustrie (VDA). The standards produced often differ in the definition and implementation of the concepts, in this work I adopted the standards defined by the International Standard Organization (ISO). In figure 1.5 can be seen that the efforts in developing newer standards grew in the last twenty years. Indeed, the adoption of these standards might increase the reproducibility of the research and the possibility to compare results and data collected by different research groups or institutions. However, the study and the adoption of ISO standards by the academia is limited probably because, unlike other international standardization consortium (e.g. W3C), the standards provided by ISO are not open access. ISO assigned a specific technical committee (TC 213) devoted to the creation of standards related to Dimensional and geometrical product specifications and verification. For analyzing the costs for buying the standards and their development I have created a data set of all the standards developed by TC 213.



From 1962 to 2019 ISO technical committee 213 developed 259 standards (comprising deleted and withdrawn documents and excluding the 24 standards under development) the total commercial value of these documents is 12623.52 euros. Of these, I estimated that between 60 and 70 standards might be useful for implementing the software and hardware solution for performing a metrology analysis on artworks. The cost for acquiring these standards is around 5k euros, but of course it might vary depending on the project.

1.4.1 The choice of the standards

I selected the standards taking into account the application on Cultural Heritage objects. Most of the standards related to filtration and the computation of the metrological parameters are relevant to the characterization also of Cultural Heritage objects. These parameters, and the filtration techniques for acquiring them, have been used for characterizing the surface of CH objects [50]. Also the standards related to the reference specimens (wedges, gauge blocks and reference profiles) are important for assessing the performance of the instrument also in the Cultural Heritage sector[67]. I have excluded from the selection standards related to instruments such calipers, technical drawings, geometrical tolerancing. Furthermore, standards related to Coordinate Measuring Machine might be less relevant to the Cultural Heritage sector due to the trends towards non-contact measurements.

1.5 Discrete representations of the surface

Modern metrology instruments (viz. figure 1.1 at page 4), after the required processing, output one or many discrete values representing a distance of the point of the object from a reference point or plane (e.g. from the lens or from an imaginary plane). In this section I define the main terms and the mathematical representations of the data that will be used during the dissertation.

A **profile** can be represented as a series of distances acquired along a rectilinear trajectory. A **surface** describes instead an area of a 3D object. In most cases, I will describe profiles and surfaces as arrays. In the standards this representation is called **data-matrix**[89]. However, I differentiate between **arrays of distances** and **arrays of height variations**. From my experience, this differentiation is often unnoticed by the users of the data that are led to errors when analyzing the data provided.

nD array of distances

A simple surface profile can be represented as a 1-dimensional array of the kind:

$$P = [d_1, d_2, \dots, d_i,] \quad (1.1)$$

where d is the distance from a reference line (e.g. the trajectory of the instrument lens). For some applications, we might want to consider the points connected and hence consider this structure as a **polygonal chain**⁴.

A portion of a surface can be represented as a 2-dimensional array, of the kind:

$$S = \begin{bmatrix} d_{1,1} & d_{1,2} & \dots \\ \vdots & \ddots & \\ d_{k,1} & & d_{k,j} \end{bmatrix} \quad (1.2)$$

where d still represents the distance but from the instrument reference plane or trajectory and (k, i) refers to the indexes. We will refer to this type of data structure with the term **nD array of distances** where n denotes the number of axes of the array: one for the profiles, two for the surfaces and three for what we call **surface stacks**. This representation necessitates that the distances between a measurement and the adjacent one are constant but not necessarily equal among the different axis. For instance the distance between $d_{1,n}$ and $d_{1,n+1}$ must be the same for every n but it does not have to be necessarily the same of the distance between $d_{i,1}$ and $d_{i+1,1}$. So every nD array of distance could require from one to n additional terms defining what we can call **scan-step** in the context of scanning system **pixel size** for imaging systems or **sampling step** when the surface comes from the sampling or discretization of a continuous signal or function⁵. For encompassing all this definitions the generic term **increment** is used in ISO 25178-72:2017[89].

⁴**Polyline** and **linestring** are terms normally found in computer science.

⁵Unfortunately, often, the term lateral resolution is used, but in fact the lateral resolution can be much lower compared to the scan-step.

A 3D array of distances can be a very handy structure for multilayer material, we can think of this structure as a surface stack where the third dimension can be a distance but also represent time lapses. It is worth mentioning that the dimension of the array does not correspond to the dimension of the object mapped, for instance a 2D array of distances can represent a portion of a surface while a 3D-array of distances can represent the evolution of a surface in time so can describe four dimensions.

nD array of height variations

If the distance is referring to a line or a plane we must define the **position of the reference line or plane**, in other words at what every single distance corresponds. We may find the term **depth image** in many books. Most of the time if we output directly this data structure from an instrument the distance measured will be from the probe above the surface to the surface itself. Thus, greater distances are interpreted as valleys of the surface and smaller distances as peaks. If we subtract a reference plane the interpretation will be the opposite.

This may seem obvious to the operator who performed the analysis but may not be so evident for an external user of the data, and the results can be completely misinterpreted if the reference plane is taken for granted. For this reason, in this dissertation, we make a distinction between arrays of distances and arrays of height variations. An **array of height variations** is composed of values that are referring to a virtual plane or form, for instance, a nominal form fitted to the data. Hence heights can assume also negative values while distances are for definition positive. For convention, we use the letter z for indicating that we are dealing with a height variation.

$$P = [z_1, z_2, \dots, z_n] \quad (1.3)$$

Sometimes instead of a parallel plane the distances are referring to a point or an area. This is the case of **range imaging** and so in this case the output is called a **range image**.

Other conventions used in literature: the confusion between visualization and dimensions

A 2D array of distances can be produced and hence be visualized as a 3-dimensional object, the user may be tempted to refer to this data as 2.5D (two-and-a-half-dimensional) because it contains also information regarding the position in the third dimension, the usage of this term, in my opinion, should be avoided because this term is usually related to the visual perception⁶ of the data and not the data structure itself or its dimension from the mathematical point of view. Furthermore, the term 2.5D can be confused with the Hausdorff dimension that we encounter later on this dissertation.

⁶ three-quarter and pseudo-3D are also found in literature, the latter term even if less in vogue is actually the most preferable in the context of visual perception. An analogous concept is expressed by the term *Trompe-l'œil* in history of art.

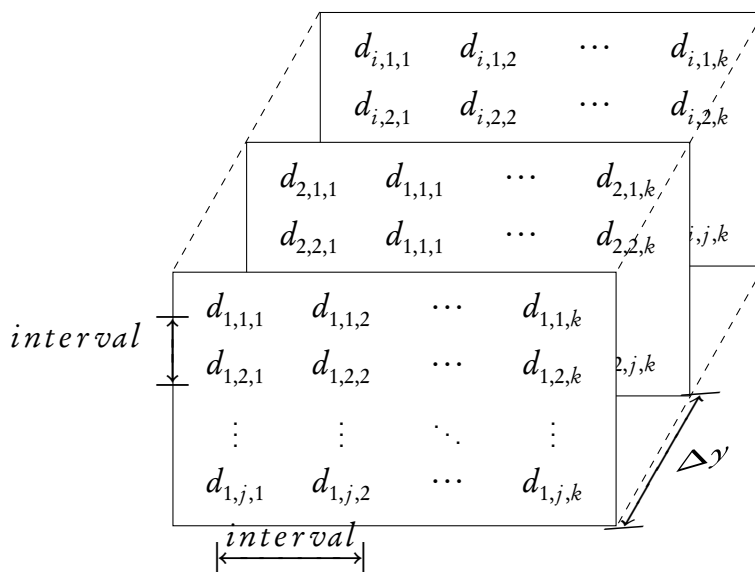


Figure 1.6: A representation of a stack of 2D-array of distances.

2D and 3D arrays of generic scalars

A large amount of analytic data can be described with the N-dimensional array (e.g. hyper-spectral or multi-spectral cubes etc. etc.). We call these representations **data matrices**. Some techniques, for instance X-ray tomography can retrieve the density of the material and hence output (after transformation of the data) a 3D array with scalars representing densities. For retrieving the interfaces usually an algorithm (such as marching cube algorithm for 3D arrays) is used: a threshold is used for delimiting the borders of the interface and obtaining what is called an **isosurface** (or **isoline** for 2D objects). Thus the interface found depends on the threshold chosen for separating the phases that the user wants to study. The output is a series of coordinates that delimit the surface, a list of n-tuple.

List of n-tuple

A more flexible way to represent the surface is using lists of coordinates with respect to an arbitrary origin point. In a more formal way we can define it as a list of n-tuple:

$$\begin{aligned} & [(i_1, \dots, i_n), \\ & \quad \dots, \\ & (i_1, \dots, i_n)] \end{aligned} \tag{1.4}$$

Where n is two for a profile and three for a surface. This structure gives us the possibility to describe complex object where a continuous interface has points with only one coordinate different from the other. They have also the advantage that can be not ordered and not-evenly spaced, because the order does not contain topologic information (in the nD-array of distances neighbour values meant that the distance was next to each other). Many formats used in computer graphics

and 3D scanning uses this data structure. **Point clouds** can be described as a set of triples (3-tuple). Where each triple contains the coordinates (X,Y,Z).

The advantage of the arrays compared to lists of n-tuple

Even if the n-tuples are more flexible compared to the arrays the main advantage of the arrays is their usability. For describing a flat surface we necessitate only the values regarding the height or distance, the shape and the increment. While for the point-clouds we necessitate for each point the two coordinates. This usually allows saving almost two thirds of the memory required for dealing with an equivalent surface described as a point cloud. Furthermore, many operations are facilitated using the arrays because they assure evenly spaced measurements.

1.6 Summary

In this introduction, I briefly explained the difference between **surface metrology** and **dimensional analysis**. An overview of the performance of the instruments used in these two fields has been given analyzing a data set collected from the nominal specifications provided by the manufacturers. The conoscopic holography sensors (treated in this dissertation) have intermediate performance between instruments normally employed for surface metrology and for dimensional analysis, thus they could be helpful for:

- retrieving dimensional and roughness information with the same system.
- multi-scale analysis, thanks to the high variation on the available working ranges.
- positioning automatically other instruments/probes with high accuracy:
 - developing of multi-modal system.
 - automatizing and increasing the reproducibility of the experiments.
 - allowing the collection of a large amount of data.
- data fusion between low-resolution and high-resolution techniques.

However, the application of surface metrology and dimensional analysis to CH objects is not straightforward. I discussed the main requirements and problems:

- non-invasiveness of the technique used.
- the portability of the technique.
- previous knowledge and development of surface metrology was based on empirical knowledge acquired on millions of pieces produced by factories.
- Cultural Heritage objects are unique pieces with materials that can change over time or due to environmental conditions.

- we need to create exploratory tools for analyzing unique materials without an *a priori* knowledge of them (as it was for the industry).
- collecting knowledge on artistic materials in a controlled and reproducible way might be helpful for improving our knowledge on surface metrology of Cultural Heritage objects.

I proposed a workflow for creating and analyzing collections of samples. For increasing the repeatability and the possibility to compare data collected from different research groups I analyzed the benefits and the costs of the adoption of ISO standards related to surface metrology using a data set.

In the next chapter, we will see how to encode the information of reference samples collection using a new tool developed during this thesis for facilitating the analysis of flat samples collections.

2

Automating the creation of flat samples collections

The chapter treats problems and methodologies for creating and analyzing samples collections of a wide range of materials used in artworks in a standardized manner. It describes a new tool developed during the thesis that produces a file format for creating, describing and analyzing flat sample collections.

Introduction

Reference samples collections in the Cultural Heritage research praxis

The creation and the analysis of **reference samples collections** is an important step in the research on conservation of Cultural Heritage (see figure 1.4 at page 11). The Getty conservation institute established in the early 1990s the GCI Reference Collection [55], one of the greatest repositories of artist materials. In fact, almost every institution and research group dealing with the conservation of Cultural Heritage produces reference materials collections. To name but a few, we can find researches based on reference samples collection for painting materials[5, 38], illuminated manuscripts materials[2] and metals[119]. However, this process is often not standardized hence the possibility to access the information of the original sample collections and the data set produced is not always granted. Other researchers or sometimes, after some years, even the same researchers who produced the collections might not be able to reuse effectively the samples collection.

	Wide (mm)	Height (mm)	Depth (mm)
Microscope slide (ISO 8037/ 1)	70	25	1
Microscope slide (geological)	75	50	1
Microscope slide (petrographic)	46	27	1
A7	81	114	-
ISO9227	150	70	1 ±0.2
ISO9227 (organic coating)	150	100	1
A4	210	297	-

Table 2.1: Common standardized dimensions that can be used for easing the process of creating samples collection.

Strategies for standardizing the creation and analysis of reference samples collections

Several laboratories have automated the analytical process for creating sample collections and acquiring the analytical data. In medical laboratories, automated analysers are used for analyzing liquid samples. These analyzers take advantage of **sample holders** following specific standards, for instance, microplates following ANSI/SBS 1-2004 ANSI/SBS 4-2004 standards. For testing some materials efficiently are already available several standards defining the dimension of the samples and the procedure to perform for instance (ISO 9227:2017[94]). For the automated analyses of complex parts, “pick-and-place” robots are used and commercially available[137]. For allowing a standardized process both the sample holder and the samples must have well defined dimensions. In table 2.1 I report some standard dimensions that can be used for standardizing the creation of the samples collection.

In the case of samples collections that are conserved for a long time, it is more convenient to design the sample’s holder around the sample collection and keep the samples holder for storing effectively the samples and possibly facilitating their analysis. In this project, I focused on the standardization of flat samples collection, which is probably the most common type of samples collection used in Cultural Heritage research, with the aim of improving the usability of these data sets. For facilitating this task I developed a Python module for generating a file to describe sample collections and that can be eventually used for producing and analyzing in an automated way the collection itself. In doing so I took into consideration the following requirements:

- The reference collection must be fully described.
- The samples holder should be used as a reference system, so there is no need to move every single sample individually.
- The format must be machine and human-readable.

2.1. The workflow for creating the samples collection

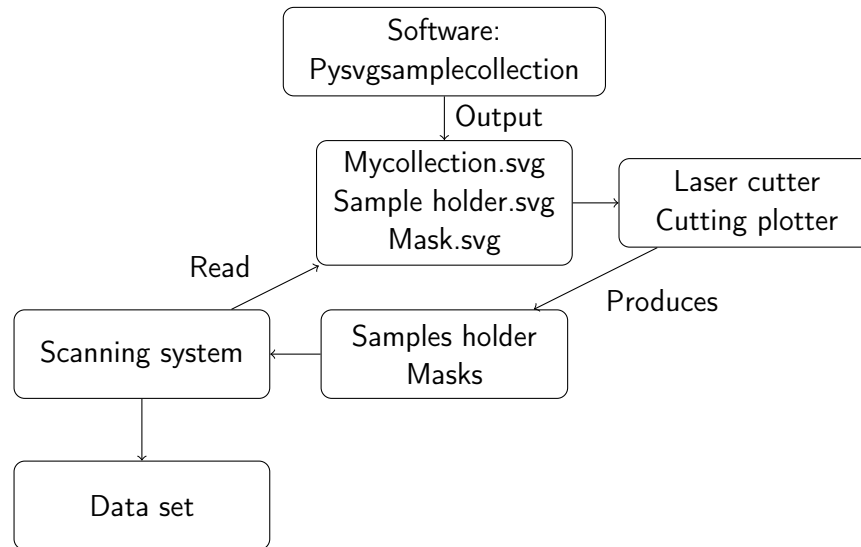


Figure 2.1: The procedure for creating and analyzing samples collection with the tool created during the project.

- The sample holder dimensions possibly should not exceed the instrument stages limits
- The sample holder should be built so that can be easily shipped to other laboratories.
- It must be possible to extract easily the positions of the samples for sending them to the positioning system.

2.1 The workflow for creating the samples collection

Figure 2.1 shows the workflow proposed for creating and analyzing the samples collection. The researcher uses the software tool to programmatically create the samples collection, as described in the following section (2.2). The output is a series of scalable vector graphic (SVG) files. SVG files are XML-based text format that can contain information in a structured way and at the same time can be read as an image allowing non experienced users to visualize the structure of the sample collection using any web-browser. The main SVG file contains all the information regarding the samples collections: materials used, coatings applied and their position in relation to the samples holder. The SVG file is structured so that it can be read by several machines capable of producing the samples holder, the samples and the masks used for easing the production of the samples. Common machines that can be used for this scope are laser cutters or cutting plotters. The **laser cutters** are programmable machines able to cut different materials following a programmable path, while **cutting plotters** perform the same function but are usually limited to sheets of soft materials such as paper and textile. Using these files as an input the machine can cut or, if needed, engrave the samples and the samples holder as designed by the researcher. The researcher can hence apply coatings and treatments.

Once the physical reproduction of the samples collection is completed, the sample holder with the samples can be placed on the scanning system that, using the information contained in the same SVG file, can automatically scan each sample or selected samples and areas. A further advantage is that the data set produced is already annotated. For instance, if the researcher scans each sample entirely, using the SVG file it can automatically retrieve the area with certain coatings or treatments he previously indicated when creating the SVG files using the aforementioned tool.

2.2 The tool for creating the samples collection



PySVGsamplescollection allows the creation of reference samples collections in a programmatic way. The source code can be found at: <https://github.com/giacomomarchioro/pySVGsamplescollection>

The general idea presented in section 2.1 is practically implemented developing a Python module that I called *SVGsamplescollection*. The listing 2.1 shows a basic example of the usage of the module for creating a samples collection of fifteen samples. This example serves only for illustrating the process and is simplified for brevity and clarity. All the design of the experiment must be carried out by the researcher before designing the collection. Here we suppose that the researcher found that 15 samples are enough for his research, and he wants to see the residues of varnishing on these samples after the exposure to UV light and the cleaning with a solution of acetone. The collection can be created and described using the following code:

```

1 from svgsamplescollection import SamplesCollection
2 mycollection = SamplesCollection()
3 mycollection.name = 'Test samples collection'
4 mycollection.add_creator('Joe Foe')
5 mycollection.publisher = 'University of Verona'
6 mycollection.set_sampleholder_dimension.A4()
7 mycollection.set_sample_dimension.Microscope_slide()
8 mycollection.set_number_of_samples(15)
9 mycollection.create_sample_holder()
10 mycollection.add_step("Cut the samples from a wood laminate")
11 mycollection.populate_with_samples('wood')
12 mycollection.add_step("Cover with vermilion in egg tempera all
    the samples except one.")
13 for sample in mycollection.samples[1:]:
14     sample.add_layer("vermilion egg tempera", "brush",
        width_percent=0.9)
15 mycollection.add_step("Add the varnish from the first to the
    fifth sample")
16 for sample in mycollection.samples[1:5]:
17     sample.add_layer("varnish", "brush", width_percent=0.7)
18 mycollection.add_step("Irradiate samples using UV light.")
19 for sample in mycollection.samples[::2]:
20     sample.add_treatment(process="uv curing",

```

2.2. The tool for creating the samples collection

```
21         parameters = {"duration": "5 h",
22                       "wavelength_nm": "290"},
23         height_percent=0.5)
24 mycollection.add_step("Clean the samples using acetone.")
25 for sample in mycollection.samples:
26     sample.add_treatment("cleaning", "acetone", width_percent
27                          =0.5)
28 mycollection.insert_alignment_MTF_standard()
29 mycollection.insert_scalebar()
30 mycollection.insert_standard()
31 mycollection.save_svg()
32 mycollection.save_masks_svg()
33 mycollection.save_dxf()
```

Listing 2.1: Example of creating a samples collection programatically using SVGsamplescollection Python module.

A minimum knowledge of programming is required for fully understanding this example.

In lines 1-8 we import the module, we create an instance of the class and we set the name of the collection (Test samples collection), of the author and institution, the dimension of the sample holder (A4), and the number and the dimensions of the samples (fifteen samples with the size of a standard microscope slide).

In line 9 we create the sample holder. The module will output an error if the samples cannot fit on the sample holder otherwise it will automatically space the samples as an array.

We must divide the creations in **steps** using the function `add_step` that accepts the description of the step that will follow (viz. line 10).

In line 11 we create the samples assigning the material to *"wood"* in this case. Now that we have the samples we can add further information regarding other materials and processes that characterize them. When designing this format I defined two main attributes: the *layer* and *treatment* attribute.

In lines 13-14 we add to each sample (IDs from 1 to 14) except the samples with ID 0 a layer of vermilion in egg tempera. Within the *layer* attribute we can assign two arguments: *material* and *process*. The *material* field is meant to be used for describing the materials present in the layers while the *process* is meant to be used for describing the process used for applying the materials. The parameter *width_percent* is used for defining the horizontal extent of the layer, for instance, a *width_percent* of 0.5 means that half of the sample is covered with the material or treated.

In line 10 we add as materials vermilion and egg tempera using as process a brush.

In lines 16-17 we apply a varnish layer, using the same procedure but only to the first 4 samples [1:5] (the right limit is exclusive) and limited to half of the samples.

For steps that do not involve the direct application of new layers but their modification we use the function `add_treatment`. That can accept the type of process and the parameters used during the process as shown in lines 16-18 (UV curing) and lines 19-23 (cleaning with acetone). In the first case the notation `::2` means that we will apply the treatment to the sample every other sample (the first,

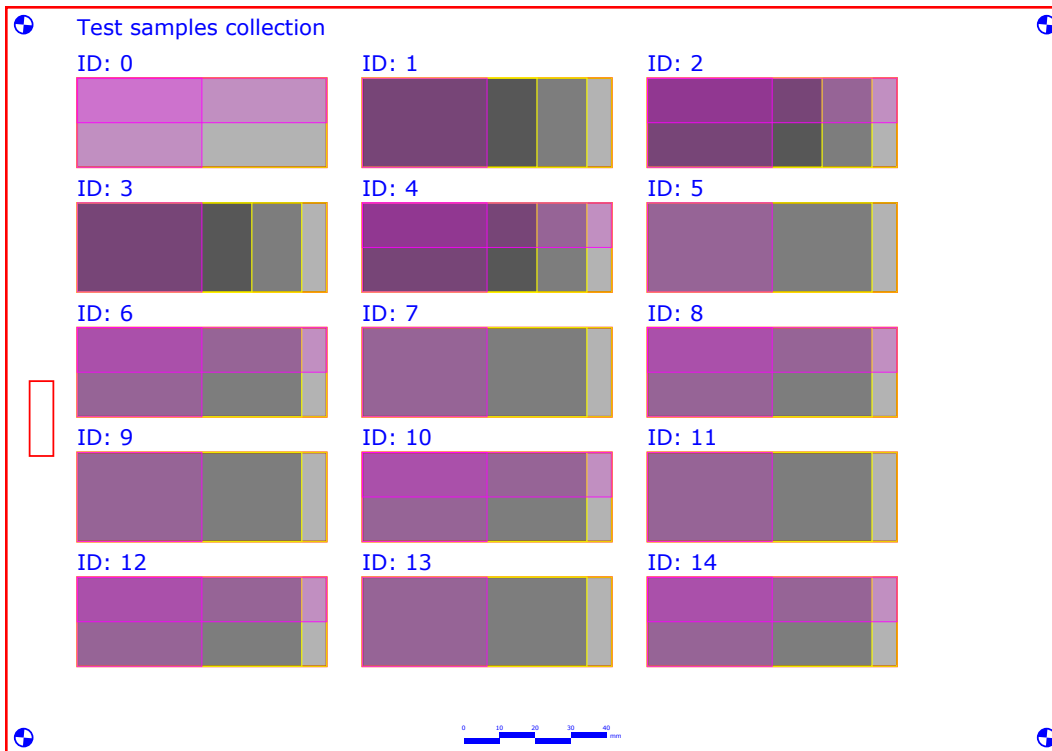


Figure 2.2: The output file containing all the information regarding the samples and the sample holder.

the third etc. etc.) in this case specifying the `height_percent` we cover the whole width but only a portion of the height of the sample.

Lines 27-29 are used for placing a scale bar, a housing for a reference target, and reference markers these are particularly useful for assessing the alignment of the scanning system and for aligning the imaging analyses not referenced to the scanning system.

Eventually, in lines 30-31 we save the main SVG files and separately the *masks*. The masks can be used during the manufacturing process of the sample collection. They can be produced in the same way as the sample holder using laser cutters or cutting plotter. Each mask covers the whole samples holder except for the extent of a specific group of layers or treatments. For instance, the mask related to the treatment of cleaning the samples with acetone (lines 25-26) covers the whole sample holder except for the first half of each sample. In this way when the researcher is preparing the sample collection he can apply the mask on the top of the samples for limiting the risk of committing mistakes and increasing the speed and accuracy of applying the treatment. The masks can be reused in the creation of other samples collections, even though often also information regarding the process or the material to be applied are engraved above the sampled area.

This process might apparently be complicated for people not used to scripting, but in fact often the user does not have to write the whole script from scratch but just adapt the example scripts that get closer to the target application.

2.3 Conventions and suggestions

As a convention, I started the numbering of the samples from zero. I use the sample with ID 0 as a reference hence I usually leave it untreated or only partially treated. Often a small portion (a strip of about ten percent of the width of each sample) is left completely untreated as reference. Leaving this space allows to study also the interaction at the borders of the treatments or the layer and is often useful for measuring the layer thickness.

Another important function of a reference band on one specific side of the samples is to have asymmetric samples. This is very important if the samples can be removed from the samples holder, symmetrical samples could be inadvertently rotated causing errors when registering the samples in spatio-temporal studies.

Regarding the color coding of the lines in the SVG files, I kept the conventional color coding of the laser cutter. Red lines (RGBA: 255, 0, 0, 255) are defined as cut line hence they will be cut if the SVG is used in combination with a laser cutter. Blue lines and areas (RGBA: 0, 0, 255, 255) will be engraved with a depth depending on the laser parameters used, so everything appearing as a blue area or line will eventually appear as black depending on the material used for creating the sample holder.

2.4 Description of the modified SVG file format

As previously mentioned the SVG is a file format based on Extensible Markup Language (XML). In this section, we will have an insight into the particular implementation of the SVG file format that I defined for this specific task.

```

1 <svg baseProfile="full" height="210mm" version="1.1" viewBox="0
  0 297 210" width="297mm" xmlns="http://www.w3.org/2000/svg">
2   <metadata>
3     <rdf:RDF xmlns:dc="http://purl.org/dc/elements/1.1/"
  xmlns:rdf="http://www.w3.org/1999/02/22-rdf-syntax-ns#"
  xmlns:rdfs="http://www.w3.org/2000/01/rdf-schema#">
4       <rdf:Description dc:date="2020-07-18 18:48:18.093112"
  dc:format="image/svg+xml" dc:language="en" dc:publisher="
  University of Verona" dc:title="Test samples collection">
5         <dc:creator>
6           <rdf:Bag>
7             <rdf:li>John Doe</rdf:li>
8           </rdf:Bag>
9         </dc:creator>
10        </rdf:Description>
11      </rdf:RDF>
12    </metadata>

```

Listing 2.2: Example of creating a samples collection programatically using SVGsamplescollection Python module.

I used the `viewBox` attribute to define the coordinate system (in this case 297 units wide and 210 units high). And then `width` and `height` attributes to define the measurement units in this case millimeter. Even though for some SVG elements the units can be specified in the attributes (e.g. `width="70mm"`) to be consistent with

complex SVG elements that do not allow the definition of the units of measurement, I decided to indicate the unit of measurement only on the header of the SVG file.

The first element contains the basic metadata (creator, date, title, institution (using the `dc:publisher` term) encoded on the widely accepted standard Dublin-Core[42] and using the Resource Description Framework (RDF)[148].

After the header, other two elements (`<text>`, `<rect>`) are used for printing the title of the samples collection and the external borders.

```
1 <image id="backgroundimage" />
2 <text fill="blue" font-family="Verdana" font-size="9.0" x="20" y
  ="12.0">Test silver</text>
3 <rect fill-opacity="0" height="210" id="collection_border"
  stroke="red" stroke-width="1" width="297" x="0" y="0">
4   <title>{
5     "1": {
6       "description": "Silver samples are cut and fixed to the sample
7         holder.",
8       "status": "?",
9       "date": "?"
10    },
11    "2": {
12      "description": "Silver samples with ids ranging from 1 to 8
13        are ceased using a graver.",
14      "status": "?",
15      "date": "?"
16    },
17    "3": {
18      "description": "A nitrocellulose lacquer is used to protect
19        the silver samples.",
20      "status": "?",
21      "date": "?"
22    },
23    "4": {
24      "description": "All the samples are cleaned using acetone.",
25      "status": "?",
26      "date": "?"
27    }
28  }</title>
```

Listing 2.3: The definition of the collection borders and the description of the steps.

It is important to notice that all the other title tags `<title> ...</title>` are not used for describing the actual title of the sample collection but for describing the content of the elements. Inside the title tags are reported the information relative to the element (layers, treatments, steps) using the JSON schema[100]. When opening the file using a browser the user can see the information as a tooltip through mouse over interactions. The title tag of the rectangle element defining the border of the sample collection contains the list of steps that we defined previously and the status and the date, if the step has been already carried out.

The other information can be still retrieved in a standard manner de-serializing the text of the title tag.

The information regarding the sample collection are organized in groups. In SVG group of similar objects are enclosed between the group tags `<g> ...</g>`. All the samples positions are inside a group with `id="samples_position"`. Each sample is described by a rectangle, describing the dimensions and a text that contains the ID of the sample.

```

1 <g id="samples_position">
2   <rect
3     x="20"
4     y="20"
5     id="0"
6     width="70"
7     height="25"
8     stroke="red"
9     stroke-width="0.5"
10    fill-opacity="0" />
11  <text
12    x="20"
13    y="18"
14    font-family="Verdana"
15    font-size="5"
16    fill="blue" >
17    ID: 0 </text>
18  [...]
```

Listing 2.4: The group containing the samples positions.

A second group contains information regarding the samples and their treatments. Rectangles are used also here for indicating the position and the extent of each sample, layer and treatment. Inside each samples a `<title>` tag is used for storing the fields containing the description of the layers and the treatments. In this way, when the SVG is opened in a browser the user can retrieve the information regarding the last layer passing on the top of each layer. The browser will display a tool-tip with the information.

```

1 <g id="samples">
2   <rect
3     x="20"
4     y="20"
5     id="0"
6     width="70"
7     height="25"
8     stroke="yellow"
9     stroke-width="0.4"
10    stroke-opacity="0.8"
11    fill-opacity="0.3" >
12     <title{
13       "material": "wood",
14       "process": "?",
15       "thickness_microns": 1,
16       "status": "?",
17       "step": 1,
18       "applied_date": "?",
19       "removed_date": "?"
20     }</title>
21   </rect>
```

```

22
23 <rect
24   x="20"
25   y="20"
26   id="0"
27   width="35.0"
28   height="25"
29   stroke="magenta"
30   stroke-opacity="0.8"
31   stroke-width="0.3"
32   fill="magenta"
33   fill-opacity="0.2" >
34   <title>{
35     "process": "cleaning",
36     "parameters": "acetone",
37     "status": "?",
38     "applied_date": "?",
39     "layer": null,
40     "step": 5
41   }</title>
42 </rect>
43 [...]
```

Listing 2.5: The group section containing the information regarding the samples.

These are the mandatory parts of the file format. At the end of the file are present the groups containing the definition and position of the scale bar, the alignment markers and the housing for an optional reference target standard. As we will see in the next section this defined but yet flexible structure allows querying the samples collection for reading the information needed.

2.5 Reading and querying the SVG

Knowing the structure of the files allows to manipulate them very effectively using tools able to phrase XML data structures. In the implementation of the tool, I provided the possibility of selecting layers with keywords in their description and also of performing spatial queries, as explained later.

```

1 from SVGsamplescollection import ReadCollection
2 mycollection = ReadCollection('Test samples collection.SVG')
3 mycollection.get_treatments_position(WITH='acetone', WITHOUT='
   varnish')
```

Listing 2.6: Example of querying a samples collection programatically using SVGsamplescollection Python module.

For instance, the researcher might want to select a region of interest (ROI) where are present some materials and are not present some treatments. For instance, related to the previous example, the researcher might want to select the areas that are varnished but not treated with acetone. In this case, we took advantage of Shapley a Python library for manipulation and analysis of geometric objects [56]. The results of this query are the IDs of the sample and the coordinates of the areas that meet the criteria imposed by the researcher.

2.6. An example of the manufacturing process of the samples collection



Figure 2.3: The creation of the samples collection using an industrial laser cutter and the masks for easing the application of the layers. From left to right, on the first row: cutting of the panel, resulting panel with the border and positioning of the first mask. From left to right on the second row: positioning of the second mask, painting of the areas and final result.

The coordinates can be eventually used in combination with a positioning system for automating the analysis of the samples or specific parts of samples collection.

2.6 An example of the manufacturing process of the samples collection

The creation of the samples and the samples holder is not strictly bound to a specific manufacturing process. However, this rigorous design method allows taking advantage of different tools for improving or automating the creation of the samples collection.

Figure 2.3 shows the steps for producing a basic samples collection. The sample holder is cut using an LVTC 1390/100 laser cutter from a XylTECH[®] composite fiber. For cutting, the speed of the cut is set to 20 mm s^{-1} and the power of the laser to 50-60% while for the engraving the name of the samples the speed of the cut is set to 120 mm s^{-1} and the power of the laser to 10-20%. Besides, the sample holder also a frame is cut from the same piece of composite fiber. The frame can be used for positioning the sample holder and the masks. The masks for this project are cut from NOVAFLEXIBLE[®] polypropylene sheets (speed of the cut is set to 35 mm s^{-1} and the power of the laser to 50-60%) and they can be used for guiding the operator in the addition of the layers, as shown in figure 2.3.

If the researcher wants to control the layer thickness there are several possibilities to achieve better control of the thickness depending on the application. For layers with thickness from several microns to millimeters masks with a known thickness can be used combined with spatulas for a coarse control on the layer

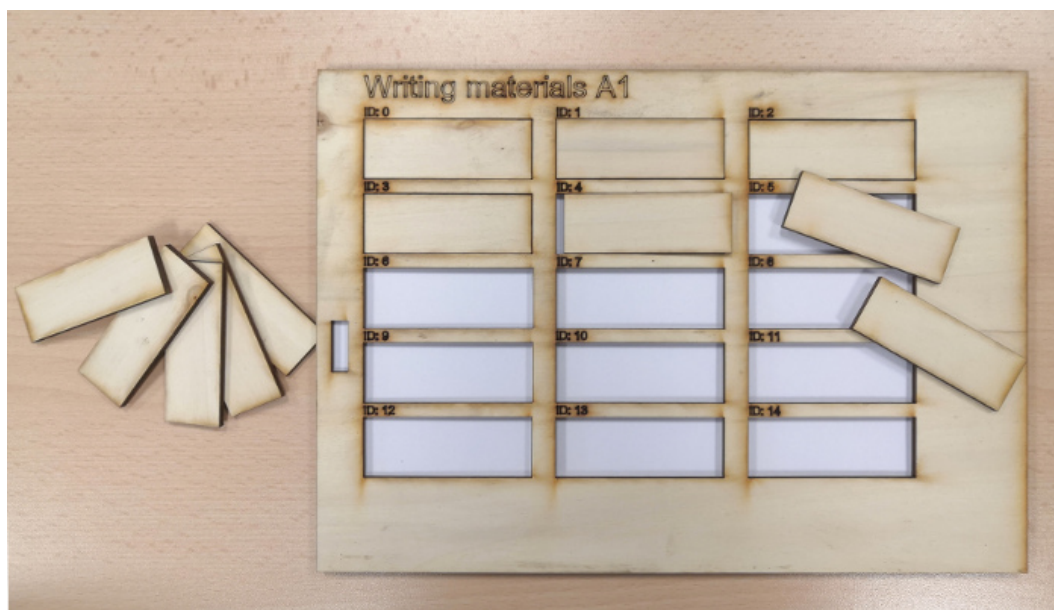


Figure 2.4: The creation of a samples collection with samples cut from a poplar panel.

thickness; a more precise control can be achieved using micrometer film applicators. The actual thickness of the layer might vary after the filmation process requiring a direct measuring of the film thickness using an appropriate measuring device.

For allowing wider compatibility with different laser cutters the .svg file of the sample holders and the masks can be converted into a .dxf file using a routine provided inside the module. Using masks for the creation of the layers does not always guarantee the best results for the creation of the layers, but are often very effective when the construction step involves the irradiation of a specific part of the samples. For instance, if we want to artificially age using UV light only a part of the samples.

Once, the sample collection has been completed it can be placed in a positioning system and the coordinates of the samples retrieved as explained before can be used for automating the analysis.

In figure 2.3 the samples are unmovable, however, in case the sample must be analyzed using instruments with a sample stage with limited space the sample area can be cut to produce a housing for movable samples as shown in figure 2.4. In figure 2.4 the samples are made of the same material of the samples holder (a poplar panel) but they can be cut using a separated file from any other material.

2.7 Summary

Reference samples collection are widely used in the current Cultural Heritage research practices and in other fields. The way to describe and create flat samples collections can be improved.

In this chapter I have proposed a methodology for increasing the efficiency

of the creation, description and analysis of reference flat sample collection. The methodology take advantage of a particular implementation of a well established and accessible format such SVG for describing and visualizing the collection and the sample holder that can be used as reference system.

Using an open-source tool that I called pySVGsamplescollection it is possible to facilitate the encoding of the information and the querying of the SVG file for retrieving the position of the samples and areas with different combinations of layers and treatments.

The information contained in the file can be used for automating the creation of the samples collection as well as the masks for easing the application of the treatments by means of laser cutter or cutting plotter.

The creation of the reference sample collection is the first step of many research projects, the analysis of the samples is the next step. In the next chapter, we will discuss the strategies for scanning the object of the analysis that might be the reference sample collection or an artwork.

3

Scanning strategies and their application to areal surface metrology with conoscopic holography probes.

This chapter analyzes the possible scanning strategies and their implication on the scanning system. It defines formally the scanning patterns and modalities and their influences on the acquisition that can be used for implementing most of the scanning systems. Finally the knowledge gained is used for implementing a scanning conoscopic holography system for acquiring the areal topography measurements.

3.1 Introduction

As shown in table 3.1 several scanning systems have been developed specifically for the diagnostic of Cultural Heritage. Some of these researches led to the development of commercial products[118, 139]. Their success in this field is mainly due to the fact that the heterogeneity of the materials may render ineffective single-spot sampling of the surface[60]. Hence, the ability to image or scan an area or the whole surface is becoming crucial in the application on Cultural Heritage objects. In this field some drawbacks of scanning techniques such as the time requirements that are limiting their adoption in industry and in medical application are less relevant, and long acquisition times are usually worth the benefit of the wide-field analysis. An understanding of the different scanning systems and of the basics concepts of mechatronics is needed to completely evaluate the influences of different scanning approaches on the analysis and the data that they produce.

In the first part of this chapter, I will discuss the general aspects and the definition of the terms of scanning instruments. The concepts explained can be applied

	Publication	Commercial products
VIS-NIR spectrometry/multi-spectral	[101, 49, 40]	
XRF-EDXRF	[147, 126, 6, 70]	[149, 118]
Raman	[20]	
Conoscopic holography	[52]	
Acoustic microscopy	[102]	
FT-IR	[9, 114]	
PIXE,PIGE	[60]	
XRD	[178]	

Table 3.1: References to some scanning systems developed for the diagnostic of Cultural Heritage

to most of the scanning instruments and used to accurately describe the system developed.

The last two sections apply the concepts to the development of a scanning conoscopic holography systems studied in this dissertation.

3.1.1 Choosing the right positioning system

One of the first problems when designing a scanning system is to choose and design the correct positioning system. In this project, I focused on the creation of systems based on motorized linear translation stages. Although, 6-axis articulated robots seems an appealing solution, in practice the cost, the portability and the safety are probably limiting their adoption in this field, to the best of my knowledge only some applications for easing the stereo-photometric reconstruction of the object are reported in literature [155, 58]. Most of the scanning systems developed for metrology application (viz. [168, Chapter 5]) and for Cultural Heritage applications (cf. table 3.1) feature linear translation stage.

The main components of a linear stage are the motor, an optional encoder, an actuator, a carriage, and a controller. The **encoder** is used for retrieving the position of the carriage. For this purpose, it usually records the rotations of the motors (**rotatory encoder**) or less frequently some spatial signal parallel to the actuator (**linear encoder**). The **controller** drives the motor and can receive feedback from the encoder when operating in closed-loop mode and drive the motor accordingly. The motor is connected to the carriage by means of an **actuator**, which is generally a component that transforms the rotatory motion of the motor into the desired motion, in this case, a translation. There are mainly two types of actuators used for this task: screw actuators and belt actuators. **Screw actuators** are usually more accurate in the positioning but are more sensitive to dust and dirt from the environment. When developing set-ups for in-situ measurements in restoration or archaeological sites special care must be taken for avoiding dirt entering inside the screw mechanism that is usually not sealed. Small quantities of dirt may irreversibly damage the thread and require expensive maintenance.

On the other hand, **belt drive actuators** are less accurate but, at the same time,

less sensitive to dirt infiltration. Furthermore, positioning systems based on belt drive actuators usually travel larger distances compared to lead screws actuators (that are usually limited to two meters). This aspect might be crucial for designing systems able to acquire larger works of art. Hybrid designs that feature belt actuators for coarse positioning and lead screw actuators for fine positioning are an option to overcome the limits of both technologies. As a matter of fact, Scan4Reco consortium choosed this solution for developing the multi-modal system.

The panorama of positioning systems is very vast is worth mentioning air bearings and linear motors. In particular linear motors could have better performance compared to ball-screw systems however, these are usually confined to laboratory operation and hence less adaptable to in-situ operation. While piezoelectric positioning systems have a limited travel range and hence their application is limited to the analysis of very small areas.

Two or more linear stages can be assembled together to perform the scanning. The **XY configuration** is mostly used for moving the object rather than the probes while **XZ configuration** is the most common configuration for in-situ analyses. A third axis can be mounted for allowing a further degree of freedom, often used for building systems with sensors that require to be at a precise distance from the surface. There are mainly two variants to the **XYZ configuration**, depending on the position of the Z axis.

3.2 Scanning analysis

Two main scanning modalities are defined in [168]: static acquisition and dynamic acquisition. In **static acquisition** the probe or the sample is moved step-by-step along the desired trajectory and the acquisition is performed with both in a still position¹. The movement can be followed by an **idle time**, that is a waiting time to dampen the vibrations induced by the motion before starting the acquisition of the measurement. In **dynamic acquisition**² the acquisition is carried out while the probe or the sample are moved. The disadvantage of the static mode acquisition is mainly the required time to perform the scan, because of the continuous moving, stopping and waiting the acquisition can become extremely long. Dynamic acquisitions offer a drastic increase in the speed of the acquisition, because the acquisition is performed in motion and the idle time is limited to the scanning offset. A **scanning offset** is a portion of the motion trajectory where the probe does not acquire any measurement. The offset can be added at the beginning and at the end of the single profile to dampen the vibrations due to the acceleration. The first scanning offset is called **run-up** while the offset at the end of the acquisition is called **over travel**.

Moving the probe can be beneficial when the probe irradiates the artwork with a laser, in this case, the thermal stress is reduced. Moreover, if the sensor is sensitive to speckle noise, acquiring the data while the probe is moving can reduce considerably the speckle noise produced by the surface[191]. In the case of techniques

¹ [191] defines this as discrete digitizing.

² [191] defines this as continuous digitizing.

such as conoscopic holography — that we will encounter later — it can be an important factor for increasing the repeatability and the quality of the measurement. For this reason, to the best of my knowledge dynamic acquisition mode is often the best modality to implement for scanning systems and the only option for acquiring millions of data points in an acceptable amount of time with a scanning system. The main drawback is that the spatial resolution in dynamic acquisition mode is usually worse. This is due to the fact that the sampled area increases due to the motion of the probe while acquiring the sample as we will see in the following section.

3.2.1 Factors influencing the sampled area in dynamic acquisitions

The fact that the measurement is performed during a movement has important implications on the spatial resolution of the measurement and the area exposed to the probe interaction. A sensor that is acquiring a signal with an integration time t_{int} during a stationary motion —with constant acceleration— will keep collecting data while moved for a length equal to:

$$\vec{l}_e = t_{int} \cdot \vec{v}_s \quad (3.1)$$

Where \vec{v}_s is the velocity of the linear stage. Zapico et al.[191] call l_e **exposure length**. That can be interpreted as the length during which the sensor is exposed, or better collects the signal. If we know the area that we are sampling with the specific probe during the static acquisition it is easy to calculate an approximated sampled area during the dynamic acquisition. For instance, the equation 3.2 can describe the contours of the sampled area.

$$\left| \frac{x}{w/2} \right|^{w/r} + \left| \frac{y}{h/2} \right|^{h/r} = 1 \quad (3.2)$$

This equation defines a superellipse, with width w and height h and rounded corner of radius r . It can be noticed that when w, h and r are equal to one, the equation describes a circle with radius one. When $r \ll w$ the shape approximates to a rectangle. In this example, I assume that the probe in a static acquisition mode is sampling an area that can be delimited by the contours of the equation 3.2 with width w of 3 microns, height h of 7 microns and r of 2 microns. With these parameters equation 3.2 defines an ellipsoidal shape center at the origin of the axis as shown in figure 3.1. Similar shapes are often encountered when working with probes based on non-circularized edge-emitting laser diodes that usually have different divergence angles³.

If the probe moves along the x direction, with a velocity of 3.5 mm s^{-1} and integration time of 1 ms, the exposure length l_e will be from equation 3.1 of $3.5 \text{ }\mu\text{m}$. We split l_e in its two components along the two directions of motion x, y . In this

³beam profiling the emission of the probe can be useful for determining the shape of the spot.

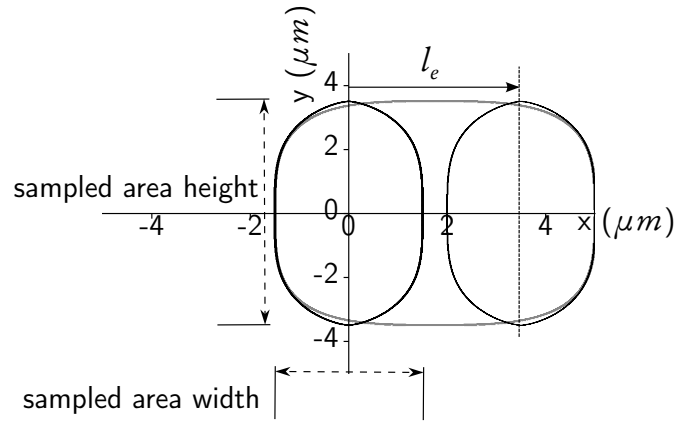


Figure 3.1: The sampled area represented by a super ellipse at the initial position and after the movement along the x direction of the exposure length l_e . The gray line shows a superellipse with width equal to the width of the original sampling area plus the exposure length.

case, because the scanning motion is parallel to the x axis, l_{ey} is zero and l_{ex} is $3.5 \mu\text{m}$. The final contours of the sampled area can be hence calculated with the following equation:

$$\left| \frac{(x - l_{ex})}{w/2} \right|^{w/r} + \left| \frac{(y - l_{ey})}{h/2} \right|^{h/r} = 1 \quad (3.3)$$

The second superelipsed centered at $(3.5, 0)$ in figure 3.1, illustrates the results of 3.3 with the aforementioned parameters. It can be noticed that the overall area sampled during this travel is equal to the sum of the sampled area during the static acquisition plus the area of the rectangle obtained multiplying the height of the spot size and the exposure length l_e . For measures along one of the two axes this can be generalized in the following equation:

$$A_{tot} = A_s + l_{ex} \cdot h + l_{ey} \cdot w \quad (3.4)$$

Where A_s is the area sampled during a static acquisition and the other parameters are the same as in the previous equations. When analyzing the optical transfer function we have to take into account that the area between the vertical axes of the two superelipses is sampled twice compared to the remaining area.

As an addendum, for transitions along one of the two axes, an approximate area can be drawn using equation 3.3. For instance, for the case where the translation is along the x axis the superellipse defining the overall total sampled area will have a width equal to $w + l_{ex}$ and centroid at $(l_{ex}, 0)$. The result is plotted with a grey line in figure 3.1. It can be noticed, that it only approximates the real area, and the error can vary depending on the parameter used for defining the initial super ellipses.

3.2.2 Triggering synchronization and data transfer from the sensor

The acquisition of the data from the sensor may be triggered by different external events. Triggering the acquisition using a fixed interval of time (**time domain pulsing**) causes unevenly-spaced sampling due to the slight variation of speed during the motion. A better approach for scanning techniques is to trigger the acquisition of the sensor with the absolute position recorded by the axis (**spatial domain pulsing**)⁴. For instance, in the system in figure 3.8 *a* page 50 we trigger the acquisition using the encoder of the horizontal axis so that after the carriage travelled a specific distance from the starting point (that I call **scan step**) the controller sends a signal to the probe. The probe once received the signal, acquires the single measurement. Spatial domain pulsing ensures that the measurements are equally spaced. However, regardless of the modality chosen, the reasoning explained in section 3.2.1 still applies. Accelerations cause changes in the sampled area and hence in the spatial resolution. Another important aspect is that the trigger pulse and the probe integration time must be synchronized, thus the probe often can be used with a frequency equal to the trigger pulse frequency or their multiples.

The data transfer is the next step in the acquisition pipeline. The probe can send the data collected directly to the main control unit i.e. computer. This mode is usually called **stream mode** because it allows streaming virtually infinite data to the main control unit. The main problem using this mode is that the data transfer rate between the probe and the computer depends on the communication between the two systems and usually can not be triggered. The other option is to store the data values in a **memory buffer** inside the probe and then transfer the data contained into the buffer at regular periods. I refer to this mode as **buffer mode** but it is also called **block mode** or **scope mode**[169]. When high sampling rates are used, storing the measurement into memory buffers internal to the probe is usually preferred because it allows triggering, faster data logging and prevents communication error. The main limitation of the buffer mode is that the memory buffer has usually a small memory capacity, hence the data must be transferred to the main memory at regular intervals (for instance after the collection of a single profile). In fact, is not advisable to perform long runs in a single profile during spatial domain pulsing in buffer mode, because although we are triggering the acquisition of the data, the frequency of the clock of the probe must stay synchronized with the frequency of the trigger which is usually from the axis encoder. During long runs because of jitters and variations from the nominal clock frequency some missing values might occur.

The last passage is storing the data in non-volatile memory. After the data is transferred from the buffer to the computer, all the single lines can be stored in the RAM and pre-processed otherwise each line can be written on the hard-disk. This last approach frees the memory each time the data is transferred from the buffer to the RAM thus allowing to perform scans that can potentially take advantage of the whole computer storage.

⁴different vendors may call it Position Synchronized Output (PSO) or Position Synchronized Triggering (PST).

3.3. Scanning patterns for single-spot acquisition

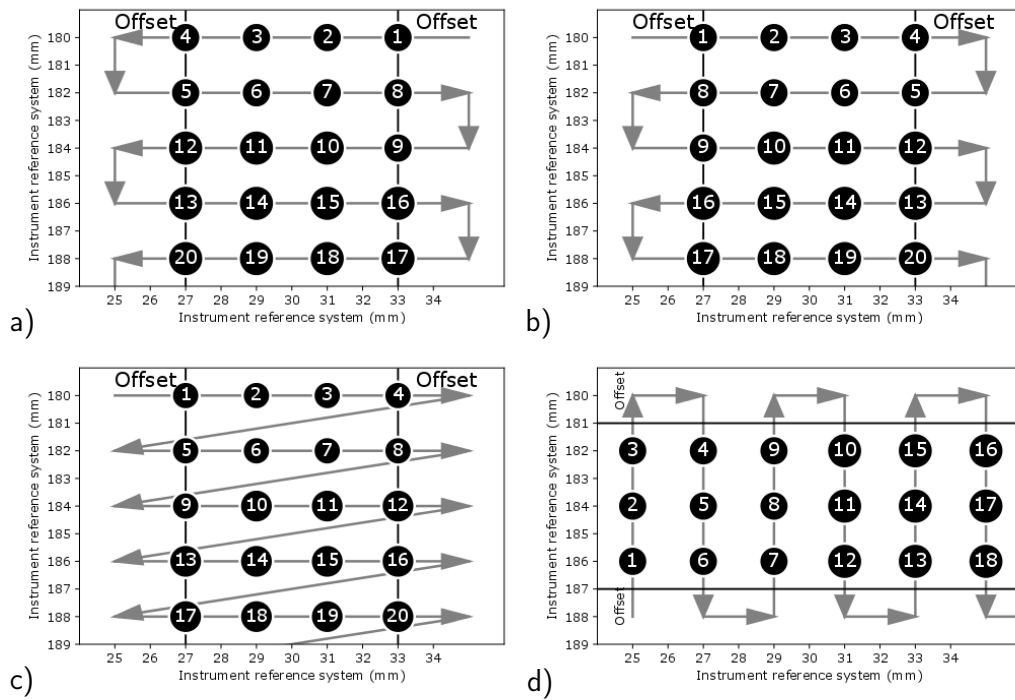


Figure 3.2: Some of the different scanning patterns that can be used for scanning an area with indexes indicating the sequential number of measurement. Notice that only the pattern c (which is usually called raster scan) follows *row-major order*.

Performing a dynamic acquisition triggered by a spatial pulsing in buffer mode is in most cases the best choice for implementing the scanning system. It allows an evenly spaced sampling and a reliable data transfer. Transferring the data to the hard-drive at the end of each scanned line allows exploiting the whole memory of the computer. In the next section, I will explore different scanning patterns that can be used for maximising the performance of the system and how the concepts explained in these sections can be applied for the correct implementation of the scan.

3.3 Scanning patterns for single-spot acquisition

There are different scanning patterns that can be performed using XY configuration of linear stages. The simplest scanning patterns are based on sampling along linear trajectories with only one axis moving while acquiring the data. More complex scanning patterns may implement spiral, zig-zag and Lissajous trajectories[172].

These latter trajectories although would allow acquiring data continuously without idle times, are usually not practical for two main reasons:

- difficulties in reconstructing a 2D-array of distances or height variations once acquired the data.

- when working in buffer mode must be solved the problem of emptying the buffer without creating artifacts.

the first reason is linked to the fact the resulting measurements are not evenly spaced and hence it is required to interpolate the value for retrieving an array of distances of height variations (that I adopted for the processing).

The second reason is due to the fact that usually buffer's capacity is limited. If the measurements required for the acquisition are greater compared to the measurements that can be stored in the buffer size, the system at a certain point must stop for emptying the buffer. Otherwise, if the data transfer from the buffer is performed while moving along the trajectory, the data will have gaps during the buffer emptying process. In both cases, this event could be a source of artifacts hence seems more advisable to adopt simpler patterns.

The patterns that I am studying in this section can be described by repeating combinations of simple rectilinear trajectories. The acquisition will be performed only during the motion along one axis (we call this axis the **fast axis**), while the motion on the other axis is used for re-positioning the probe in the next column or row. As described previously, at the beginning and the end of the motion of the fast axis there is normally a **scanning offset**, (see figure 3.2). This part of the trajectory is used for damping the vibration produced by the acceleration and hence no data values are acquired in this part of the motion. If the stage is subject to a constant acceleration equation 3.1 will become:

$$\vec{l}_e = \frac{1}{2} \vec{a}_s \cdot t_{int}^2 + \vec{v}_{si} \cdot t_{int} \quad (3.5)$$

Where \vec{a}_s is the acceleration of the stage and \vec{v}_{si} is the initial velocity. Higher acceleration will normally produce stronger vibrations so it is important to accelerate the probe slowly. However we must be sure that when the scanning offset is finished we are at the target stationary velocity, otherwise, l_e will vary with time and we will have different sampled areas and hence different spatial resolution along the scan. In general, the minimum acceleration a_m that we have to apply for reaching the target velocity v_f after a scanning offset l_{so} can be calculated using the following motion equation:

$$\vec{a}_m = \frac{\vec{v}_f^2}{2 \cdot \vec{l}_{so}} \quad (3.6)$$

The same value can be used for decelerating the probe during the scanning offset at the end of the trajectory.

It is important to notice, for the following reconstruction of the matrix, that the profile contains also the scanning offsets. Hence, if we start a scan with a scanning step s_x from x_i to x_f with an offset l_{so} the number of points n we will record in a single profile is equal to:

$$n = \frac{|(x_f - x_i)| - 2 \cdot l_{so}}{s_x} + 1 \quad (3.7)$$

The same, of course, applies to the other directions.

3.3.1 The definition of the scanning patterns

It is very important to agree a common definition of the patterns, this is essential to properly reconstruct the data matrix from its binary representation once the data has been collected but might be also useful for asses artifacts due linked to the time variation of the sample. The classical **raster scanning** (figure 3.2.c) is usually not convenient when the time for acquiring a single line is long, because the axis has to move back to the beginning of the line every time. Figure 3.2 shows some possible scanning patterns: pattern *a,b,d* are usually called **snake scans**[105, 184]. They offer a considerable time saving, and are hence more efficient for performing the scan. If the data has been collected and stored in contiguous memory addresses, all the information about the scanning pattern must be provided as meta-data. Hence for reconstructing the data matrix besides the matrix dimensions an univocal definition of the scanning pattern must be provided, this information might be useful also for assessing other bias as we will discuss in the next chapter.

In this dissertation, I propose the following convention for indicating the scanning pattern in a meta-data field. I categorize the axis movement in: right, left, up and down in relation to the probe. I use the initials the direction of the movements (r,l,u,d) for indicating the scanning pattern that will be repeated during the whole acquisition. If during the movement the data is acquired the letter is capitalized, if the movement is only used for positioning the probe the letter is left in lower case. For instance, the scanning pattern *a* in figure 3.2 can be indicated as LdRd, the scan moves first to left, acquiring the data, then down, without acquiring data, right, while acquiring the data, and finally down to the next row. Scan patterns *b* and *d* can be indicated respectively as RdLd and UrDr. Any raster scan pattern can be still indicated using this convention, for instance the scan pattern *c* in figure 3.2 can be described as R(1d) where (1d) indicates that the two movements are performed together and hence is equal to the diagonal movement. We can see that there are in total eight possible raster scan patterns (R(1d), L(rd), R(1u), L(ru), U(dr), D(ur), U(d1), D(u1)) and eight possible snake patterns (RdLd, LdRd, RuLu, LuRu, UrDr, U1D1, DrUr, D1U1). Each pattern acquires the data values in a different order and hence must be considered different. For the user familiar with computer science R(1d) produces a C-contiguous array hence with a row-major order of the elements while D(ur) produces F(ortran)-contiguous array hence with a column-major order of the elements.

3.3.2 Misalignments due to dynamic scans.

When we are performing scans in dynamic acquisition mode we have to consider the factors highlighted in section 3.2.1. In the case of scans using snake scan patterns if the starting points of the acquisition are aligned we will have a misalignment of the fast axis depending on the direction of motion. As an example we will examine the RdLd scan in figure 3.3 *a*. The scan uses x as fast axis starting at the coordinate 0 and ending at coordinate 0.4 with a scan step of $100\ \mu\text{m}$. Assuming an ideal system, the probe will receive the pulse for acquiring the measurement always at the same x coordinates $C = (0.0, 0.1, 0.2, 0.3, 0.4)$ regarding the direction of motion. However, the direction of exposure length \vec{l}_e will vary depending on

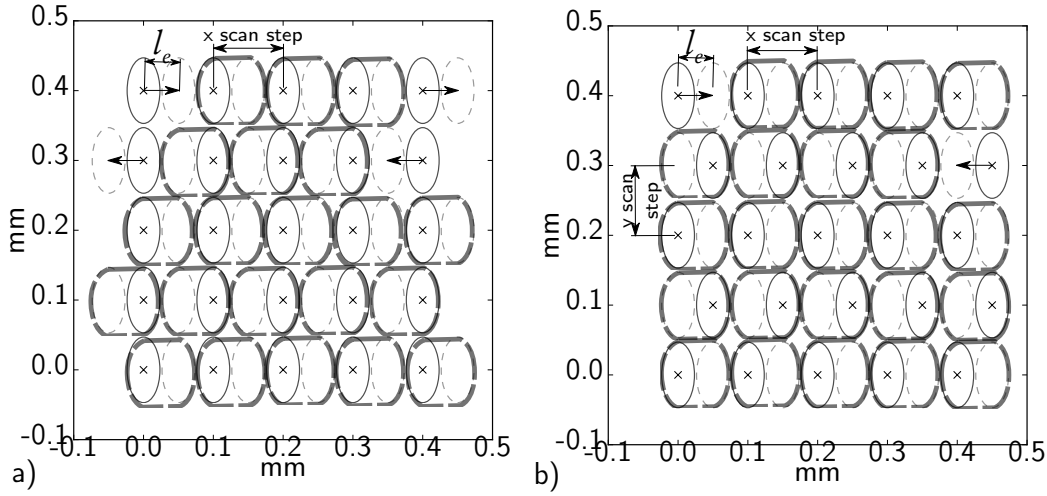


Figure 3.3: Snake pattern scans during dynamic acquisition scans. a) without sampled area centroid align b) after correcting the starting position for aligning the centroids of the sampled areas. The dashed thin line indicates the final position of the optical spot size. The thick gray dashed line indicates the overall sampled area. The x indicates the coordinates where the measurement start.

the direction of motion. For a scan from the initial x coordinate x_i to the final x coordinate x_f with the optical spot size of width w the even lines will acquire data from $x_i - w/2$ to $x_f + \vec{l}_e + w/2$ while the odd lines will acquire data from $x_i - \vec{l}_e - w/2$ to $x_f + w/2$.

This misalignment can be corrected before acquiring the matrix as in figure 3.3 *b* simply by shifting the acquisitions coordinates of the odds lines of \vec{l}_e in the direction opposite of motion.

In post-processing the error can be corrected by interpolating the points and recalculating the profiles using a new set of coordinates. We have to bear in mind that for instance the actual center of the sampled area is shifted of $\vec{l}_e/2$. In this example, if we want to correct the odds lines the x coordinates of the data points are equal to $[x_i, x_f] - l_e/2$ finally the coordinates at which to evaluate the interpolated values will be $[x_i, x_f] + l_e/2$. The same approach can be used for correcting the even lines instead of the odds one. An alternative approach is to recalculate the value at the original starting point. Thus, the coordinates at which to evaluate the interpolated values will be in the interval (x_i, x_f) . In this case, the first and the last element of the lines are excluded from the evaluation. We call this process **centroids alignment** because at the end of this process each final sampled area of the single spots will have the centroid aligned with the next row and column. Correcting the sampled area centroids in post-processing can have some benefits in avoiding aliasing while sampling the signals on the surface, however the computational requirements required for re-computing the corrected aligned scan are often too demanding. The correction of the scanning pattern before the acquisition might be the best solution in most cases.

Besides the approach chosen for correcting this misalignment, the strategy used must be reported when disseminating the data.

3.3.3 Point, profile and areal measurement

The user must be aware of the differences in the various acquisition types. To summarize, we have seen that we can perform the analysis in a single spot in a stationary position, we can repeat this procedure along a linear path and have a static acquisition of a profile. Eventually, we can acquire the data while moving the probe performing a dynamic acquisition. We have seen that the results of these acquisitions are different. The result of these types of scan is eventually a collection of aligned profiles. In metrology there is a strong separation between profile and areal measurement: different procedures and algorithms are used depending on whether the input data is a profile or an areal measurement. Some questions arise: can the output of the scans shown in the previous sections be considered as an areal measurement or shall we consider this data as a stack of multiple profiles? Are these scans comparable with areal measurements performed with instruments able to acquire simultaneously the distances over an area (e.g. white light interferometry)? This question cannot be answered if we do not have a complete characterization of the system. If the scan is performed accurately: the sampled area is symmetrical and the centroids of each sampled area are evenly spaced. The scan measurement may not only be considered an areal measurement but also be free from optical distortions that affect the range imaging techniques. Unfortunately, it is not only difficult to obtain the aforementioned conditions but often these conditions are also difficult to assess. An easy test for getting an insight on these aspects can be performed by acquiring the same sample rotated by 90 degrees and subtracting the two scans, once they have been properly aligned. A well designed scan should show no differences between the two scans.

Using reference standards as we will see in the next chapter is another option but it requires a careful selection of the standard. Indeed, scans that do not produce a measurement with homogeneous sampling can still be used for extracting meaningful information but the approach for extracting this information is different, hence it is crucial that we have a complete description of the scans and scan pattern used.

3.4 Conoscopic holography principles and applications

The concepts explained in the previous sections can be applied to most of the scanning systems currently available and can be used for the implementation of multi-modal scanning systems based on linear stages. In this section, I will apply them to the design and description of different systems based on Conoscopic Holography sensors that we designed in our laboratory.

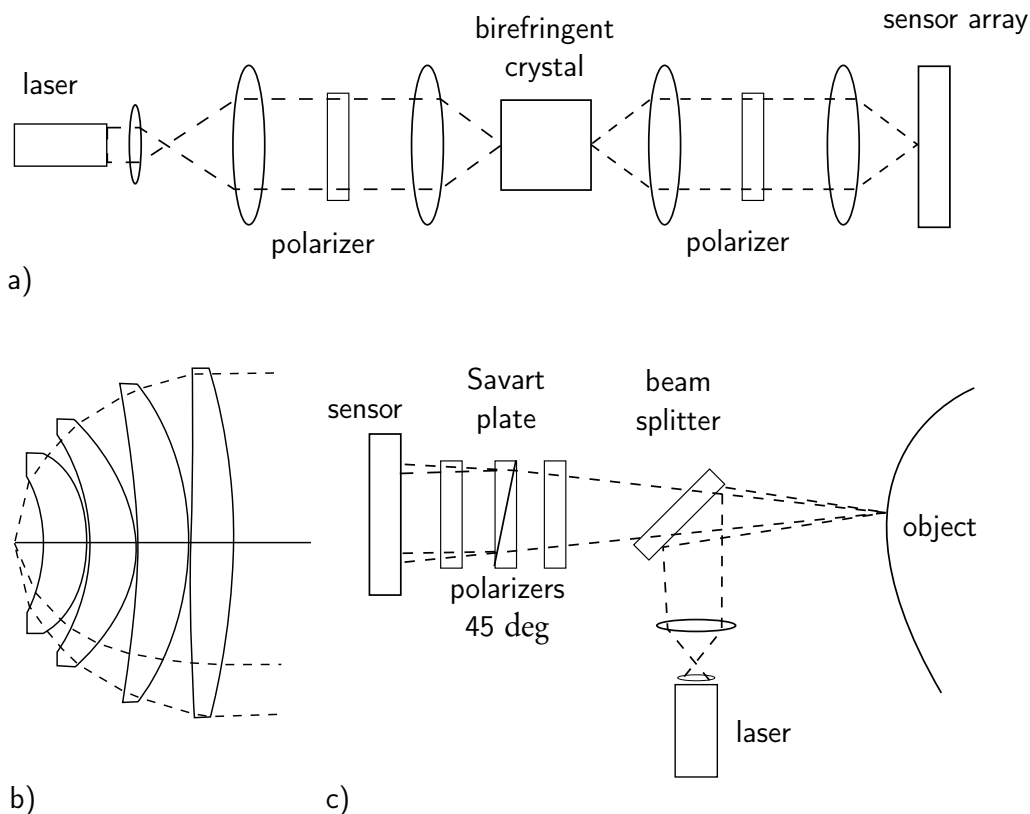


Figure 3.4: Different set-ups related to conoscopy. a) a conoscopic interferometer for studying the properties of a birefringent crystal [182] b) a portion of arrangement of lens for studying the angular distribution of rays (no interference involved) [36] c) shearing interferometer rangefinder as shown in Häussler et al. [66].

3.4.1 Conoscopic holography rangefinders

Conoscopic holography rangefinders are amongst the possible devices that can be used for micro-metric measurement of distances. These devices coupled with positioning stages, can acquire the topography and accurately position other probes in the proximity of the samples. The physical principles that cause the conoscopic interference pattern is well-known [12, 135], and it is used in different application for studying the properties of crystals[182, 133].

The conoscopic holography rangefinders have been developed since 1980 and they are basically a particular implementation of shearing interferometry based on birefringent crystals. This particular usage of conoscopic interference patterns for retrieving distance measurements has not been extensively investigated and has not yet been included in the classification surface texture measurement methods (ISO 25178-6 2010). For this reason, in this section we will cover in more detail the different set-ups available.

3.4.2 Disambiguation of the terms

As the name suggest conoscopy (from Ancient Greek κώνος cone σκοπέω examine) allows to analyze a cone of light. Hence, often with the term **conoscope** are catalogued instruments for measuring the angular distribution of light, based on special arrangements of lens called conoscopic lens as in figure 3.4 *b*. Conoscopic holography uses instead the interference pattern produced by a birefringent crystal to retrieve information about the cone of light. In this case the basic set-up is almost identical to a **polariscope** (also called conoscope) used in mineralogy, where the two polarizers are rotated for investigating the different crystals properties. For investigating the properties of crystals, a similar set-up is called **conoscopic interferometer**[182] (see 3.4 *a*). In general, because the birefringent crystal produces a copy of the wavefront with a small displacement that causes the interference, the conoscopic holography can be categorized as **shearing interferometry**. Hence, many set-ups similar to the conoscopic holography are grouped under the class of shearing interferometer rangefinders.

3.4.3 The physical principle of conoscopic interference pattern

Figure 3.5, shows a typical set-up for generating conoscopic interference patterns. The rays coming from a point P pass through a first polarizer and then impinge with uniaxial birefringent crystal. At this point due to the birefringent crystal, two rays are formed. The ordinary ray (r_o) travels with a constant index of refraction while the extraordinary ray (r_e) propagates with an index of refraction depending on the direction of propagation, which is determined by the angle the incident ray interacts with the crystal. When these two rays interact on the sensor plane they form an interference pattern. The interference pattern depends on several parameters: indexes of refraction, axis and length of the crystal, filtering and eventually the position of the light source that determine the angle of incidence of the rays.

3.4.4 Rangefinders based on shearing interferometry with Savart plates and Wollaston prisms

The idea behind shearing interferometry (conoscopic holography) range finders is to keep all the parameters listed in the previous section fixed and irradiate the point P using a monochromatic source. Analyzing the interferogram produced, it is hence possible to associate a frequency/phase to a range of positions of the point P. After calibration, it will be possible to retrieve the distance from the point P and a reference point (e.g. the lens of the acquiring system). The set-up shown in figure 3.5 is however unpractical for such purpose due to some biases. The first rangefinder based on shearing interferometry was built by Häussler et al. [66] (figure 3.4.c). This set-up uses a Savart-plate for creating the two wavefronts. Wollaston prisms have been used in different set-ups for measuring displacement[69] or for range imaging[115], some of them are patented [57].

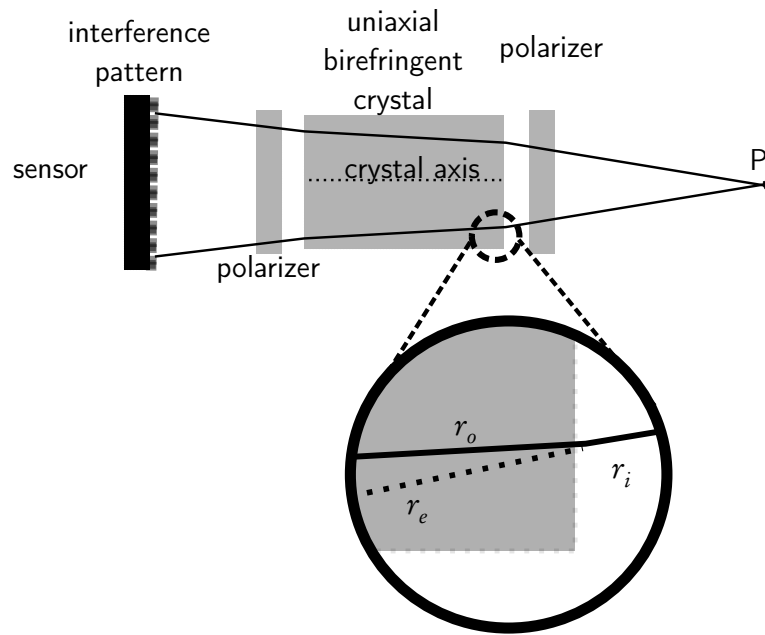


Figure 3.5: A schematic of a simple conoscopic holography set-up. The light back-scattered at the point P pass through a series of polarizers and a birefringent crystal. When a ray r_i hits the crystal it is splitted in a ordinary ray r_o and an extraordinary ray r_e .

3.4.5 Conoscopic holography rangefinder with quarter-wave plate

One of the first conoscopic holography set-up[30] used a quarter-wave plate switched by a light-valve, that produced two interference patterns on a CCD camera. The two-dimensional array was later reduced to a one dimensional signal, analyzed for extracting the phase. A similar set-up has been used for studying the possibility to create a conoscopic range-imaging device[127]. Both these set-ups have not been commercially available and they remained mainly proof of concepts.

3.4.6 Linear conoscopic rangefinders: ConoProbes

The conoscopic holography sensors commercially available today (viz. 3.6) feature different patent technologies. They are commercially called Cono-probes[165] and are produced by an Israeli company called Optimet. The main improvement of the ConoProbes regarding the aforementioned systems is due to the arrangement of two birefringent crystals with their axis shifted by 45 degrees[164], re-assembling the set-up proposed by Häussler et al. [66]. Speckles are one of the main problems in this kind of range finders[65]. Conoprobes use light modulators and wedges to mitigate their negative effects on the interferogram[162]. In figure 3.6 we can see a typical arrangement. A laser diode emits a beam (wavelength 655 nm) that passes through a staircase illuminator[162]. The light is directed through the lens using a lateral displacement beam splitter. The lens focalizes the beam onto the object. The backscattered radiation is collected by the same lens and directed through the two birefringent crystals and a polarizer beam splitter that is used to irradiate two linear CCD sensors. On each CCD sensor is

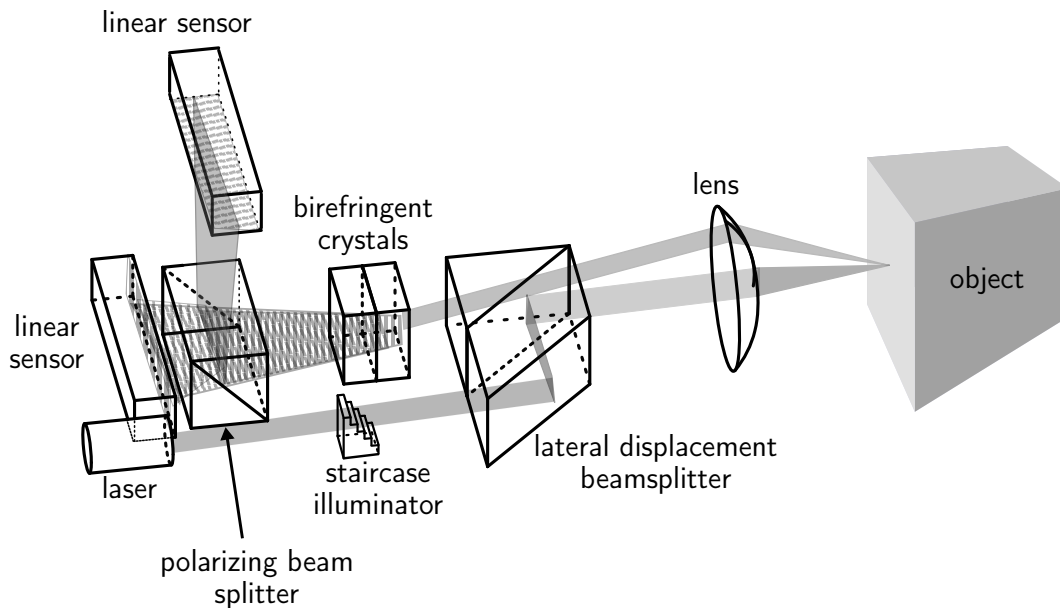


Figure 3.6: A reconstruction of a possible schematic of a linear conoscopic holography range finder (ConoProbe).

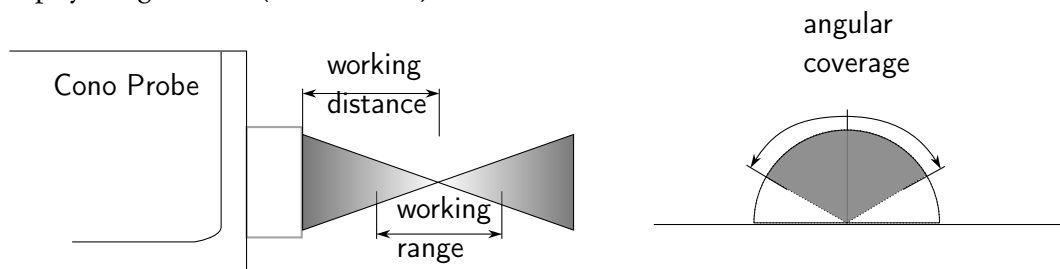


Figure 3.7: Drawing of a side view of a ConoProbe. The laser is focused to a point that corresponds to the working distance or standoff. The measurement range defines the maximum extent of the measurement. While the angular coverage is linked to the steep of the surface.

collected an interferogram, these two interferograms are combined and used for calculating the distance. In the Cono-Probes all the analysis of the interferograms is carried out inside the probe by a field programmable gate-array (FPGA) and the output of the computation is stored in the buffer or streamed to the communication box.

The ConoProbes are denoted by a number indicating the kHz and a suffix. Besides the standard conoprobe are available other two Conoprobes the ConoProbe-10HD and the ConoProbe-3R. ConoProbe-10HD provides higher accuracy while ConoProbe-3R is optimized for measurements on specular and transparent materials. Each probe can be coupled with a set of interchangeable lenses. In table 3.2 are reported the nominal specification for each configuration as provided by the manufacturer.

Depending on the lens the measurand must be positioned at a different **working distance** (or standoff). At this distance, the laser is focused on the surface and the spatial resolution is highest as shown in figure 3.7. During the analysis the ob-

Lens type	Probe	Accuracy (micron)	Working Range (mm)	Laser spot size (micron)	Angular Coverage
16	ConoPoint-3	2	0.6	20	150
50	ConoPoint-3	6	8	37	170
75	ConoPoint-3	10	18	47	170
100	ConoPoint-3	15	35	63	170
200	ConoPoint-3	70	125	105	170
25GH	ConoPoint-3HD	1	0.6	12	150
50H	ConoPoint-3HD	2.5	2	19	150
25N	ConoPoint-3R	1	1	5	5
50N	ConoPoint-3R	2.5	5	16	3
75N	ConoPoint-3R	4.5	9	25	1.5

Table 3.2: Specification of the ConoProbe systems (lens and probe) used during the project.

ject should stay at the working distance and must be acquired within the **working range**: a range of distances where the quality of the measurement is optimal. Outside the working range the measurements suffer a strong decreasing of the SNR that may cause invalid measurements and in some cases inverted measurements. Lenses with high performance have usually a shorter focal length that allows focusing the laser beam in some tenth or microns or less but obliges to operate at short working distances with a restricted working range. The user must find a trade-off between the high-resolution and the maximum height step that can be acquired with a single scan. Furthermore, we have to consider that working very close might pose some risk for the safety of the artwork.

Another important figure of merit is the **angular coverage**: given a hypothetical hemisphere with the base perpendicular to the optical axis of the system, the angular coverage represents the portion of the hemisphere that can be acquired. The angular coverage is expressed using an angle with the vertex coinciding to with the hemisphere centre. As shown in figure 3.7. An angular coverage of 180 degrees means, that the probe is able to acquire measurements at each point of the hemisphere. While for instance, an angular coverage of 60 degrees means that the probe can acquire measurement only on the points of the sphere that are between $\pm 30^\circ$ from the axis passing from the pole of the hemisphere as shown in figure 3.7.

3.5 Design and implementation of scanning conoscopic holography systems

During the project, we implemented different modular systems based on Conoscopic Holography sensors and micrometric linear stages. In this section, I describe the initial requirements for implementing the scanning and the implemented solutions.

3.5. Design and implementation of scanning conoscopic holography systems

	Min. incremental motion (micron)	Backlash (micron)	Design resolution (micron)	Axis speed (mm/s)	Travel range (mm)
M-414.3DG	0.1	4	0.023	3	300
M-531.DDB (Active drive)	0.1	-	0.1	50	305
L-509.40AD10	0.8	0.3	0.06	50	100

Table 3.3: Specification of the linear stages by PhysikInstrumente selected for creating the system.

3.5.1 Requirements for implementing an optimal scanning conoscopic holography set-up

As shown in table 3.2 conoscopic holography systems focus the laser in an area with maximum width ranging from 5 to 105 μm we need a minimum incremental motion of the stage of at least less than a quarter of the laser spot width. For mitigating the problems caused by speckle noise [65] we must be able to perform dynamic acquisitions. In dynamic acquisition, the speckle noise is reduced by the fact that the signal is average during the exposure length [191]. Thus the linear stages should have an encoder and the possibility to use the encoder signal to trigger the acquisition of the ConoProbe range finder. For acquiring a considerable area of the sample we need stages with a travel range of at least ten centimeters. Working with large areas the stage must be able to reach a velocity of at least 10 mm s^{-1} , using such velocity it is possible to acquire approximately one squared centimeter in four minutes with a scanning step of $50 \mu\text{m}$. Higher velocities can be used only in particular cases, the probes have a maximum sampling frequency of the CCD of 3 kHz. This means that are able to acquire at best a measurement every 0.3 ms. Working in dynamic mode, from equation 3.1, it means that the exposure length at 10 mm s^{-1} will be $3 \mu\text{m}$. Follows that at 20 mm s^{-1} we will have exposure length greater of the laser spot size of the ConoPoint-3R with the 50N lens causing a sampling area with an aspect ratio different from one and hence a distorted acquisition. Taking into account that the sampling frequency of the ConoPoint that must be set for acquiring many materials is usually one or two times lower the possibility to increase the velocity over 50 mm s^{-1} maintaining a sampling area with an aspect ratio close to one is limited to few configurations (e.g. Cono-Point-3 with 75,100,200 mm lens).

The linear stages selected for the creation of the different systems are listed in table 3.3. All the stages use DC motors and ball bearings for minimizing friction, thus allowing very high accuracy in the positioning. The trigger is generated by a rotatory encoder and is transmitted by a controller.

For allowing the acquisition of triggered data at high velocity without jitter or general communication problems it is preferable to implement the acquisition in buffer mode implementing the scan using snake patterns. The easiest solution is

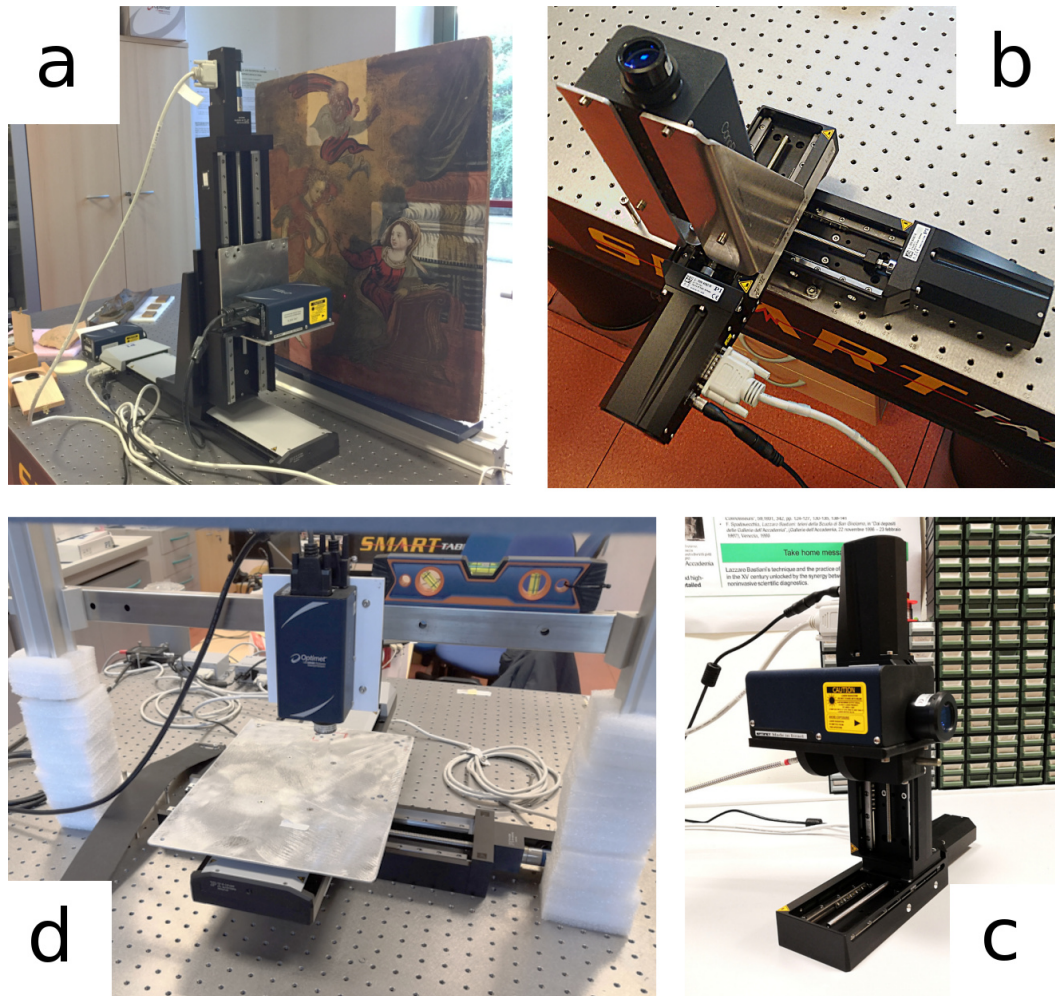


Figure 3.8: The scanning systems developed during the project. a) the vertical XY version for on site measurements of vertical surfaces b) XZ version developed to be attached to a robotic arm c) a portable vertical XY version d) the XZ version for laboratory measurements of small and medium-size samples.

to implement a RdLd with acceleration and deceleration during a scanning offset at the beginning and at the end of the line.

3.5.2 The solutions proposed.

The four systems developed during the project are shown in figure 3.8.

The first configuration (figure 3.8 a) is designed to be used on site. The scanning system is composed of two linear motorized stages, a M-531.DDB by Physik Instrumente with maximal speed of 50 mm s^{-1} for the horizontal axis and of 3 mm s^{-1} for the vertical axis (P.I. M-414.3DG). The horizontal axis is the fast axis that triggers the acquisition with a TTL pulse sent by the encoder. The maximum encoder resolution is $0.1 \mu\text{m}$ while the maximum error in the whole range is $1 \mu\text{m}$. All the motors and the positioning of the following systems are controlled by two C-863 Mercury Servo Controllers connected to a PC.

During the laboratory analyses, the system is placed on a SMART UT2 optical

table (by Newport) for damping the environmental vibrations.

The second configuration (figure 3.8 *b*) was the first prototype to be mounted at the end of the robotic arm build in Scan4Reco project. In this configuration, the scan is on the X and Z axis. To have a lighter configuration the linear stages (two L-509.40AD10 by Physik Instrumente) have a travel limited to ten centimetre. The support connecting the ConoPoint to the stage is custom and produced by BBZ S.r.l..

Anther configuration was built to be mounted as end-effector of the robotic arm (figure 3.8 *c*) was designed using the same axes. In this case the part connecting the probe to the axes can be 3D printed and contains a hole for connecting a bifurcated fiber optics such as QR400-7-UV-BX by Ocean Optics thus allowing the collection of spectroscopic data in the range from 350 nm to 1050 nm.



The design of the adapter for connecting the ConoPoint to the L-509.40AD10 linear stage is available online at the following link: <https://grabcad.com/library/conopoint-xx-1509-1> and can be 3D printed.

Finally, a horizontal version of the system can be built using two micrometric stages in a XZ configuration as shown in figure 3.8 *d*. This system is particularly suitable for measuring flat samples collection or small artworks that can be placed on the measuring plate. Also this configuration uses a M-531.DDB and M-414.3DG linear stages by Physik Instrumente using the faster M-531.DDB for performing the acquisition and the slower M-414.3DG for repositioning the probe to the next row. A custom adapter is needed for connecting the M-414.3DG to the M-531.DDB stage.



The designs of the adapter for connecting the M-414.3DG to the M-531.DDB linear stage, and the design of the plate for positioning the samples are available online at the following link: <https://grabcad.com/library/m4143dgm531ddbssystem-1>

3.6 Summary

Many scanning systems have been developed for Cultural Heritage diagnostics and probably more will be developed in the future. These systems are collecting important data that must be described and reusable. Unfortunately, often the technical knowledge of the manufacturers is not transferred to the researchers and hence the systems might be poorly described undermining the interpretation and the usability of the data collected.

I have presented an agile but rigorous introduction to the design and description of scanning system fusing a scattered literature and researching on the influences of the modalities on the acquisition.

Starting with the definition of the positioning systems used for performing the scanning I gave an overview of the main two scanning modalities (dynamic and static acquisition) highlighting how they affect the sampled area.

I used super-ellipses for describing the sample area and the influence of the scanning motion on it.

After introducing the triggering and the synchronization of the data and the most common ways in which the data is transferred, I proposed a convention for describing the most common scanning patterns.

In section 3.4 I wrote a literature review of the conoscopic holography and the evolution of the design of range-finders based on this principle that led to probes now commercially available as ConoProbe.

Based on the specification of the probes and the concepts explained in the previous sections I explained the choices made for developing the systems used in this dissertation.

Eventually, I reported the systems developed during the project using commercially available hardware and providing the design of the custom parts needed for completing the systems.

4

The data analysis and characterization of the surface

This chapter discusses the data analysis with a particular focus on the surface topography data. It describes the processing carried out using the software for processing the data developed during the project and includes the description of some new algorithms tested for the analysis of heterogeneous surfaces.

4.1 Storing the data

Every data analysis process starts from importing the data and understanding its structure. In this section, I describe the main possibilities and choices made for storing the data retrieved by the metrological system.

4.1.1 Level of processing

Different levels of processing might be applied to the data for making it more accessible. The processing can be carried out by the hardware during the acquisition or by the user when reorganizing the data set: the processing might include filtering, reconstruction of the matrix and detection of the outliers. It is difficult to obtain completely unprocessed data because often some processing is carried out in real-time by the hardware. In general, sharing less-processed data allow a more transparent workflow and a better chance to identify artifacts and apply corrections. On the other hand, unprocessed data require a number of steps to be finally analyzed that could lead to errors during the data analysis by users not familiar with the system. One common solution is to store an unprocessed version of the data and a processed user-friendly version. In this project, I decided to provide

both unprocessed¹ and processed data so that both user needs could be met.

4.1.2 Unprocessed data


The data at the lowest level of processing that we can get from the ConoPoint probes are the computed distances. All the processing done on the conoscopic patterns is not accessible by the end-user. The distances are saved as binary (float32) to a file with extension `.dist` for each distance we can save also the signal to noise ratio, an index of the total amount of signal collected by the detector, and an incremental measurement identifier which is used for determining missing values. All these data are saved in different files with the respective extensions: `.snr`, `.total`, `.tag`. Eventually, in an ASCII header file with extension `.hdr` are stored the scanning parameters such as the axis velocity the dimension of the scan and the starting and ending points.

4.1.3 Processed data

During the last decades, several formats have been developed to store information coming from surface topography techniques in a more standardized and accessible way. ISO commission attempted to standardize the structure the metadata of the file format for some of them (AFM and SPM with ISO 28600:2011) and give a general overview of the software measurement standards in ISO 5436-2:2012[89]. Nevertheless, there are still a lot of ambiguities regarding the usage the terms for describing the file. This is also partially due to the increased number of techniques used in the field of surface reconstruction that require particular data structures to store all the relevant information regarding the acquisition of the surface. Amongst the possibilities, I have selected three file formats that from my own experience can be used effectively for sharing processed data.

X3P

In 2008 OpenGPS[®] consortium tried to address the aforementioned issues, and overcome the current limitations of ISO 5436-2 with an open format called `.x3p`[37]. This format is now part 72 of the ISO 25178 but at the moment is unmaintained by the OpenGPS consortium and now is partially maintained by OpenFMC (Open Forensic Metrology Consortium). During the project, I developed the only Python parser available for reading and writing files using this format and I released the code open-source.

	<p>pyx3p is a module that allows to read and write <code>.x3p</code> files using Python. It can be freely installed from the following online repository: https://github.com/giacomomarchioro/pyx3p</p>
---	--

¹In this dissertation I call unprocessed data the data with the lowest level of processing that the data-provider can share.

gwy

Gwyddion[130] is a popular open-source program for analyzing data produced by AFM, MFM, STM, SNOM/NSOM and in general any data that can be described as a 2D data matrix. The .gwy format can be used for sharing the data allowing the user to access it and analyze it directly with an open-source software with a graphical user interface. I used this format for sharing data with restorers and conservation scientists.

HDF5

HDF® groups[174] implemented this scientific format for describing heterogeneous data set. The meta-data of .x3p files can be mapped to this format, while any array can be stored in a hierarchical manner. I have adopted this format for sharing most of the data collected during the projects amongst computer scientists.

4.2 The signal of the surface

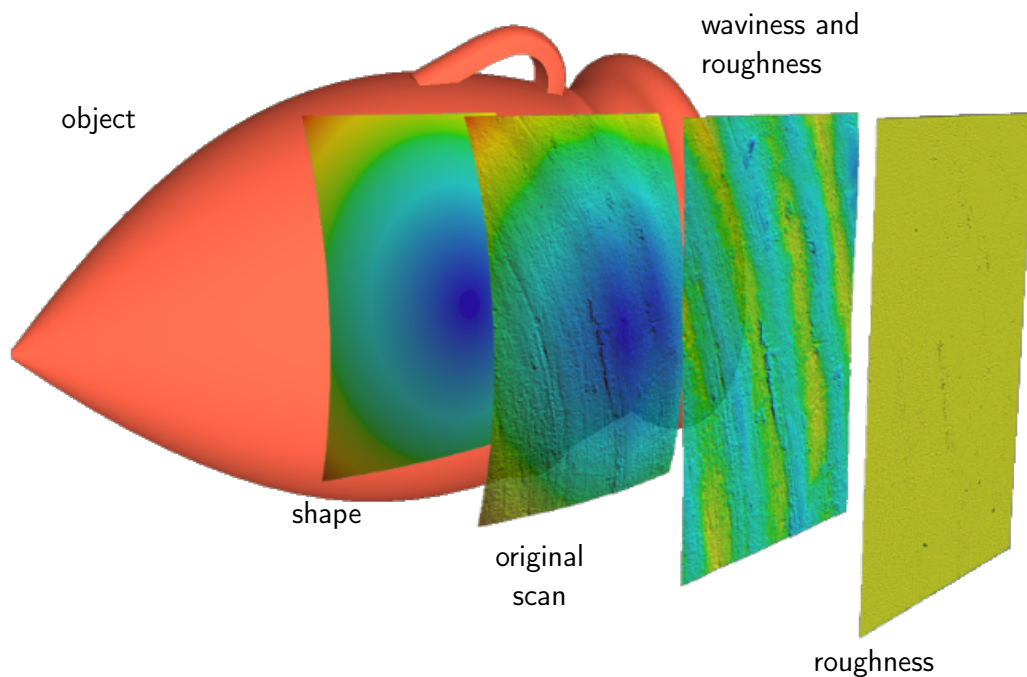


Figure 4.1: Scan of a fragment of archaeological amphora using ConoProbe-3 (lens 75 mm), superimposed on an exemplification of a 3D model of an amphora. The original scan has been decomposed in its components: shape, waviness (with roughness) and roughness.

Many concepts developed in industrial surface metrology apply on artworks. Cultural heritage objects are, in fact, examples of ancient manufacturing techniques. Conventionally[186, Chapter 2], metrologists separate the surface into three main components the form, the waviness and the roughness. The **form** refers to the

shape, or a portion of the shape, of the object, investigated. The **waviness** is instead a periodic signal, this signal is often associated with the traces left by the tool used for shaping the object. In the industry is often due to the machining of the pieces under construction. Eventually, the **roughness** is linked with the finishing of the object surface and material and, in general, is considered as a chaotic signal. The surface may not be isotropic, the predominant direction of the features of the surface is called **lay**. In figure 4.1 we can see a scan performed with the conoscopic holography profilometer on a fragment of an amphora. The original scan can be decomposed by fitting a second order polynomial to its shape and its waviness. In this case, the waviness is due to the shaping of the amphora on the pottery wheel that produced a clear lay on the surface. The roughness can be extracted using Gaussian filters, and showing scratches and high frequency signals produced during the manufacturing and its conservation history. The classification of the surface features in these three categories serves for a first understanding of the object 3D geometry. Many different signals, due to different processes applied on the surface, can be observed and studied (these may be due to the surface finishing, cleaning and restoration [183], natural curvature of the panels, the structure of the warp-yarn of the paintings[51], canvas imprint, engravings and inscriptions[52]). There are no precise boundaries between these components but they serve as a starting point for the understanding of the cultural heritage object. One of the aims of the data analysis in surface metrology is to separate and characterize these signals. However, the role of the historian, restorer and archaeologist is crucial on the following interpretation of the outcomes of the analysis. The potential benefits of analyzing this information are manifold. Firstly, we can have insight into the production process of the object, what tools and techniques have been used. Secondly, we can have insights on the conservation history of the object, assessing variation of roughness and or surface features linked with degradation processes or evaluating the invasiveness of cleaning methods and their impact on the visual appearance. Eventually, because most of the non-invasive techniques interact with the surface, we can potentially fuse the data for increasing the accuracy of the measurements and correcting the influences of the surface.

4.3 The processing workflow

For extracting meaningful information from the surface data, a considerable amount of processing must be carried out. The steps that I adopted for executing this process are summarized in figure 4.2. The data-matrix is reconstructed from the flattened binary file containing the distances and the dimension of the array stored as meta-data. An algorithm identifies the positions of the missing values and inserts NaN for realigning the matrix. At this point, the quality of each single distance measurement is assessed using specific indicators of the goodness of the interferogram such as the SNR and the total signal recorded for each distance provided by the probe. From the quality control, we can map bad values (i.e. measurements that did not meet our quality criteria) into masks. Masks are arrays of Booleans with the same size of the data matrix array and with values equal to True where we want to exclude the respective distance values from the following calculations.

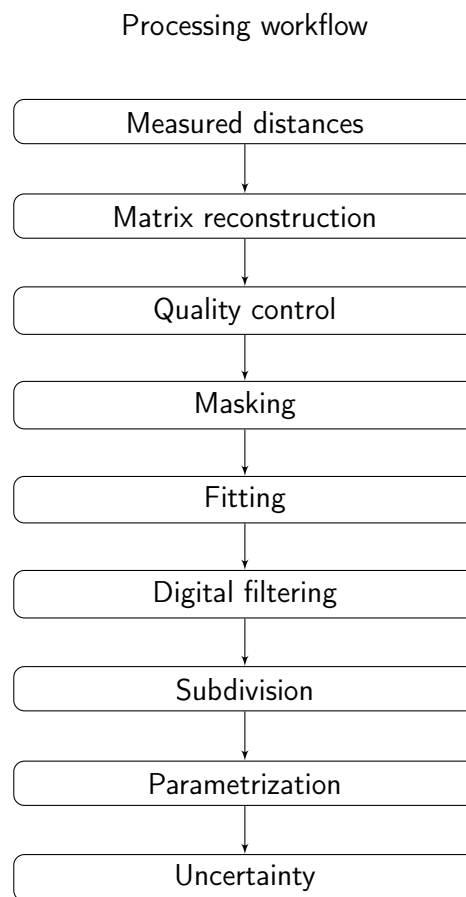


Figure 4.2: Metrology surface data-analysis workflow re-adapted from [129].

Depending on the shape of the object we can perform a fitting of the data for removing its shape using only the distances that met our quality control criteria (the unmasked values). We can then apply different filtering techniques for extracting the signals from the surface. The result of the filtering process is usually subdivided in sampling lengths (or more rarely in sampling areas). Finally, when we have our set of profiles, the parametrization consists of analyzing the distribution of the heights using different statistical parameters that describe particular aspects of the distribution. Of course, to each of these steps, is associated an uncertainty, the estimation of the overall uncertainty is hence an important step for the final results.

In the next technical sections, we will explore in more detail each step of the workflow and the software that I developed for analyzing the data.

I decided to structure the next sections following the workflow in figure 4.2 for giving a clear idea of the necessary steps and connections. The reader will encounter during some sections the metrological parameters (e.g. P_q , P_a , S_q , Sk_w etc. etc.) that will be defined in detail in section 4.10. The reader can read that section first for understanding what these parameters describe, even though for this introduction is sufficient to know that they are statistical descriptors of the distribution of heights.

4.4 The tool developed for analyzing the data: “micropro”

Currently, there is no dedicated software commercially available created for analyzing the data produced by the conoscopic holography scanning system. Although it is possible to map the distances recorded by the microprofilometer to other common metrology formats used by most of the metrology software, this software is not able to handle the auxiliary data regarding the acquisition collected by the probe that is helpful for assessing the quality of the measurement furthermore is harder to integrate custom processing in preexisting software. Hence I implemented a Python module that allows to perform different operations on a single surface or automatizing the computation on multiple surfaces, and design reproducible procedures for analyzing the data. The tool is build on the top of different existing libraries for array manipulation (Numpy[132]) scientific data analysis (Scipy[179]), image processing (OpenCV[19]) and scientific visualization (Matplotlib[71] and Mayavi[144]). It allows to analyze the data and perform different algorithms interactively using the console or writing Python scripts.



Micropro is a module that allows the analysis of the data produced during the project. It can be freely installed from the following online repository: <https://github.com/giacomomarchioro/micropro>

The module is integrated with the database containing further information regarding the sample, and is intended as a tool for manipulating directly the RAW

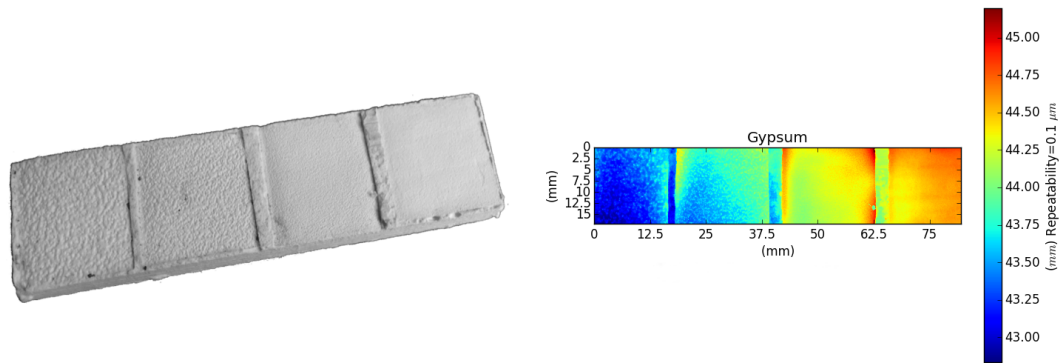


Figure 4.3: On the left, a gypsum sample with different surface textures, each of the four areas has decreasing roughness from left to right. On the right, the scan acquired with the microprofilometer. The distances matrix reconstructed shows the distances from the probe to the sample encoded using a colormap.

output of the systems and/or exporting it in more accessible formats. It can export annotated data sets in the major formats used for storing surfaces (.x3p,.sdf,.ply) and data set (.hdf5,.gyw,.mat). In the following sections, we will see more in detail the processing workflow associated with each step and we will explain how the methods have been implemented.

4.5 Matrix reconstruction, quality control, and masking

For reconstructing the data matrix the module reads the binary file into memory and reshape the matrix with the distances using the matrix dimension retrieved by the metadata. During the acquisition process, to each distance value is assigned a tag, a consecutive number from 0 to 255, if for some reason the probe could not read some value during the profile scan we will encounter an interruption of the series when reading consecutive tags. For identifying these interruptions we can insert NaN values in place of the missing values (in this way we ensure that the rows are aligned). We save the position of the missing values on a separate matrix. At this point, we have a 2D-array of distances from the probe to the object. We reconstruct in the same way two other arrays one containing the SNR for each distance measured, the other containing the total signal collected (abbr. Total). For an optimal measurement for each value of the distance array the software checks if the following conditions are met for each distance measurement:

- the distance recorded is within the working range of the lens.
- the SNR is greater than 512 (equal to 50%)[35].
- the total signal collected is between 1600 and 18000 counts[35].
- is not a NaN value.

	Acceptable	Optimal
Total	900-1200, 1600-1800	1200-16000
SNR	>30% (307 levels)	>50 % (512)
Working rage	Within	Within
Tilting	<2°	<1°
Laser power	> 10	> 10

Table 4.1: Quality parameters suggested by the manufacturer, for achieving acceptable and optimal measurement. The tilting refers to metrology measurement of flat surfaces.

If the measurement does not meet one or more of the previous conditions, the module excludes the value from the following computations. For doing so, I create a mask, that as mentioned early, is a Boolean data type array with the same dimensions of the data array that represents invalid values as True. The usage of masked arrays allows to maintain the original value of the data matrix and exclude it from the computation when needed. I used the implementation of a masked array provided by Numpy[175]. From the point of view of the performance, this implementation is less efficient but it allows better handling of operations on multiple surfaces. The uncertainty introduced by calculations over areas with NaN and masked values must be considered case by case.

For a first control of the quality of the data, I introduced a mandatory assessment of the quality parameters listed in table 4.1. When the file containing the scan is opened for the first time the user is asked to evaluate the reconstruction of the matrix based on plots showing: the distances of the object with respect to the optimal working distance, the SNR, the Total, the tilting and eventually a plot where all the values that did not meet the optimal quality parameters are masked. For the acquisition of whole squared sample (such as flat reference coupons as described in Chapter 2) I also provide a function for automatic detection of the corners of the sample for assuring that all the sample has been acquired.

For each resulting plot, the user must decide if the data passed or failed the test. In the case, the scan passed all the tests, a quality control file indicating that the measure passed the tests is saved in the data structure of the original file. In the case the scan failed any of the tests, an analogous file is saved stating that the scan failed the tests. In both cases, the quality control file contains: the results of each test, the name of the operator and the date of the tests. If the user opens a file that did not pass the quality control test, a warning is printed to the console.

The implementation of the quality control step forces to critically assess the quality of the scan, despite the subjectivity of the evaluation it drastically reduces the probability of introducing scans with poor quality into data sets. The quality check is particularly important in the case of surface metrology, where, as we will see in the in chapter 5, the uncertainties and the sources of errors are greater, but it can be extended to any other technique. Recording the outcome of the analysis, labelling the good and the bad scans, furthermore allow to train models for automatic assessing of the quality of the data. For this reason, it is important to record the name or an ID of the operator that performed the quality control of the data

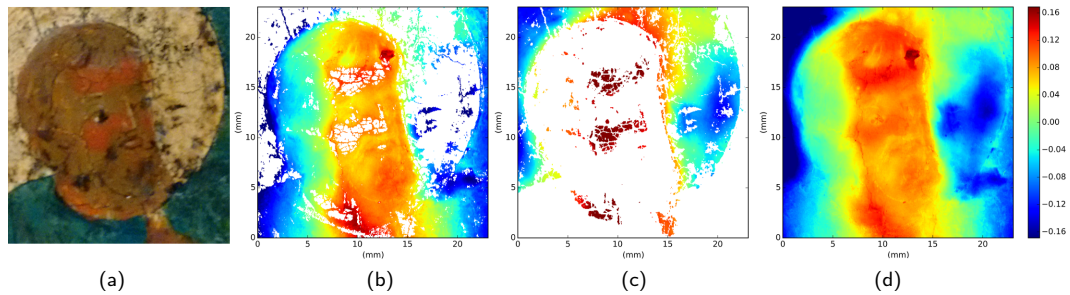


Figure 4.4: Acquisition of a portion of a Russian icon (a). Acquiring the green vest requires high-laser power because green usually absorbs at the wavelength of the laser, the aura is overexposed and hence masked (white values) (b). For acquiring the highly reflective aura the laser must be kept at low power (c) the scans were merged using the methods in section 4.6(d).

and preserve also bad measurements.

Figure 4.3 shows a scan of a test sample made of gypsum with four areas with different roughness. I will use this test sample for illustrating the results of some of the algorithms that I developed.

4.6 Improving the quality fusing multiple scans

When scanning material with high reflectance differences at the laser wavelength (655 nm), is not always possible to acquire all the area with the right exposure in a single scan. For mitigating this issue it is possible to scan the sample more times with different laser powers and fuse the data matrices so that only the optimal result is kept in the final matrix. I implemented two different approaches for performing these tasks. The first approach compares the SNR matrices pixel-wise and records the indexes and the matrix where the SNR is greater. This approach can give good results in most of the cases however has some drawbacks that must be considered. The first one is that because we are acquiring the surface with different laser power the spatial resolution might change between the two measurements. Higher laser power produces a lower-spatial resolution because the backscattered radiation comes from a larger area. Even for slight improvements of the SNR, the values are interchanged between the two matrices. The resulting matrix is hence composed of interspersed values from the two original matrices. Besides the difference in spatial resolution, other misalignments can arise if the two scans are not properly registered. The second approach is based on the use of masks. These masks are retrieved as explained in the previous section and hence are a combination of different quality parameters. From the data array acquired with the lower laser power (hence higher spatial resolution), we extract the good values (unmasked), we replace the corresponding values of the array acquired with high laser power with the extracted values. Using this method we ensure that we are preserving the values with the best spatial resolution and we limit the interspersion of the values of the two arrays. Another advantage of this method is that we can easily calculate the mask of the resulting array simply performing a matrix mul-

tiplication between the two original masks. The main disadvantage is that some values with higher SNR of the high-power laser data matrix might be substituted with values with lower SNR of the other matrix. Figure 4.4 shows the application of these approaches for solving this issue during the acquisition of a Russian icon.

An analogous procedure can be performed when the object has height differences higher than the working range of the probe. When a measurement is performed outside of the working range it has usually a greater error or extremely high numbers. In this case, we can acquire multiple scans re-positioning the part of objects within the working range of the lens. However, we must take care that the alignment between the scans is maintained.

4.7 Fitting

Fitting is an important instrument in the toolbox of the metrologist. It allows to find simple idealized shapes (refer as **nominal forms**) that best represent irregular surfaces. In wide area metrology even artworks with simple shapes such as icons or panels often deviate considerably from simple shapes or portions of them. Hence, many authors use different strategies for characterizing the curvature or the deformation of the surface from the nominal form. Besides fitting the whole surface[136], one possible approach is to subdivide the artwork surface into its elements and to fit the single elements[134].

In the context of robotic positioning systems with many degrees of freedom, the fitted shape can be used to calculate trajectories that allow maintaining the probe perpendicular to the surface. Allowing to filter the shape component during the acquisition and do not incur in the distortions due to the shape removal algorithms, which we will discuss later.

In this section, I focus on the usage of fitting for separating the approximate shape of the object from the other aforementioned components such as waviness and roughness. In this way, we can look at the distances data matrix no more as absolute distances from the probe to the object but as a positive or negative deviation from the fitted shape, what I call 2D-array of height variations, and pose the basis for the following data analysis.

4.7.1 Short introduction to the least-square fitting for surface metrology

A detailed revision of the fitting process applied to surface metrology can be found in literature [129, Chapter 14]. Given a set of values and their coordinates, the aim of the least-square fitting method is to find the parameters of an equation so that the sum of the squares of the differences between the value computed using the equation and the original value to be fit is at its minimum. In our implementation, I solve this problem using linear matrix equations. I used Numpy[132] for computing a vector m that minimizes the squared Euclidean 2-norm $\|D - mA\|_2^2$ computed for different equations describing the shape to be fitted in the general form $Am = D$, where D , in our case, represents the distances measured by the microprofilometer and A is the *coefficient matrix*. For fitting a profile, we can use

the equation of the line $d = mx + q$ rewritten as $Ac = D$, where c are the coefficients m and q of the best fit to be found. When the values are stored as nD-array of distances, that is the case for the implemented microprofilometer and many metrological instruments, the coordinates $x_{1,1} \dots x_{i,j}$ (and $y_{1,1} \dots y_{i,j}$ in the case of a surface) must be calculated based on the dimension of the data matrix. The nD-array of distances is vectorized, i.e. converted into a column vector, as the matrices representing the coordinates of each point. Hence A and D are represented as follow:

$$A = \begin{bmatrix} x_1 & 1 \\ x_2 & 1 \\ \dots & \dots \\ x_n & 1 \end{bmatrix} \quad D = \begin{bmatrix} d_1 \\ d_2 \\ \dots \\ d_n \end{bmatrix} \quad (4.1)$$

Once computed the coefficients, each point of the fitted line can be calculated from the equation $d = c_m x + c_q$.

For a plane with equation $d = m_1 x + m_2 y + q$ the matrix A become:

$$A = \begin{bmatrix} x_{1,1} & y_{1,1} & 1 \\ x_{1,2} & y_{1,2} & 1 \\ \dots & \dots & \dots \\ x_{i,j} & y_{i,j} & 1 \end{bmatrix} \quad (4.2)$$

The point corresponding to the fitted plane can be hence computed using the retrieved coefficients. $d = c_{m_1} x + c_{m_2} y + c_q$ multiplied by the coordinates where the surface was sampled.

Up to this point, we dealt with first-order degree polynomial. Increasing the order the system of equations allows fitting curved surfaces. As an example of the second-order curve fitting, the following equation is used for performing the form removal of the amphora shape shown in figure 4.1. The polynomial used is in the form $d = m_1 y^2 + m_2 x^2 + m_3 xy + m_4 y + m_5 x + q$ the matrix A hence become:

$$A = \begin{bmatrix} y_{1,1}^2 & x_{1,1}^2 & x_{1,1} \cdot y_{1,1} & y_{1,1} & x_{1,1} & 1 \\ y_{2,1}^2 & x_{2,1}^2 & x_{2,1} \cdot y_{2,1} & y_{2,1} & x_{2,1} & 1 \\ \dots & \dots & \dots & \dots & \dots & \dots \\ y_{i,j}^2 & x_{i,j}^2 & x_{i,j} \cdot y_{i,j} & y_{i,j} & x_{i,j} & 1 \end{bmatrix} \quad (4.3)$$

These are the most common polynomials that can be used for fitting the data and they have been implemented in the module that I developed, however, the user might want to implement specific polynomials to deal with other shapes found during the investigations.

Outliers and bad measurements can drastically reduce the effectiveness of the fitting. Furthermore, the user may consider excluding from the least squares fitting abnormal surface peaks or valleys and including them later on the following computations of the metrological parameters. For these purposes, the Boolean masks introduced in the previous section can be very effective.

$$X, Y, D = \begin{bmatrix} x_{1,1} \\ x_{2,1} \\ x_{1,2} \\ x_{2,1} \end{bmatrix} \begin{bmatrix} y_{1,1} \\ y_{2,1} \\ y_{1,2} \\ y_{2,1} \end{bmatrix} \begin{bmatrix} d_{1,1} \\ d_{2,1} \\ d_{1,2} \\ d_{2,2} \end{bmatrix} M = \begin{bmatrix} \text{True} \\ \text{False} \\ \text{False} \\ \text{True} \end{bmatrix} \Rightarrow A = \begin{bmatrix} x_{2,1} & y_{2,1} & 1 \\ x_{1,2} & y_{1,2} & 1 \end{bmatrix} D = \begin{bmatrix} d_{2,1} \\ d_{1,2} \end{bmatrix} \quad (4.4)$$

The vectorized boolean masks $vec(M)$ can be used for extracting from the arrays only the coordinates and the corresponding distances of the measurements that meet our criteria (the unmask value, `False` in the array M). The resulting matrices A and D can be used instead of the original matrices for computing the best fit.

4.7.2 Analysis, levelling, form removal and rotation

The coefficients calculated from the fitting can be used for characterizing the surface, just to name a few, some of these coefficients can represent the curvature, the tilting of the surface or a radius of a hypothetical cylinder fitted to the object. In this workflow, instead, we use the fitting for removing the shape component from the scan. This step is normally called **levelling** if the shape can be approximately represented by a line or a plane, or **form removal** if the shape has some curvature[90]. Levelling, in particular, is commonly used when the optical axis of the probe is not completely orthogonal to the surface to be measured which is very common when we position the system manually.

As explained early, once we have determined the coefficient of the equation used for the fitting, for each coordinates x (or x, y in the case of surfaces) we can compute the distances of fitted shape, we denote the matrix containing all the computed distance as F . The surface with form removed is hence the subtraction $D-F$, where D is the matrix containing the distances. Because, in case of optical range finders, the matrix D often contains the distances from the probe to the object, we perform $F-D$ so that the peaks of the surface are represented by positive values and the valleys by negative values.

This method for removing the form determine some error in the reconstruction of the surface. For understanding better the influences and the errors I performed some experiments on a synthetic profile. In figure 4.5 (left plot) we can observe the subtraction of the values calculated on a fitted line from an arbitrary synthetic sinusoidal profile, with an amplitude of 2 units and wavelength of 6 units. After the subtraction, the profile result distorted, with the peaks of the profile shifted to the left. For avoiding the distortion, the profile must be rotated. In the right plot of figure 4.5 I show the same profile after applying a counterclockwise rotation matrix R to each pair of x, d values:

$$R = \begin{bmatrix} \cos \theta & -\sin \theta \\ \sin \theta & \cos \theta \end{bmatrix} \quad (4.5)$$

The resulting profile is almost undistorted, however, as we can see from the trajectories of the points of the right plot in figure 4.5 the distances between the

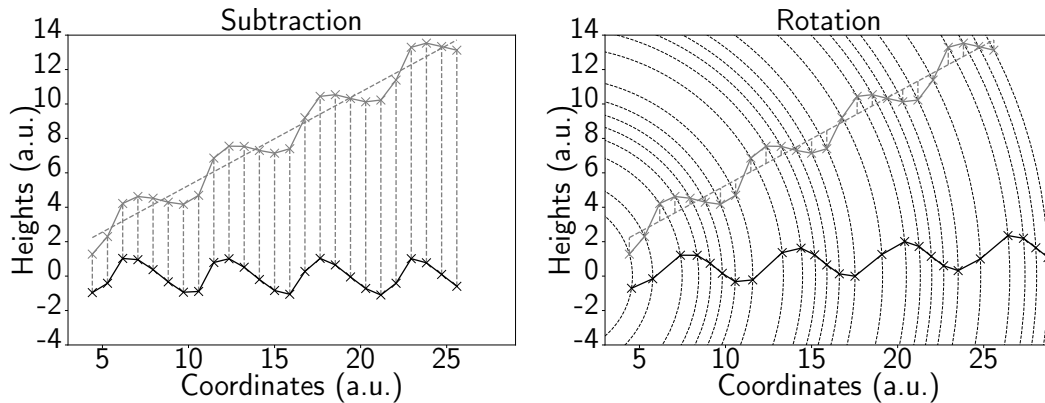


Figure 4.5: Comparison of the procedure for removing the tilting of a profile. On the left, the value computed on the fitting line (dotted grey) is subtracted to the original profile (grey marker). The resulting profile (black markers) is shown below. On the right, the original profile (grey markers) is rotated using a rotation matrix and the angle computed from the tilting. The original profile should have amplitude of 2 units and wavelength of 6 units.

measurement varies. Hence, for obtaining evenly spaced measurement a second step involving the interpolation of the values is needed. The interpolation is not always free of risks, thus it is preferable to evaluate if the disadvantages of performing this operation are justified.

For this purpose, we can evaluate the results of the transformations of known synthetic data. For instance, we can generate a set of synthetic profiles starting from an untilted profile with the same features of the previous (Amplitude=2, $\lambda = 6$) and rotating each profile known angle using a rotation matrix. In this case, I performed a linear interpolation to retrieve the distance value for the same set of x coordinates. Eventually, we can compute some metrological parameters for each synthetic profile after the subtraction or the rotation for each angle. I computed some of the most common metrological parameters: Psm (average peak distance), Pq (standard deviation of the heights), Pa (average heights), Pt (max height distance), Psk (skewness of the distribution of heights) and Pku (Kurtosis of the distribution of heights). In figure 4.6 we can see that the parameters are affected differently. After the subtraction, in this case, the average spacing between the peaks (Psm) decreases while the other parameters related to the amplitude of the profile (Pt, Pq, Pa) tend to increase. On the other hand, the rotation matrix maintains the computed parameters close with the values computed on the surface untilted. Computing the relative error is particularly useful to understand the sensitivity of the parameters to tilting of the sample. From figure 4.7 we can see that in this case, the Psk parameter is particularly sensitive to the tilting of the surface. For this synthetic profile, we can observe that most of the benefits of the rotation matrix over the simple subtraction appear to be evident when the profile is tilted more than 5 degrees.

The results here reported, are specific of the synthetic profile under investigation and can not be easily generalized. Furthermore, we must consider that the rotation matrix is computed using the known angle, in the real scenario the ro-

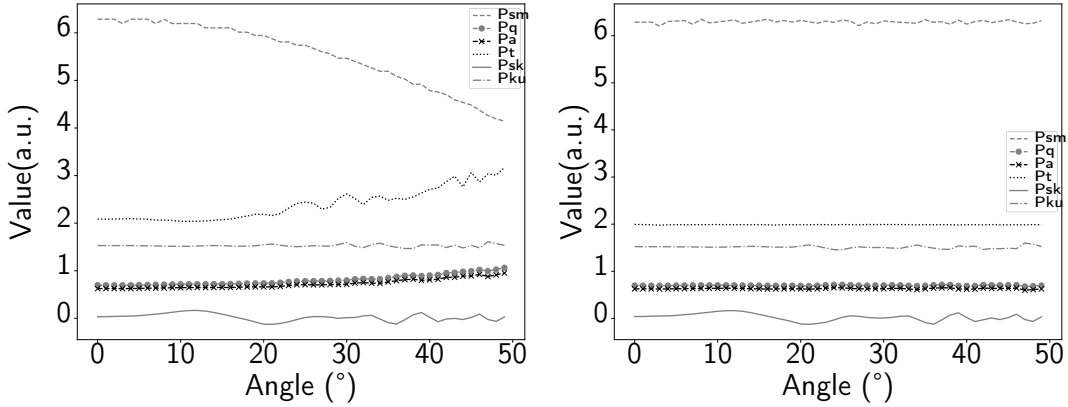


Figure 4.6: The effects of subtraction (left plot) and rotation (right plot) on the computation of some metrological parameters (P_{sm} , P_q , P_a , P_t , P_{sk} , P_{ku}) computed on a synthetic sinusoidal profile ($A=2$, $\lambda = 6$).

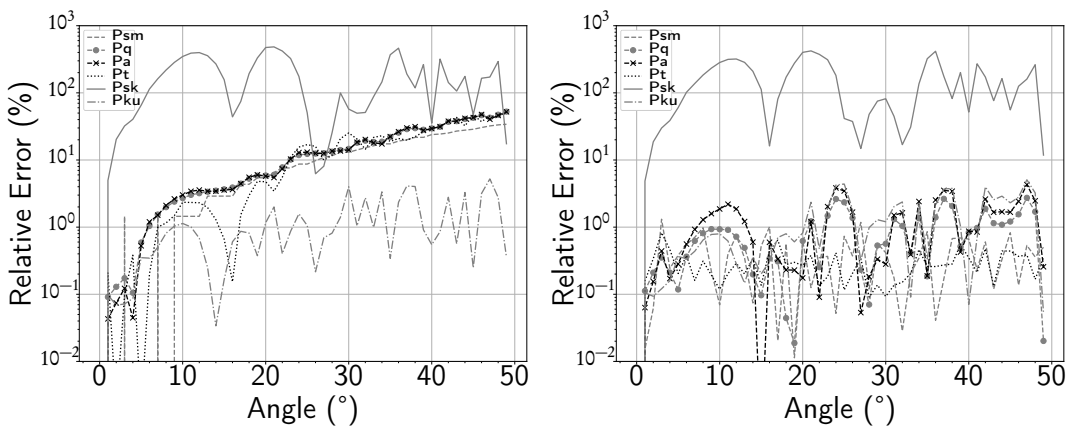


Figure 4.7: The relative error (log scale) computed at different angles against the values with the profile parallel to the direction of scanning. On the left plot, the relative error of subtraction and the right plot relative error of the rotation on the computation of some metrological parameters (P_{sm} , P_q , P_a , P_t , P_{sk} , P_{ku}) computed on a synthetic sinusoidal profile ($A=2$, $\lambda = 6$).

tation angle θ is unknown and must be determined, for instance computing the arctan c_m , where c_m is the angular coefficient of the fitted line. Determining the angle increases the error in the transformation, and eventually, this can undermine the advantages of the rotation matrix for moderate tilting. If we are measuring flat areas is often preferable to try to minimize the tilting before starting the scan rather than rely on the form removal algorithms. As a rule of thumb for optimal acquisition, we set our maximum angle of tilting to one degree. After the quality control, if the sample result with a tilting greater of one degree in any direction (x or y) the position of the system is corrected and the scan is repeated. Measuring various samples data set with the system I induced that with tilting lower than one degree the subtraction method usually is the most convenient. On the other hand, if the surface or the portion of the surface is very inclined ($>10^\circ$) and the system cannot be positioned perpendicular to the surface the rotation matrix can be used for reducing the distortions. High frequency signals are more sensitive to tilting off of the surfaces, hence these guidelines serve only as an indication and must be verified case by case depending also on the signals that we want to isolate with the techniques explained in the next section.

The output of these operation is called **primary profile** or **SF surface** for areal measurement.

4.8 Digital filtering

Digital filtering plays a key role in the analysis of surface metrology. ISO 16610:2015 is the reference standard regarding filtration techniques applied in metrology[75]. Digital filtering aims to select signal within a precise bandwidth that is usually delimited by **cut-off wavelengths** that suppress most of the wavelengths that go beyond the desired range.

Digital filtering is usually performed after the form removal process, but can be also applied before this step for removing the **micro-roughness** that usually contains high-frequency noise produced during the acquisition (usually caused by vibrations, dark current, and in the case of conoscopic holography by speckles). The signal from the ideal surface undergoes two other filtering processes before the digital filtering. The optical transfer function of the system act as a low-pass filter, suppressing wavelengths below the spatial and axial resolution of the system. The calculated optical transfer function, however, is not determined only by the specification of the system but also by environmental factors (e.g. vibrations, deformations) that induce movements of the system object-probe.

We must be very careful in this regard because we might apply a low-pass filter starting from a frequency range that was already heavily filtered by the measuring system. Thus, the following results of the parametrization are relative to a different bandwidth compared to that one indicated by the cut-off wavelengths. One of the most common filters is the Gaussian that can be implemented for filtering profile [76] and areal measurement[83]. A detailed explanation of the implementation can be found in literature [129, Chapter 5] the weighting function is the

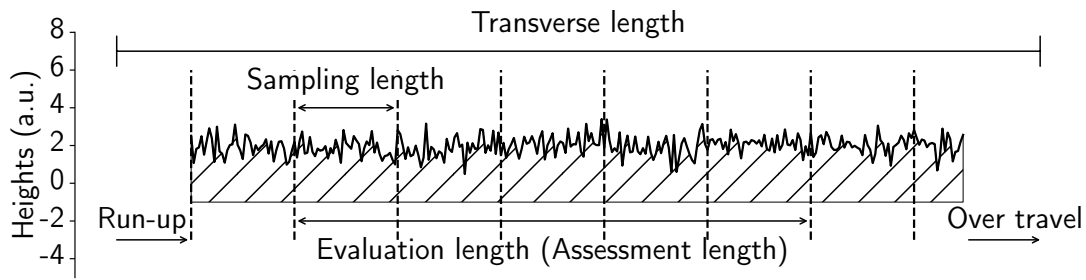


Figure 4.8: Subdivision of the profile parts re-adapted as shown in [14]. Run-up and Over travel are the offset of the measurement.

following:

$$S(x) = \frac{1}{\alpha \lambda_c} \exp \left[-\pi \left(\frac{x}{\alpha \lambda_c} \right)^2 \right] \quad (4.6)$$

Where $\alpha = \sqrt{\ln 2/\pi} = 0.4697$ while λ_c is the cut-off wavelength that allows us to set the bandwidth of the filter. Traditional **Gaussian filters** may not be effective when in the surface are present features, such cracks, holes and well-defined structures. This is, unfortunately, the case of most artworks surfaces, where many different processes left chaotic signals. For overcoming these issues **robust Gaussian regression filters**[159] have been included in ISO 16610 for profile[79, 80] and areal [84] measurement. The ISO technical committee added several new filtering techniques for profile and areal measurement these include spline [77], wavelets [78] and morphological filters[81, 82, 85]. These techniques, even though their implementation is not always straightforward, add new possibilities to filter effectively complex heterogeneous surfaces as those commonly found in artworks. Blateyron[16] summarizes in his work the techniques and the workflow shown in ISO standards, while for more details on the implementation other references are available[143]. The ISO nomenclature for the output is the following: after applying a low-pass filter we obtain the **waviness profile** (**SF surface** for areal measurements) while after applying the high-pass filter we obtain the **roughness profile** (or **SL surface** for areal measurements).

4.9 Surface subdivision

One important step before the processing is the subdivision of the measured surface in parts[92]. In the case of a profile, the whole length comprising the offset is called **transverse length**. A portion of the profile is selected for the analysis (**evaluation length**). The evaluation length is subdivided into parts (usually five) with equal **sampling length** as shown in figure 4.8. The sampling length is usually equal to the cut-off chosen during the digital filtering step discussed in the previous section. The choice of the cut-off and sampling length has many important implications on the following processing. Historically, the sampling length and the cut-off were empirically determined analyzing hundreds of samples and choosing “the length of assessment over which the surface roughness can be considered rep-

representative”[186, p.10]. Rank Taylor Hobson found the optimal sampling length to be 0.8 mm analyzing machined metal pieces. The results found by Taylor Hobson were later included and extended with further research in ISO 4288:1996[92]. However, they can be hardly generalized to every surface and in fact, this standard should be replaced by ISO 21920 in the future [95, 96, 97]. The choice of the correct cut-off and sampling length is determined by many parameters comprising also if the surface presents some periodic signals or not. In particular, in the case of artworks, the cut-off and strategies defined in ISO 4288:1996 must be taken *cum grano salis*, and the choice should always be motivated.

4.9.1 Varying sampling length or area approach

To overcome the limitations of the current guidelines, a possible approach is to study the effects of a vast range of different cut-off and sampling lengths and evaluate the metrological parameters for each cut-off and sampling length. The results can be used not only for identifying the best values to use but also for understanding the homogeneity and the behaviour of the surface. This approach is used, for instance, by Bigerelle et al. for studying the abrasion on stainless steel[15].

As discussed in [168, Section 7.2], the concepts of sampling length and evaluation length can be extended to areal measurements as **sampling area** and **evaluation area**. I implemented different algorithms for subdividing areal surface into sampling areas of increasing size. The first algorithm starts with a small sampling area in the centre of the sample. The sampling area is increased in successive steps until the border of the sample is reached. For each step are computed the metrological parameters under investigation. The area can be squared or having the same aspect ratio of the sample. I found this algorithm is particularly useful when measuring reference samples or region of artworks where cleanings trials have been performed. The borders of many samples have often metrological properties very different from the centre of the sample. In case of application of coatings or cleaning processes part of the untreated sample might be included or the borders can accumulate materials due to different phenomena. Hence, it is crucial to select only the area that is representative. This method, however, does not show which portion of the area is contributing more to the overall estimation of the metrological parameters. For instance, if the initial region of interest is not centred some sides of the sampling area may encounter soon the discontinuities of the borders, while other homogeneous areas are left outside the computation. For overcoming this issue, I implemented a second algorithm that can map the inhomogeneities of the roughness. The 2D-array of heights is subdivided in squared sampling area with the same side starting from the upper left corner (figure 4.9). For each step, the side of the squared sampling area is increased. If the side of the evaluation area is not a multiple of the side of the sampling area – as in figure 4.9 c– the values at the borders are discarded. In this way, we ensure that the number of measurements in each square of the same subdivision step is the same. Once, we have subdivided the area or the profile in sampling units several parameters can be calculated for describing the surface. In figure 4.10 we subdivide the test sample shown figure 4.3, in squared areas with side of fifty measurements. After levelling and filtering

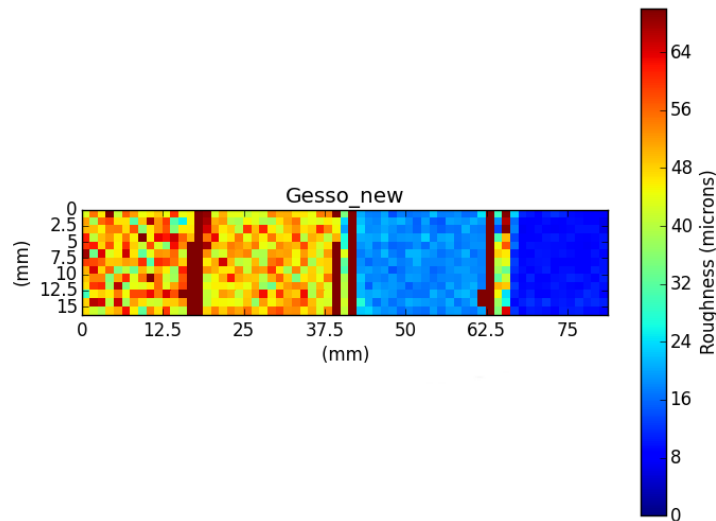


Figure 4.10: Roughness parameter S_q computed after subdividing the filtered sample surface (figure 4.3) into sampling areas with a side of 1.25 mm. Some artifacts are visible on the borders between the two patches. These are due to the fact that the cells happen to be between the steps dividing the patches.

the low-frequency signals, we computed the root mean square parameter S_q (that will be defined in 4.10.3) for each cell. In this case, every pixel of the figure 4.10 indicates the roughness computed over 2500 measurements and it is equivalent approximately to an area of 1.5 mm^2 . We can notice how it is possible to identify that the four square regions have decreasing roughness from left to right. When the sample has high steps as can be seen in figure 4.3, the filtration algorithm might produce some artefacts that cause atypical peaks or valleys that produce high values of roughness (dark red columns separating the four cells).

It is also possible to perform the algorithm with overlapping areas subdivisions. In some cases, this might be beneficial because when the samples are inhomogeneous it allows making a larger sampling and more accurate statistics. The main drawback is that when we reconstruct the distribution image (viz. figure 4.9) it is harder to associate the values that produced the result with the location on the image, losing part of its effectiveness in estimating the homogeneity of the surface.

4.9.2 Irregular sampling area

In some cases, these algorithms might also be applied before filtering or form removal. Furthermore, for very heterogeneous surfaces squared areas are not always an effective subdivision for mapping the roughness variations across the sample. In particular in the case of regions of the surfaces with irregular borders if the cell encompasses height variations between a region with different roughness the computed roughness is not representative of the surface. This is very likely in heterogeneous surfaces such as artworks. I tested different algorithms to segment the

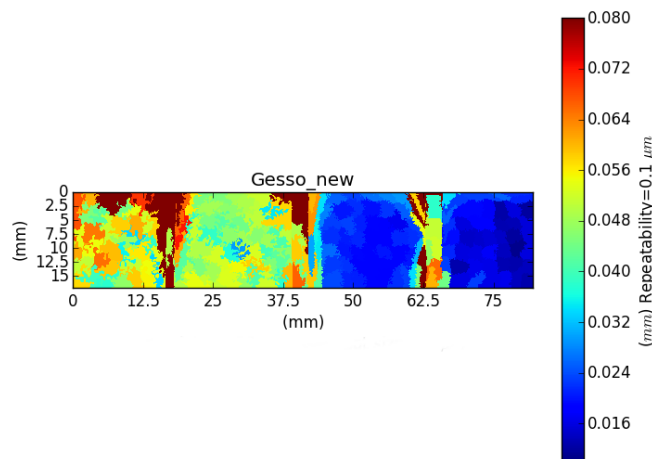


Figure 4.11: The result of the subdivision of the sample surface (figure 4.3) using the SLIC algorithm and computing, for the sampling areas enclosed in each super pixel, the roughness parameter S_q (that will be introduced later with the equation 4.11).

surface inhomogeneous areas. The algorithms that I tested are normally applied to image processing and allow segmenting the homogeneous areas of the image (in case of images with similar colours). The segmented areas are called **super pixels**. I tested the compact watershed algorithm proposed by Neubert and Protzel [131]. Some watershed algorithms, in fact, as we will see in section 4.11 are already used for computation of areal features parameters and are part of ISO 25178:2012-2 [87] but here we use them for selecting the sampling area. Another algorithm that I tested is the Simple Linear Iterative Clustering (SLIC) algorithm [3]. This algorithm performs the clustering in a 5D space. The first two dimensions are the space coordinates and the other three the colour space. Usually, the CIE Lab colour space is used. In the case of surfaces, we can input the same normalized heights matrix for all the channels. Another approach is to work in the RGB space and input a three-dimensional array where in addition to the heights matrix we can use other data that are relevant to the classification. One possible choice is to use the SNR matrix and the matrix recording the total light collected (abbr. Total) as the other two channels. In this way, we can subdivide the surface into areas that have as well as approximate the same heights also similar SNR and Total value. Because the SNR and the Total matrix are linked with the material present in the surface, this approach might prove effective in separating the contribution of the properties of the material in the surface topography. Of course, for this kind of algorithm the user cannot choose the side of the sampling area but rather the total number of super-pixel to be identified.

4.10 Calculation of metrological field parameters

In this section I describe the common metrological parameters and the choices made for the implementation in the developed software.

4.10.1 Introduction to the ISO conventions

The characterization of the surface is performed computing for each sampling area specific metrological parameters. Usually, for profile measurements, the result is the average of the computation performed in at least five sampling lengths. These parameters are subdivided into three main categories: amplitude, spacing and hybrid parameters. The **amplitude parameters** refer to the statistical characterization of the heights. **Spacing parameters** are instead linked to the spatial distribution of the peak and the valleys. Eventually, **hybrid parameters** estimate feature of the surfaces that can be included in both classes. Metrological parameters are usually indicated with a capital letter (P,R,W or S and V) indicating if the profile has been computed on the **P**Primary profile, the **R**oughness profile, the **W**aviness profile or on the areal **S**urface or **V**olume. This letter is followed by a lower case letter identifying the algorithm (e.g. q, sk, ku)².

The mathematical computation of the parameter may differ between various standard, here, as an example, I show the implementation of ISO 4287:1997 [91] for profile, and for areal measurement ISO 25178-(1-3) [86, 87, 88]. The software implementation of the algorithm may also differ depending on the algorithms used. In the following paragraph, I will explain the rationale of the choices I made for implementing some of these parameters in the software that I developed and the recommended implementation.

4.10.2 Profile parameters

As a first example we take the calculation of the roughness profile parameter Rq , the root mean square height. Rq is defined in ISO 4287 – 1996 section 4.2.2, other roughness profile parameters can be found on the NPL website[171]. The calculation of this parameter for a profile described as a continuous function is the following:

$$Rq_i = \sqrt{\frac{1}{l} \int_{l_i}^{l_f} Z^2(x) dx} \quad (4.7)$$

Where l is the sampling length starting at l_i and ending at l_f , and Z are the distances from the reference line.

Because nowadays the instruments acquire a series of discrete values, an efficient way to compute an approximated value is to redefine the parameter computation as a summation:

$$Rq_i \approx \sqrt{\frac{1}{n} \sum_{i=1}^n z_i^2} \quad (4.8)$$

²these letters are not written as subscript.

Where n is the number of points comprised in the sampling length and z_i is the distance value at index i . This approach is very efficient from the computational point of view and has been adopted in the implementation of our software. However, is not the suggested approach by ISO 4287 – 1996. Which instead is based on the interpolation of the discrete values using a natural cubic spline. This cubic spline is used for computing the integral form of the metrological parameters within each sampling length (as shown for the parameters Rq in equation 4.9). Specifically, l_i and l_f become the starting and the ending point of each sampling length.

Besides the computational requirements, the cubic spline may also lead to unpredictable results when are present invalid values, hence I decided to implement the metrological parameters using the discrete approximation.

In both case for final estimation of the parameters is computed averaging the result obtained applying the defined formulas on each sampling length as defined in ISO 4287 – 1996. Hence, the final estimation is done using:

$$Rq = \frac{1}{CN} \sum_{i=1}^{CN} Rq_i \quad (4.9)$$

Where CN is the **Calculation Number** the number of sampling lengths evaluated (usually five). The estimation of the parameters from the discrete approximation, continuous interpolation and mathematical function is still debated and some frameworks are currently underdevelopment for assessing the differences between the results of the computations[176].

4.10.3 Areal field parameters

Part of the reasoning of the previous section can be extended to areal parameters. These parameters are indicated with the letter S or V (for volume parameters) regarding the fact that they are computed over the SF or SL surface. The root mean square height parameter of the equation 4.9 becomes:

$$Sq_i = \sqrt{\frac{1}{A} \iint_A Z^2(x,y) dx dy} \quad (4.10)$$

Where A is the area under investigation. While the equation 4.8 becomes:

$$Sq_i \approx \sqrt{\frac{1}{A} \sum_{i=1}^{n_i} \sum_{j=1}^{n_j} z_{i,j}^2} \quad (4.11)$$

Where n_i and n_j are the numbers of measurement of the sampling area. For areal parameters, the evaluation area is usually not subdivided into sampling areas. Thus the evaluation area becomes the sampling area [17]. However, in the case of heterogeneous surfaces, such artworks it is often useful to evaluate the parameters

on different sampling areas with the algorithms shown in the previous sections. The standard deviation and the distribution of the values assumed by these parameters in different sampling areas gives an insight into the homogeneity of the surface. This can be done visualizing a recomposed image of the metrological value computed on each sampling area as shown in the previous section in figures 4.10 and 4.11.

4.11 Areal features parameters

The computation of areal field parameters largely depends on the cut-off, sampling length and type of filter used. As mentioned previously the cut-offs used in metrology are derived by empirical observation in industrial fields and should be redetermined case by case for unknown surfaces. The meteorologist working on artworks is often operating blindly. Computing from complex surfaces this series of parameters can be misleading if we do not have an understanding of the surface. Another set of parameters are useful for this task are referred to **areal features parameters**. An introduction to these metrological parameters can be found in literature[18]. Many of these features are borrowed by terrain topography analyses. Their roots can be found in early works of Cayley [29] and Maxwell [33] for identifying the elements of the terrains such as dales, hills and saddle points. Nowadays for identifying these features watershed algorithms are often used. Once identified they can be hence organized in graph or tree describing the relation between each feature identified. A detailed dissertation can be found in literature[146].

The same structure can be identified on the surface at a smaller scale. Different industries have standardized their own definition and algorithms for identifying peaks and valleys in surface topography data such as PSA Renault in CNOMO 14015:1993 [1]. For computing metrological parameters, after the identification of the features is, however, important to eliminate the features produced by the measurement noise. The routine proposed by Gert W.Wolf[187], called **Wolf pruning** can be effectively used for this task and is now part of ISO 25178:2012-2 [87]. Lately, these algorithms have been constantly improved allowing the segmentation of structured surfaces[160].

4.11.1 Hierarchical Peak-Valley Analysis (HPVA)

For performing exploratory analysis of unknown heterogeneous surfaces, I proposed and implemented a method that allows to create a hierarchy of peaks and valleys and visualize each level of the hierarchy maintaining the original position of the features for eventually analyzing their relationships and distribution. This method is intended to explore the data “ as it is ” without complex transformation that can hide the direct link with the surface feature. However, it usually gives better insights if applied after the levelling or form removal. Hence, here I explain the algorithm performed on a profile P defined as a 1D-array of heights variations:

$$P = [z_1, z_2, z_3, \dots, z_n] \quad (4.12)$$

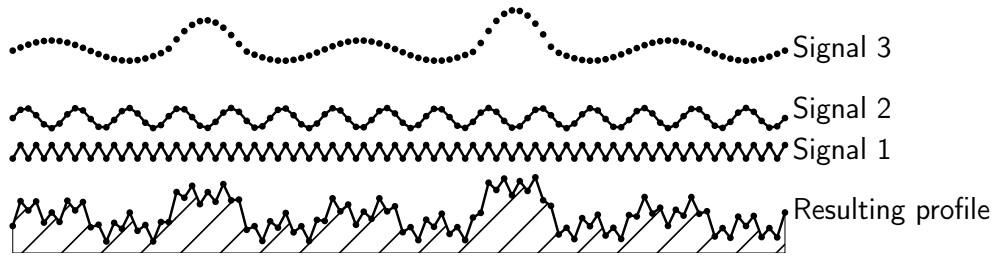


Figure 4.12: The creation of a synthetic profile used in figure 4.13 summing three different signals.

The measurement z_i is a peak if $(z_i > z_{i-1} \wedge z_i > z_{i+1})$, instead z_i is a valley if $(z_i < z_{i-1} \wedge z_i < z_{i+1})$. If we are using array of distances the definition of the peak and the valley is the opposite. When we identify the peaks or the valleys of a profile we call this list of identified features **level**.

For instance, the first level of peaks heights Lh can be described with the set-builder notation as follow:

$$Lh = [z_i \mid z_i \in)P(, z_i > z_{i-1} \wedge z_i > z_{i+1}] \quad (4.13)$$

We keep a record of the positions (indexes of the matrix) where the peak have been detected on another list Lp :

$$Lp = [i \mid z_i \in)P(, z_i > z_{i-1} \wedge z_i > z_{i+1}] \quad (4.14)$$

It is not possible to determine if the first and the last values of the profile P are peaks (or valleys), the algorithm is hence computed excluding the extremes. Followed that $Lp + 1$ correspond to the original indexes distance of the peaks in the profile P .

We can perform the same process for identifying the features recursively on the heights levels computed before until the level has only one feature left.

However, from the first level onward we must consider that we already assigned the first value of the profile to a specific feature, hence we do not have to exclude the extremes from the analysis. For instance, if we compute the first level of peaks $L1h$. We already know that the first value $L1h_1$ is peak hence if it is greater than $L1h_2$ it should consider a peak in the iteration for the next level.

In figure 4.12 we create a synthetic profile summing three different signals. The first signal is used for simulating a high-frequency periodic noise such as vibrations, while the second and the third signal can be seen as roughness and waviness signals. In figure 4.13 we can observe the results of the simulation iterating the algorithm for the detection of the peaks. We can observe that the peaks are progressively selected. The first level contains the peaks relative to signals that we assigned to the noise, roughness and waviness. Increasing the level we highlight the higher peaks.

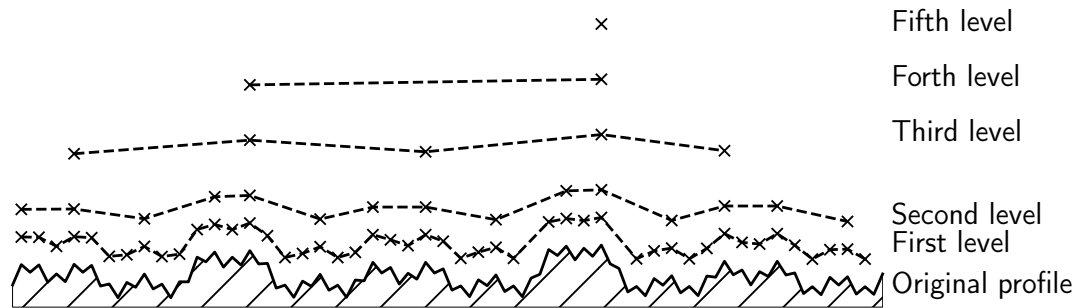


Figure 4.13: Application of the HPVA for the analysis of the peaks of the profile created in 4.12. Each level corresponds to an iteration of the algorithm on the profile below. The profiles are stacked for the purpose of visualization.

The same procedure can be applied for identifying the different valleys. The Lp and Lb list that we obtain for each level of iteration can be used for analyzing the distribution of the features. Knowing the scanning step l_s of the measurement we can, for instance, compute for each level the spacing between adjacent peaks:

$$Ls = [(Lp_i - Lp_{i+1}) \times l_s \mid Lp_i \in Lp] \quad (4.15)$$

Or the height difference between each adjacent peak:

$$Ld = [Lh_i - Lh_{i+1} \mid Lh_i \in Lh] \quad (4.16)$$

Eventually, we can combine each peaks level with the corresponding valley level. The surface between the first level valleys and the first level peaks is called **surface envelop**. We can compute the same spacing and height difference arrays (Ld and Ls) that we computed for the separate levels also for the joint peak-valley levels, but with one caveat. Is not granted that between two peaks there is a valley and vice versa. In fact, it is possible that with our definition of peak and valley no valleys or peaks are detected and the surface is modelled by precise steps. However, this possibility is not very likely in practice.

The next step of the implementation of the algorithm is to extend the algorithm to the 2D array of heights. The input array is analysed as it was composed of a series of horizontal and vertical profiles. Hence we will have horizontal levels when the algorithm is computed on the row of the array and vertical levels when the algorithm is computed on the columns.

An example for analyzing a panel lay

In figure 4.14 is shown a scan of a portion of wooden panel prepared using the traditional technique using linen canvas and gypsum. The preparation is made by the consecutive crossed coat of paint. After the levelling, removing the best plane

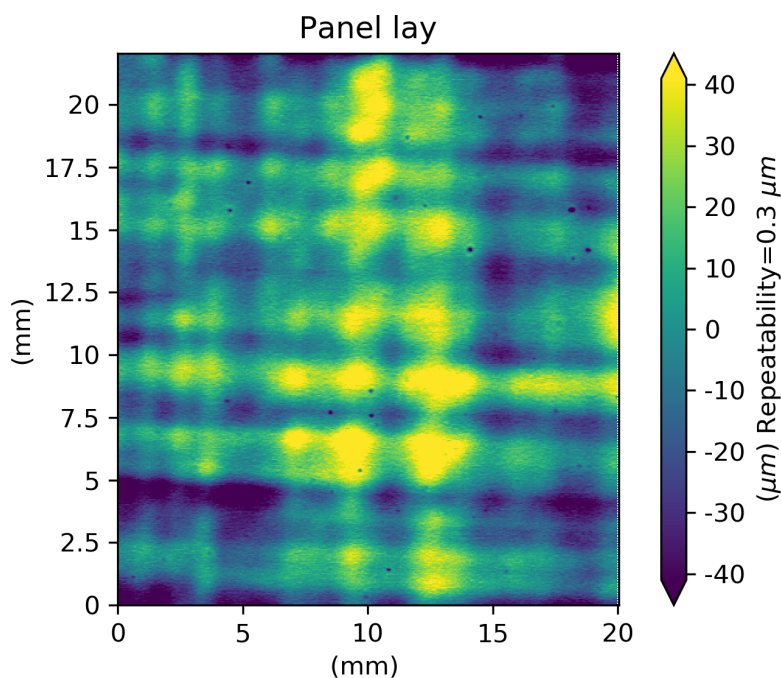


Figure 4.14: A scan of a portion of wooden panel prepared using gypsum acquired with the ConoProbe-3 lens 75 mm after levelling.

we can perceive the combined signals due to the brush and canvas. After that we performed the HPVA analysis we can reconstruct the original data matrix highlighting where the peaks or the valleys for each level are located. In figure 4.15 for facilitating the visualisation we select only the valleys levels. The first level (both horizontal and vertical) shows a high density of valleys. If we examine a detailed of the array (at the bottom of figure 4.15) we can see that the vertical level shows series of aligned valleys while in the horizontal level the valleys are interspersed. This pattern is probably linked with the scanning pattern, and hence most of the valleys detected in the first vertical level are probably noise. In the second and third level, we can instead observe vertical and horizontal patterns due to the canvas weave underneath and the brush strokes of the preparatory layer. This predominant direction in surface metrology is called **lay** [186, p. 951]. The same analysis can be performed for the peaks and the combined view peaks and valleys. The analysis of the spacing between the adjacent valleys can be performed showing the overall histogram of the differences between adjacent valleys of every single profile for the vertical and horizontal direction. Figure 4.16 illustrates the results of this computation. We can observe that the first peak of the histogram representing the vertical level 1 is very high (approximately 20000 values), the first peak indicates the minimum spacing (two times the scanning step) and in this case is probably indicating some systematic noise. The presence of some lower wavelength signals can be observed in the second and third level. The distribution of the histograms can suggest different cut-off to use during the filtering step explained in section 4.8 or used for identifying the spacing between some feature. For the last case, however, we have to bear in mind that the spacing shown by the histogram can be

interpreted as the distance between the brush stroke or the canvas weave only if these signals are perpendicular to the axes of the data matrix. In general, the proposed analysis should be used more for as an exploratory analysis for getting a first insight on the surface rather for extracting the signal. A more advanced algorithm can be found in the literature for identifying these patterns [189]. In our case, the identification of the spacing between traces left by the brush and the weave of the canvas could be improved fitting for each cluster of peaks or valleys a line. This could be implemented using RANSAC algorithms.

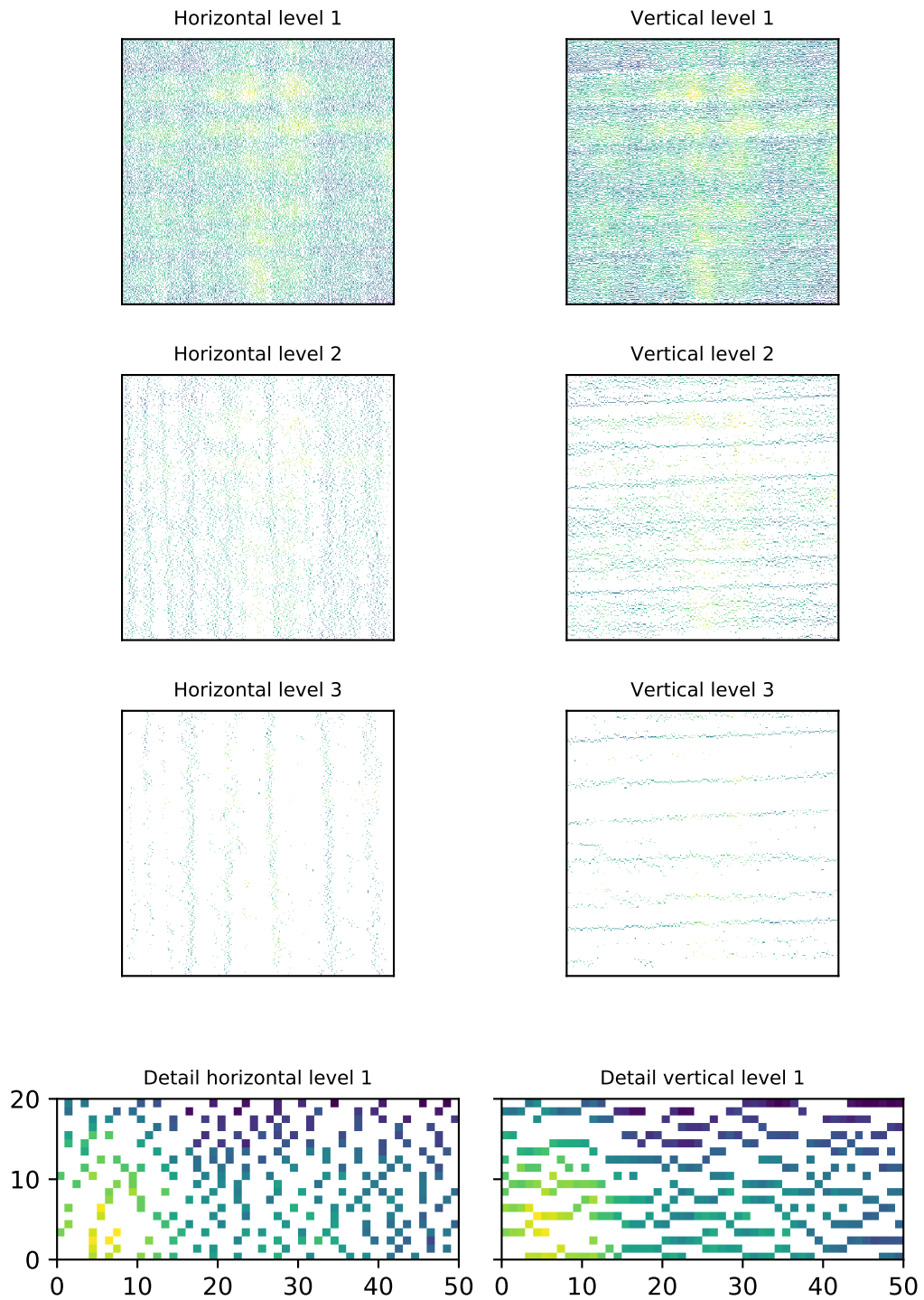


Figure 4.15: The first three horizontal and vertical levels of the valleys levels retrieved using HPVA computed on the scan shown in figure 4.14.

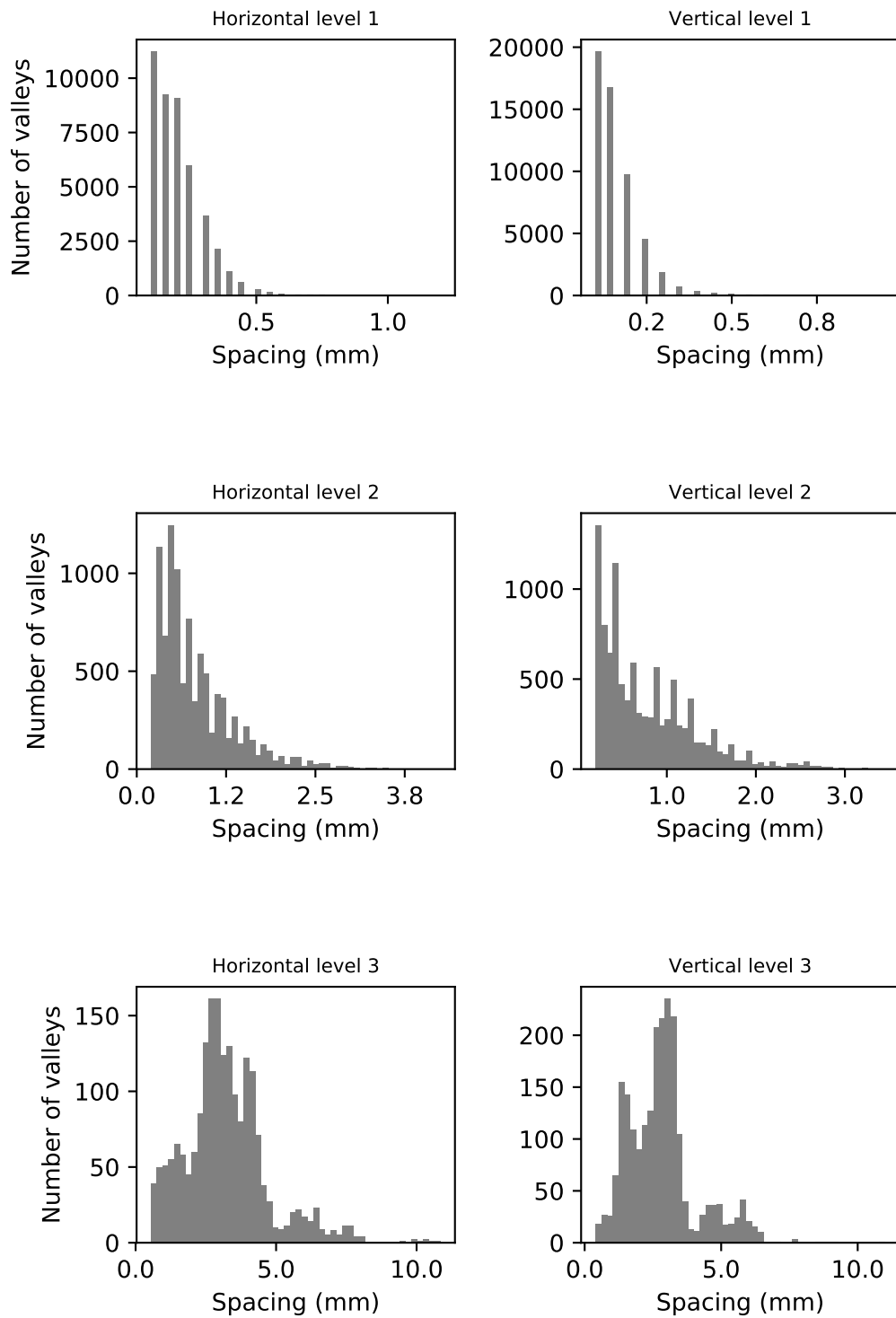


Figure 4.16: The distribution of the spacing between the valleys of the first three horizontal and vertical levels retrieved using HPVA computed on the scan shown in figure 4.14.

4.12 Summary

In this chapter, I discussed how to handle and analyze the data collected using the conoscopic holography scanning system developed.

In the first section, I have explained the different levels of data processing and I suggested three main data formats for sharing the results amongst users with different computer literacy.

For allowing the usage of .x3p file format in this framework, I developed a parser for reading and writing it using Python.

In section 4.3 I have integrated the canonical workflow for surface metrology analysis with a quality control procedure developed for the conoscopic holography system.

I have reported two algorithms for improving the quality of the measurement the first uses the values with the highest SNR the second (which to the best of my knowledge it is original) uses the masks introduced in section 4.5.

I showed how the masks can be used also during the levelling and form removal step of the workflow. Using a synthetic profile I have investigated how the levelling by subtraction affects the metrological parameters and the advantage and disadvantage of using rotation matrices.

Due to the intrinsic inhomogeneity of artworks special procedures must be implemented for assessing the in-homogeneity of the area under investigation and improving the sampling of the surface.

I have introduced different algorithms that can be used during the surface subdivision step of the workflow and to visualize effectively the roughness in-homogeneity on the surface, to the best of my knowledge the application of these algorithms to the surface subdivision in surface metrology is novel.

The first algorithm uses concentric regions of interest with area that varies progressively for each step of the computation.

The second algorithm is the extension of the algorithm proposed by Bigerelle[15] to areas, allowing a more effective mapping of the roughness.

The third algorithm uses SLIC[3] for subdividing the surface into irregular but relatively homogeneous surface areas.

I gave an introduction to the metrological field parameters that can be used on the aforementioned surface subdivisions. In particular, I have motivated the choices of using in the module developed the discrete formulas instead of computing the parameters integrating a spline fitted to the discrete data.

Another approach to surface metrology analysis is to compute areal features parameters, these parameters describe features (e.g. valleys and peaks) and their relationships.

In section 4.11.1 I have proposed and implemented an algorithm that I called Hierarchical Peak-Valley Analysis (HPVA) that identifies peaks and valleys along with the horizontal and vertical directions of the scan and regroup them in different levels depending on their relative height.

I showed how this algorithm and the resulting visualizations can be used for identifying the lay of the surface and information regarding the scan.

In the next chapter we will investigate the uncertainties and the artifacts linked

to the metrology applied to artworks with a special focus on the conoscopic holography system.

But the deity of the science of painting considers works, human as well as divine, which are delimited by their surfaces, that is, the lines of the boundaries of bodies...

Leonardo Da Vinci, A Treatise on Painting

5

Surface representations: definitions and uncertainties

This chapter introduces the reader to the uncertainties in measuring the interface. I used the coastline mapping problem as an analogy for introducing the reader to the general problems encountered in metrology. I will show different approaches for assessing the uncertainties due to the probe used and the dimensional instability of the object under investigation taking advantage of some of the results presented in two of my publications[122, 123].

5.1 Introduction

For the correct interpretation of the metrological data collected it is crucial to understand what representation of the surface we are analyzing. For this purpose it is often required to compare or combine the information from more than one technique on the same samples or on similar materials[138, 107, 113]. Often, for assessing the uncertainties, techniques with better performance or using a different physical principle are used. Hence it is relevant to have the widest understanding of the surface representation, not only at the same scale of the technique under study, but also at lower or higher scales.

In the following sections, I will firstly review the aspects and the definitions linked to the concept of surface from various field of knowledge (engineering, physics and chemistry) I will then introduce the problems linked to the determination of the surface interfaces using a parallel with the cartography that I will use through the whole chapter for easing the explanations.

At the end of the chapter, it should be clear that the subjects of study of metrology are representations of surfaces related to the probe, the way it is used and also often on to environmental conditions where the acquisitions were collected.

5.1.1 The problem of the surface definition

The concept of surface can be quite broad. IUPAC[98] suggests using this term to refer to the “*outer portion*” of the sample of undefined depth. Different compound words are used to disambiguate the meaning and will be adopted in this dissertation. The **physical surface** is defined as *atomic layer of a sample which, if the sample were placed in a vacuum, is the layer “in contact with” the vacuum; the outermost atomic layer of a sample.*

In the field of nanotechnology the term **interface** is often used and can partially replace the term physical surface because in most of the applications, particularly in the field of Cultural Heritage, the sample is not placed in high vacuum but measured in normal atmospheric condition, and we can distinguish two or more **phases**: entities of a material system which are uniform in chemical composition and physical state. Eventually, it is the definition of phase that determines the sample interface and hence our model of the boundary of the material surface. The surface unfortunately is rarely uniform and homogeneous, a more or less hydroxylized layer is present above most of the metal and organic surfaces, above this layer contaminants are usually deposited if the sample is not handle and store properly. In the field of Cultural Heritage we do not deal with what IUPAC define as **clean surface** but with surfaces where dust and dirt accumulated during the century creating several interfaces. Hence, every analysis might need to take into account these influences.

The model of the surface we are analyzing depends on the type of interaction used for probing the surface. Leach et al. [112] subdivide the interaction and the surface recorded in mainly three categories: mechanical surface, electromagnetic surface and electrical surface. The **mechanical surface** is defined in ISO 14406:2010[74] as *boundary of the erosion, by a sphere of radius r , of the locus of the centre of an ideal tactile sphere, also with radius r , rolled over the real surface of a work piece.* An important concept of this definition is that there are many different mechanical surfaces depending on the radius and, in fact, also the pressure exerted by the tactile sphere on the object. The same is true for the abstraction of the **electromagnetic surface** (ISO 14406:2010, 3.1.2)[74] where many different surfaces exist depending on the properties of the light used (wavelength, polarization state etc.). In the case of probing the surface with particles (photons, electrons etc.) IUPAC[98] defines the **experimental surface** as *that portion of the sample with which there is significant interaction with the particles or radiation used for excitation. It is the volume of sample required for analysis or the volume corresponding to the escape for the emitted radiation or particle, whichever is larger.* Unfortunately, this definition is quite ambiguous, because the first sentence seems to refer simply to the interaction of the radiation with the sample, the last sentence instead appears to refer only to the interaction with the sample that contributes to the signal recorded by the instrument, this latter sentence is hence apparently linked with the concept of escape depth. Where for **escape depth** IUPAC refers to *the distance into the sample measured from the physical surface from which all but a fraction $1/e$ of the particles or radiation detected have originated.* It must be stressed that the signal detected by the probe might be processed and filtered after that it reaches the sensor. Hence, the determination of the escape depth does not imply the determination of the

depth or the volume that contributes the most to our measurement of the surface.

A less common surface representation can be extracted measuring the variation of current density between a conductive tip and the surface to be measured varying the height of the tip. This type of surface is called **electrical surface**[112] and is used in techniques such as scanning tunneling microscopy (STM).

Eventually, similarly to electromagnetic surface, we could define an **acoustic surface** that can be retrieved measuring, for instance, the time-of-flight produced by the interaction with the object of ultra-sounds waves, mostly with frequencies in the range of Mega and Giga Hertz. This type of surface is not explicitly defined in literature but as will be shown in this chapter can be used for comparing the results obtained using conoscopic holography.

In the next sections I will present the problems related to the determination of the interfaces with a practical analogy.

5.1.2 The coastline mapping problems

The reader may find useful dealing with analogous problems at macro scale before diving into the micro and nanoscale. Historically cartographers were among the first scientists dealing with the problem of determining the boundary of interfaces[59]. Mapping an interface delimited by waves offer an interesting analogy (of course with its limitations) with the atomic level. In fact, some mathematical tools used in nanometrology have their roots in cartography. Hence, this analogy, used during the whole chapter, not only serves to introduce the reader to the concept but also it seems reasonable to try to apply to the current praxis in Cultural Heritage the concepts and the terminology developed in this field without duplicating the concepts.

If we imagine to map the coastline of a region, we could face different problems:

- How to define the water-land interface?
- What if the interface oscillates with time due to external factors?
- What instrument to use to take the measurement and at what resolution?

Besides these problems, the natural aging (in the case of the coastline, cost erosion) occurs but we consider this as the phenomenon to be measured, a measurand, rather than a factor affecting the measurement. Hence we start dealing with each problem individually.

5.2 Uncertainties in determining the interface

The first problem we may face is to decide where to define the water-land interface: shall we consider as border the wet or muddy land or only where clear water is present? Using instrumental techniques it is not always possible to arbitrarily choose what to consider the interface, hence the surface we are digitizing because, as we saw in the previous section, the interfaces that we are measuring depend on the physical principle that we are using[110]. For instance, when using an optical

technique the interface detected depends on the interaction of the radiation with the material and the processing carried out by the software for reconstructing the surface. Materials transparent to the optical radiation can cause artifacts, offset or can not be detected. Furthermore, the method used for determining the interface may give less accurate results — or artifact — depending on: the materials analyzed, the way in which we operate the instrument, and the features of the surface (e.g. steep edges). To overcome these uncertainties the following actions can be carried out:

- Identify materials that could be critical to acquire.
- Assess the performance of the instrument and its components under different conditions and over the materials identified in the previous step.
- Compare measurements of the same area with different techniques.
- Use reference standards with certified topography (and or stratigraphy).

Eventually, as we saw in section 5.1.1, the surface of a material is heterogeneous and composed of various layers with different thicknesses, which contribute in different ways to the signal collected using the instrument. In general an *a priori* knowledge of the material and its conservation status can help to predict the uncertainties in the final output. In the next subsections we will study different types of uncertainties introduced during the measurement. These uncertainties might be caused by the environment or by properties inherent to the sample under investigation. The study is carried out using different conoscopic holography scanning systems shown in chapter 3, however the tests shown here can be used for testing most of the technologies used for acquiring the surface of the artwork.

5.2.1 Materials properties critical for the acquisition

In general, most of the optical instruments for surface reconstruction and metrology work better when the surface is diffusive. The degree of transparency of the surface at the wavelength used for inspection is often a critical factor. Transparent materials can cause offset and artefacts on the acquisition, but also translucent materials may disturb the measurement because the back-scattered radiation in this case is produced by sub-superficial scattering coming from an escape depth of several millimeters. Specular objects are also challenging because the radiation is reflected at specific angles, avoiding the signal to be collected or producing highlights that saturate the detector.

5.2.2 Assessing the influences of transparent windows in front of the sensor

The transparency of some materials to the radiation used during the scan in some cases can be used to our advantage. When working in a museum it is preferable to avoid unnecessary movements of the objects from micro-climate inside the case to the laboratory. Hence, the transparency of the case windows to the laser (655 nm)

can be potentially exploited for measuring the artwork directly inside the case without the need to move the object. Another important aspect of measuring directly through optical windows, is the possibility to build a chamber for studying test materials in controlled environmental conditions and measure the objects inside the chambers without exposing the probe to the environmental conditions as shown in our study[123].

For assessing the influence of transparent windows in front of the sensor, I measured several profiles on a MB1030/M Aluminum Breadboard by Thorlabs (nominal flatness on an area of 300×300 mm of ± 150 μm) using the scanning conoscopic holography system. The breadboard is tilted at approximately 15 degrees for covering the whole working range of the probe without incurring to problems related to the angular coverage of the lens, which in this case is 170 degrees. The profiles are collected with and without the optical window using a ConoPoint-3 equipped with a 75 mm lens with a working distance of 7 cm. An average of the results is shown in figure 5.1.

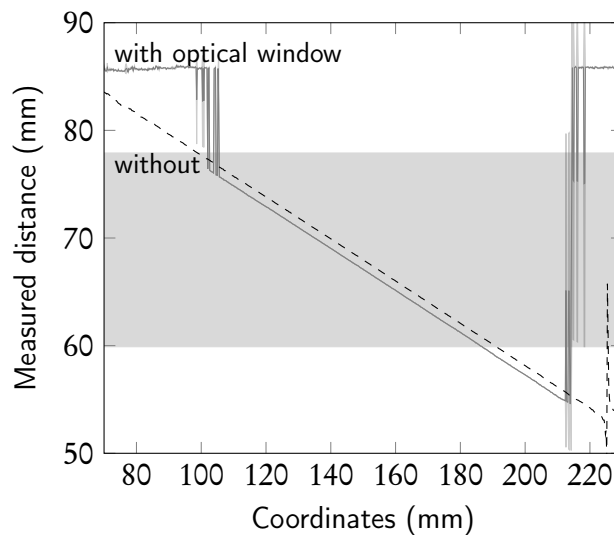


Figure 5.1: Measured profile of an inclined flat aluminum breadboard (dashed line) and of the same object thorough a 2 mm Polystyrene window (solid line). The grey band shows the nominal working range suggested by the company. The standard deviation is shown as thickness of the line. (Redrawn from data of our publication [123]).

Observing the two profiles we can see that the linearity of the distance measurement is preserved also when the transparent window is placed between the probe and the reference. If the window is stable and parallel to the motion direction it produces a fixed distance offset. Adding the distance offset to the measurement we can re-calibrate the measurement. However, we can notice that the window introduces also artefacts at the end of the working range. This results in a narrowing of the usable working range.

This study can be extended to any variation of the index of refraction of the medium between the probe and the sample. In theory, variation of the index of refraction of the air can cause uncertainties in the measurement. The fixed offset

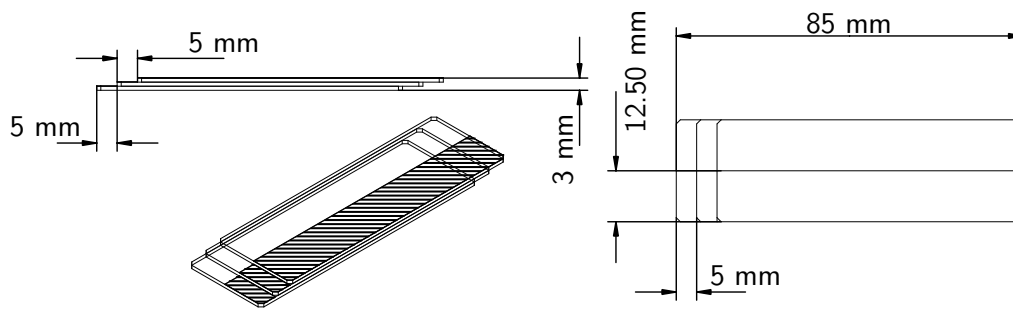


Figure 5.2: Drawings of the test object created using microscope slides. The hatched part of the sample is coated using a diffusive white tape. The distance refer to the distance between the lens and the test object.

may occur if the measurements are performed in air with a different index of refraction, while fluctuation of the index of refraction during the measurement may cause random errors. The variation of the index of refraction of the air can be calculated using, for instance, the equation proposed by Ciddor [31], however, in normal conditions the variation of refractive index of air is usually negligible.

5.2.3 Assessing the performance using half-transparent step metric test objects

For assessing the effects of scanning transparent objects or layers with the instrument I developed some test objects using materials easy to find. I built a first transparent test object using three Microscope slides by Menzel Gläser 76×26 mm with a thickness of 1 mm. I arranged the slides to form three steps. In ISO 5436-1 similar reference specimens are defined as Type A standard which are step-height standards with steps of known height. In our case, due to the high tolerances of the microscope slides thickness, I used this object for assessing the response of the instrument to transparent materials rather than for calibrating the instrument. For this scope I coated half of the samples using a white tape (PANfilm) as shown in figure 5.2. The tape used for coating half of the sample has a thickness of some microns hence can be used for creating a reference surface to be compared with the transparent surface adjacent to it. Because of the air gaps between the microscopic slides, there are a total of eight interfaces on the transparent part of the test object when positioned on the measurement plate. The test object has been measured with the different probes. Figure 5.3 shows the result using the ConoProbe-HD equipped with a 50 mm lens. I positioned the probe so that the middle step was at the standoff distance. We can observe that the measured step in the transparent part of the sample is considerably lower compared to the reference step on the coated part (dashed line). It is important to understand that the signal measured in the transparent part of the sample does not refer to the last interface (glass-air) but to the first one (between the measurement table and the air gap).

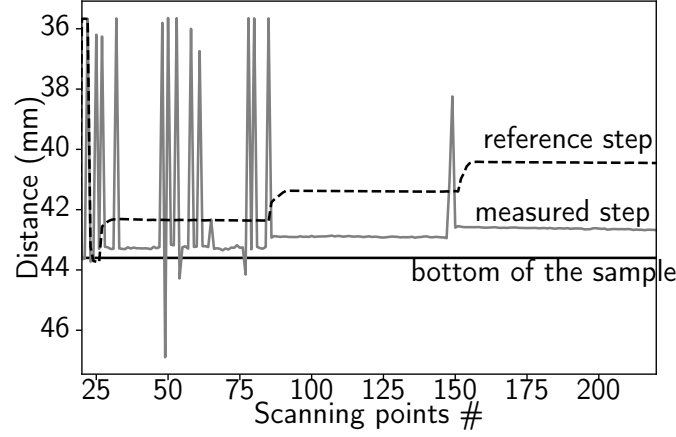


Figure 5.3: The test object measured using a ConoProbe-3HD equipped with a 50 mm lens. The dashed line refer to the measure on the opaque part of the sample, the solid line to the measurement on the transparent part of the sample.

5.2.4 A possible interpretation of the artifacts

A precise identification of the artifact can be hardly provided without knowing the processing carried out inside the probe for elaborating the interferograms. However, as explained in [163, 164] for a simple conoscopic module¹ (as shown in figure 3.5 at page 46 of chapter 3) the conoscopic corrected distance z_c is:

$$z_c = \sqrt{\frac{(\pi k_o) r^2}{\Delta\phi}} \quad (5.1)$$

where r is the lateral displacement from the geometrical axis passing through the lens and the birefringent crystal and k_o is a unit-less conoscopic parameter as defined in [163]. The phase difference $\Delta\phi$ of the two polarized wave-fronts passing through the crystal determines z_c , and this is generated from the interaction of the cone of light with the birefringent crystal. From Snel-Descartes law:

$$\frac{\sin \theta_2}{\sin \theta_1} = \frac{n_1}{n_2} \quad (5.2)$$

The refraction of the ray from the air (where $n_1 \simeq 1$) in the birefringent crystal with index of refraction (n_2) which is different for the ordinary (n_o) and extraordinary (n_e) ray can be described as follow :

$$\sin \theta_1 = n_o \sin \theta_2 \text{ with } n_1 \simeq 1 \quad (5.3)$$

$$\sin \theta_1 = n_e(\theta_1) \sin \theta_e \text{ with } n_1 \simeq 1 \quad (5.4)$$

¹The same reasoning can be applied to linear conoscopic modules used in this dissertation. Here the simplest configuration is used for sake of clarity.

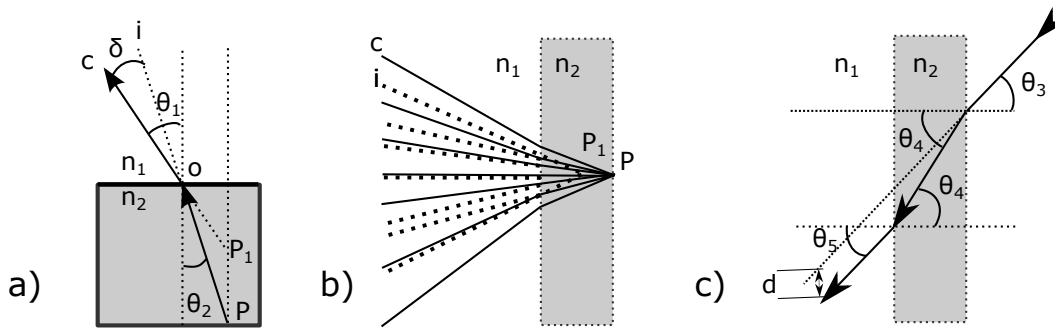


Figure 5.4: Different interactions of the light passing through transparent materials.

Where $n_e(\theta_1)$ tell us that the index of refraction depends on the angle at which the ray impinges the crystal that eventually influences the phase difference.

Figure 5.4 *a* shows different interactions of the light with transparent layers. The back-scattered radiation from the point P is deviated of an angle δ compared to the imaginary trajectory i that the ray would have followed if the two indexes of refraction were equal. The point source P generates the same wavefront of the point source P_1 in the air (as shown in figure 5.4 *b*), thus the phase difference $\Delta\phi$ is associated with the corrected distance z_c of the point P_1 creating the offset in the measurement.

Figure 5.4 *c* illustrates the case of optical windows placed between the lens and the object, as described in section 5.2.2. It can be demonstrated that the ray exits with the same angle ($\theta_3 = \theta_5$) but with a displacement d . The cone of light eventually, will appear as it was closer to the probe, generating an offset in the measurement of the distance.

It is harder to interpret the spikes and the large distances shown in figure 5.1 and 5.3 without knowing the processing carried out by the FPGA inside the probe. However, we must take into account that every interface is reflecting part of the radiation. Thus the final signal is composed of different interferograms overlapping. The algorithm used for determining the phase of the interferograms might fail to extract the phase of a single interface when these interferograms have similar intensity. Figure 5.3 at page 91 endorses this hypothesis: as we can see that the spikes artifacts appear in the edge of the steps where the probe probably is collecting simultaneously the cone of light passing from the two adjacent steps. Different artefacts appear also in the last step where the two interfaces are closer and this probably causes a mixing of the signals.

The same reasoning can be applied for interpreting the artifacts in figure 5.1 at page 89. When the two interfaces are closer the signals cannot be resolved while when the surface is too distant the back-scattered signal is too weak, probably attenuated by the interface and disturbed by the part of the laser light reflected by the transparent windows.

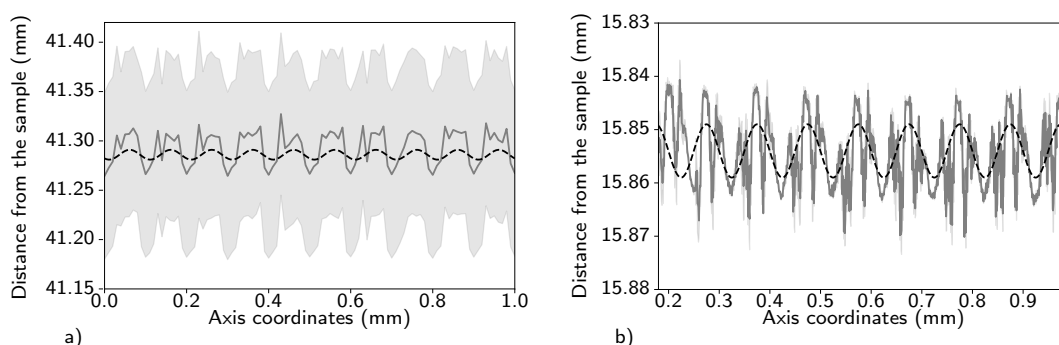


Figure 5.5: The solid gray line shows the profile acquired on the reference specimen 526X by Rubert & Co Ltd. using a ConoProbe-3HD equipped: a) with a 50 mm lens b) with a 25 mm lens. The gray area represent two standard deviations. The dashed black line is a synthetic sinusoidal profile generated with wavelength of $100\ \mu\text{m}$ and amplitude of $10\ \mu\text{m}$.

5.2.5 Assessing the performance on certified reference standard

Even though it is possible to assess artifacts testing various materials, for a quantifiable measurement of error in reproducing a surface topography a certified measurement specimens must be used. ISO 5436-1[93] defines the reference specimens for testing surface measuring instruments based on stylus. In this document, the standards are categorized regarding the morphology. These standards were initially designed to assess the performance of profile measurement using stylus profilometers but were then adopted also for optical instruments[93]. However, it must be taken into account that the performance of the instrument on the standard is often linked with the material used, this is often the case for optical instruments that are more sensitive to the properties of the materials (see section 5.2.1). Lately, ISO 25178[86] introduced various optical instruments for 3D surface areal measurements however the reference specimens of ISO 5436-1[93] are still maintained.

Reference specimens created specifically for areal optical instruments are very rare[61]. Furthermore, most of them are made only of metals and hence are an accurate estimation of the performance of the instruments on this material, while the performance might vary on other materials found in Cultural Heritage objects. However, even though I could not test the instrument on traceable certified specimen created *ad hoc* for Cultural Heritage the information retrieved using metal specimens give us an insight into the performance of the system.

For characterizing the instrument I used ISO 5436-1 type C standard that are reference specimens with a certified regular pattern. The 526X is a reference specimen made from electroformed nickel by Rubert & Co Ltd. This specimen has a regular sinusoidal pattern (hence more specifically it is classified as type C1) with a mean spacing between the peaks (R_{Sm}) of $100\ \mu\text{m}$ and the difference between the highest peak and the lowest valley (P_t) of $10\ \mu\text{m}$. In figure 5.5 the reference standard is acquired using a ConoProbe-3HD equipped with a 50 mm lens (figure a) and using a 25 mm lens (figure b). The gray line represents the average of three

profiles acquired by the instrument and the gray area is equal to two standard deviations. The dashed black line is a synthetic sinusoidal profile with a wavelength of $100\ \mu\text{m}$ and amplitude of $5\ \mu\text{m}$ generated for comparison. Bearing in mind that R_{sm} and P_t are statistical quantities and the certified surface profile will have some deviations from the ideal sinusoidal profile, we can get an insight on the order of magnitude of the error comparing these two profiles. The synthetic profile can be generated using the following equation:

$$y = \frac{P_t}{2} \cdot \sin\left(x \cdot \frac{2\pi}{R_{sm}} + \phi\right) + d_s \quad (5.5)$$

For a first estimation, we can use R_{sm} and P_t given by the manufacturer of the standard, while the two unknown variables are the distance from the reference plane (d_s) and the phase or translational offset (ϕ). After a manual pre-alignment of the profile adjusting d_s and ϕ for finding the initial guess for the unknown parameters, the reference synthetic sinusoidal profile can be fit using non-linear least squares. Thus we can calculate an estimation of the average error from the subtraction of the aligned synthetic profile (S) and measured profile (M) as follows:

$$\frac{1}{n} \sum_{i=0}^n |M_i - S_i| \quad (5.6)$$

Using the ConoProbe-3HD with the 50 mm lens I calculated an average error of $14.13\ \mu\text{m}$ with a standard uncertainty of $7.8\ \mu\text{m}$ while with the 25 mm lens I obtained a mean error of $4.59\ \mu\text{m}$ with a standard uncertainty of $3.5\ \mu\text{m}$. Because the standard was highly reflective I tested also the ConoProbe-3R with a 25 mm lens, which is the conoscopic probe optimized for the acquisition of specular materials. The results are however, similar to the ConoProbe-3HD with the 25 mm lens. I recorded a mean error of $4.50\ \mu\text{m}$ with a standard uncertainty of $2.5\ \mu\text{m}$. This is probably because although the sample is highly reflective is not specular hence we have only some minor improvements. A more canonical way of using the standard is to compute the metrological parameters and compare them with the certified values. The table 5.1 shows the results of the computed parameters and the difference with respect to the certified value. We compute Pt and Ra (arithmetical mean deviation of the assessed profile) as defined in ISO 4287:1997 [91]. I also recomputed Pt and Ra using the data obtained from the synthetic profile that I have generated.

The results indicate substantial differences between the certified value and the measured value. The specimen is particularly challenging for the probe because it presents a reflective surface and close steep edges.

Also the metrological parameters computed over the synthetic profile are slightly different from the certified value. The difference can be attributed to slight variation during the electroforming process, the algorithm, and the instrument used when characterizing the specimens. Furthermore, we have to bear in mind that these parameters are an average estimation thus it is normal that the synthetic profile might not be a completely accurate representation of the real object.

	Ra (micron)	Diff.	Pt (micron)	Diff.
ConoProbe-3HD (50 mm lens)	15.67	12.52	46.05	36.05
ConoProbe-3HD (25 mm lens)	5.37	2.22	24.91	14.91
ConoProbe-3R (25 mm lens)	6.26	3.11	22.64	12.64
Synthetic profile	3.18	0.03	10	0
Certified value (stylus profilometer)	3.15	n.a.	10	n.a.

Table 5.1: Comparison of the computed metrological parameters and the parameters measured using the different conoscopic probes. The Diff. column indicates the difference with the certified value of the standard.

5.2.6 Comparison of Conoscopic Holography measurement with Acoustic Microscopy

The usage of synthetic profile can not be always accurate for the identification of the biases because the least-square error tends *per se* to align the profile for minimizing the errors. Furthermore, as shown in the previous section the results of the assessment of the performance on certified reference standards, might not be extended to every kind of material. Because of the lack of certified standards with materials properties comparable with artwork materials it is important to assess the performance of the instruments on a wide range of materials in the form of mock-up and later on real artworks. However, the intrinsic variety and heterogeneity of the artworks often necessitates other strategies for identifying possible artifacts. The different critical aspects studied in the previous sections are usually combined together. During the analysis of artworks, it is common to work with metallic materials with multiple layers of transparent varnishes or coatings. Comparing analogous data acquired with other techniques is one of the possible routes to identify errors in the acquisition and improve the accuracy of the measurement. Comparing techniques that take advantage of completely different phenomena for retrieving the topography of the surface can be more effective for identifying the artifacts. In our study[122] I compared the data acquired with the conoscopic holography profilometer with the data acquired using acoustic microscopy.

Acoustic microscopy —as it will be explained later on— take advantage of different physical phenomena not linked to electromagnetic radiation and hence is less likely to find the same artifacts using the two techniques. Furthermore, the usage of this technique for surface metrology, in my opinion, has not received enough attention in the field [109, 112].

Acoustic microscopy uses ultrasonic waves produced by a piezoelectric transducer coupled with the object by means of a coupling gel to retrieve the topography of the object. The high-frequency and focused acoustic waves are back-scattered by the different interfaces encountered and recorded by the transducers. Processing the resulting time-of-flight signal allows computing the distance of the various interfaces.

In this study, I focused on the comparison of the digitization of the *physical surface*, hence I used only the interface between the gel and the samples from the SAM scan. I scanned a set of samples made of patinated bronze and several multi-layer



Figure 5.6: Photograph of patinated bronze mock-up with engraved the number “2” (see Fig. 5.7 for precise dimensions). Two different patination processes have been used while a stripe between them has been left as reference (left). Detail of the engraver grooves and the material scratches (right).

egg-tempera patches. A complete description of the samples and the motivation of the choice can be found in the public deliverable *A guide for multi-material palette preparation*², here I present only the information relevant to the study. I scanned these samples with the conoscopic holography setup based on a ConoProbe-3HD equipped with a 50 mm lens and compared the results with the scans on the same objects provided by Ormylia Foundation using Scanning Acoustic Microscopy (using Olympus™ 110MHz and 175MHz transducers mounted on Aereotech™ linear stages). Modern Scanning Acoustic Microscope with a conventional 300 MHz transducer can achieve lateral resolution 10 μm to 15 μm this resolution can be improved up to 1 μm with GHertz-SAM[181] and are hence comparable or better than the Conoscopic Holography sensors used in our study. Axial resolution is usually worse: with a 175 MHz transducers it is around 9 μm with detection limit 3 μm [173] while with 2 GHz transducers axial resolution can reach 0.60 μm [173].

The bronze samples were prepared by Opificio delle Pietre Dure (Florence) using the original varnish recipes, some parts of the sample are covered with the coatings (patinated) comprising the engravings, others are left without any coating for reference. Figure 5.6 shows a portion of the sample with two patinas applied and an engraving with the ID of the sample. The same areas of the sample have been acquired with acoustic microscopy and with the conoscopic holography set-up with a scanning step of 40 μm . We can observe that the acoustic microscopy scan is able to measure the grooves more accurately, the elliptical shape of the traces left by the engraver are visible and well defined. While the metal irregularities of the surface disturb the acquisition of the topography using conoscopic holography sensors. On the other hand, in the conoscopic holography scan, we can notice the small granules inside the patinated area that are not visible in the acoustic microscopy scan.

I also tested the two techniques on egg tempera data set produced by Ormylia Foundation. The egg tempera data set simulates a multi-layer egg-tempera painting using the original techniques and was made in Ormylia Art Diagnosis Center. The

²<https://ec.europa.eu/research/participants/documents/downloadPublic?documentIds=080166e5abb21b68&appId=PPGMS>

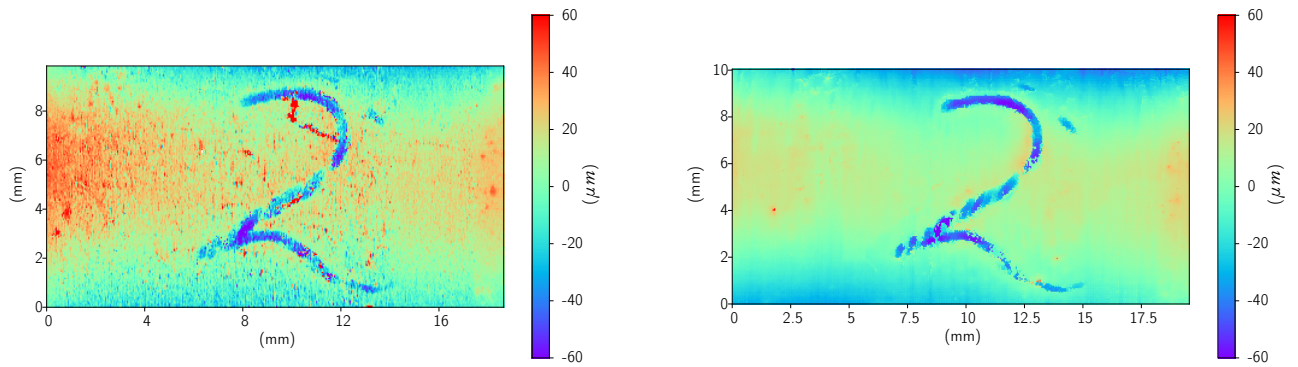


Figure 5.7: Comparison of the two techniques used for scanning a patinated bronze. On the left plot, the conoscopic holography scan, on the right plot, the acoustic microscopy scan.

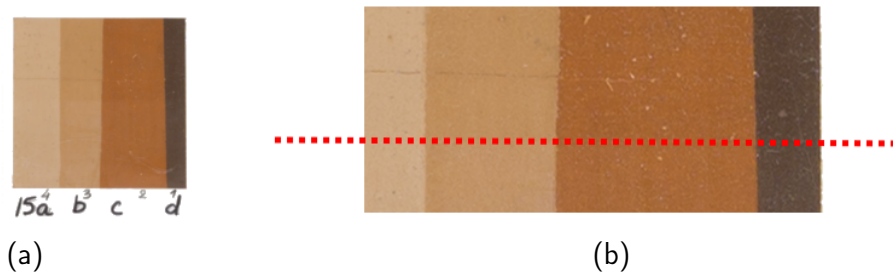


Figure 5.8: a) The egg tempera patch number 15 of the data set. Warm ochre mixed with lead white. b) The ROI investigated with the two techniques in figure 5.9. The part above dotted red line line is varnished.

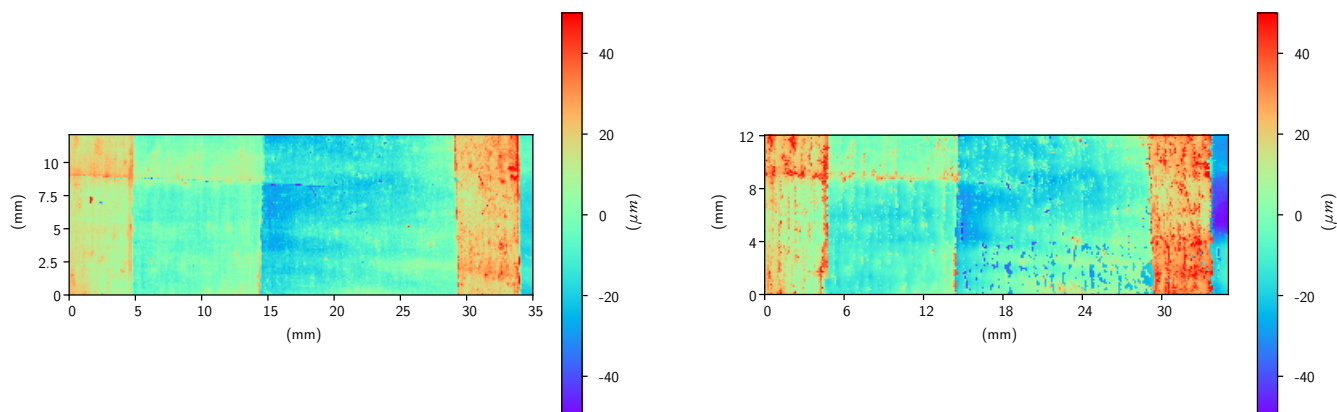


Figure 5.9: On the left conoscopic holography scan of the ROI shown in figure 5.8 *b*. On the right acoustic microscopy scan of the same area. Some artifacts can be noticed at the coordinates ($x \approx 14 - 30\text{ mm}$, $y \approx 0 - 4\text{ mm}$) these are probably bubbles formed when the coupling gel was applied.

panel is subdivided into 60 patches half of each patch has been varnished. In figure 5.8 we can see one of these patches and the region of interest (ROI). The ROI in figure 5.9 contains four different layers with decreasing reflectance. Above the red dashed line in 5.8 *b* the sample is varnished. In figure 5.9 we can see the comparison between the conoscopic holography scan and the acoustic microscopy scan. Some artifacts are visible on the acoustic microscopy scan (figure 5.9 right plot) that are not present on the conoscopic holography scan. These artefacts appear in the figure 5.9 as blue spots (that would be interpreted as negative values) on the bottom of the unvarnished part of the third paint stripe. Their origin can be probably linked to the formation of bubbles during the application of the coupling gel.

Another factor affecting the conoscopic holography measurement is the reflectance of the surface. When there is a high reflectance difference between the materials of the surface it could be impossible to optimize the acquisition parameters for acquiring the different areas in a single scan as we showed in our previous work[53]. Because acoustic reflectance and spectral reflectance are not always correlated, the combination of these two techniques can be used effectively for assessing and correcting the negative influences of the reflectance gradients.

Here I highlighted only a couple of examples of the artifacts that can be assessed, the next step is the improvement of the accuracy of the measurement and the correction of the artefacts based on the fusion of the data coming from the two sensors. This procedure that is normally called multisensor data fusion[64] however necessitates of seamless integration of the two instruments.

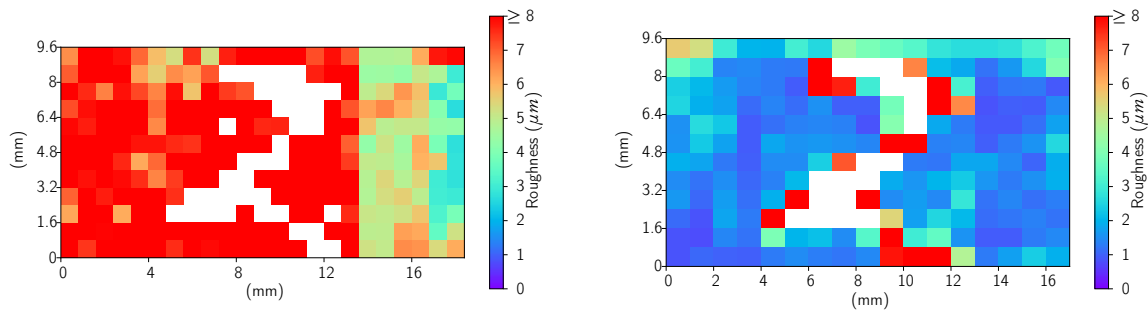



Figure 5.10: Subdivision of the conoscopic holography scan (left) and the acoustic microscopy scan (right) in $800\ \mu\text{m}$ square side patches and computation of S_q roughness parameter. A threshold has been used to exclude the patches with roughness greater than $15\ \mu\text{m}$ (in white in the picture). The roughness on the groove can not be computed effectively. Redrawn from my previous publication [122].

5.2.7 Towards a quantitative interpretation of the difference between the scans.

The quantitative evaluation of the differences between the results obtained from the two techniques poses some issues that should be addressed carefully for avoiding misinterpretations. For instance, the comparison of the results using subtractions or other methods for highlighting the differences and quantifying them into numbers have some drawbacks and requirements. First of all the two acquisitions should be carefully registered, software registration techniques are not always risk-free for this task. One particular problem is the correction of the tilting of the surfaces for avoiding errors shown in the previous chapter (cfr. Section 4.7.2). Little misregistrations can drastically affect the metrics, hence comparing for instance two profiles might be dangerous without the certainty of the exact registration of the profiles. Furthermore, we should compare scans that have not only the same scan step but also that are acquiring approximately the same sampling area, and this adds another layer of uncertainties that lower the significance of these calculations when are not done using a proper multi-modal system. I hence decided to leave these computations as external data, instead, I have highlighted the differences in the roughness computation computed on the single acquisitions.



The registration of some of the scans and the quantitative comparison can be found at the following link:
https://colab.research.google.com/github/giacomomarchioro/phdthesis/blob/master/jupyter%20notebook/Registering%20the%20arrays%20once%20they%20have%20been%20positioned.ipynb#scrollTo=jq-6x_jy0Cqn

In figure 5.10 is shown the computation of the roughness using the algorithm explained in 4.9.1.

In this case, I used a square patch with size $800\ \mu\text{m}$ after removing the tilting. Both measurements are carried out using a scan step of $40\ \mu\text{m}$ however the conoscopic holography set-up was operating in dynamic mode while the scanning acoustic microscope was operating in static mode. The conoscopic holography scan measures a roughness much higher compared to the acoustic microscope and it is able to differentiate between the varnished parts and the reference line. The scanning acoustic microscope scan shows lower roughness values due to the lower resolution of the probe. It is always wise to come back to the original surface map for interpreting the results, because as we saw in section 5.2.3 multilayered materials might be affected by artifacts that contribute to the estimation of the roughness parameters. Comparing the results with figure 5.7 we can observe that the roughness is due to small surface features (granules and engravings) and the mapping correlated with the patinated areas. The materials used in the first patinated areas formed some granules that did not dissolve causing an increase in the roughness, while on the right patinated areas a more homogeneous patina lowered the roughness caused by the irregularities of the reference surface, forming an even film.

I limited these quantitative analyses to the metal samples due to the fact that the Conoscopic Holography and the Scanning Acoustic Microscopy data sets were not acquired simultaneously neither in the same environmental conditions and this could have a negative influence in particular on hygroscopic materials that might vary depending on the environmental conditions. The next section will be devoted entirely to this topic.

One of the benefits of a multimodal scanning system is the possibility to increase the accuracy of quantitative comparison of the surface representations. A multi-modal system comprising these two sensors, as designed during the Scan4Reco project, will in fact allow to record the two measurements sequentially with a short temporal distance and furthermore can be used for a more accurate hardware registration of the two scans.

For producing a comparable scan the concepts explained in chapter 3 must not be forgotten. The sampled area and hence the lateral resolution is in fact related to the acquisition modality and only with an accurate design of the scanning the difference between the two lateral resolutions can be minimized.

5.3 Variation of the interface due to external forces

Even if we convene in the definition of the interface and we optimize our measurement procedure to identify and minimize errors and artifacts, we may experience that the interface position varies during the period of observation. The change of the position of the interface, moreover, may occur during the process of measurement compromising our survey. Coming back to the coastline mapping problem, we may experience these issues in particular during high tide or low tide of the tidal cycle. Thus, when measuring the coastline we have also to measure the level of the tide, if the cartographers measure the tide level while performing the measuring they call these measurements **tide-coordinated** otherwise if they predict the tide level using a model (mostly based on historical records) they call these

measurements **tide-predicted** [190, p. 122].

The “nano-cartographer” may face the same issues when measuring the surface of an object at the micro or nano level. For instance, the temperature or the relative humidity may affect the positions of the interfaces, because of thermal expansions or swellings due to the absorption of moisture and hence a rising in the moisture content (MC). However, reaching temperature-coordinated or MC-coordinated measurements may be harder than it seems. Measuring the temperature or the RH of the object, or worse only that of the environment, would be tantamount to the cartographer involved in the coastline mapping to know the mass of the moon: if there is not an understanding of the model governing the dynamics of the system and historical records of the object it is not possible to “coordinate” a set of parameters to the topography of the surface measured. This is due to the fact that different equilibria are involved, and could take a lot of time to reach their stationary state—assuming that it exists—at particular environmental parameters. However, if we leave the object in controlled conditions for an appropriate amount of time we can create a model for estimating factor-predicted measurements (i.e. without the need to measure directly the factor affecting the interface e.g. moisture content).

Eventually, the entire object and hence the absolute position of the interface may move while the measurement is carried out. The same, of course, applies to the observer (instrument). This is mainly due to environmental vibration, instability of the set-up and in some cases air flows. If the movement of the instrument and the surface to be measured is not controlled and taken into account the interface acquired may appear distorted.

In the next sections, I will study the methodologies for assessing this kind of uncertainties and quantify the spatio-temporal shape variations due to relative humidity fluctuations on different hygroscopic materials. The information collected is crucial for any longitudinal study involving the measurement of surface topology, or for long topography scans where environmental fluctuations might change the surface properties and morphology during the analysis. The first step of the assessment of the drift of the instruments as well as the samples properties is the identification of a ground-truth built using a stable reference material that will be the topic of the next section.

5.3.1 Reference materials

Working under controlled laboratory environmental conditions can considerably reduce the instrumental drifts related to thermal expansions and micro-movements of the set-up. In the set-up shown in my previous publication[123], the environmental variations are confined to the micro-climatic chamber. However, even in this case, some biases can happen due to the thermal expansion of the micro-climate chamber walls and this may cause a variable offset on the measurement and hence distortion (cfr. section 5.2.2). To ensure an accurate measurement, some stable and invariant material must be placed in proximity of the samples to be measured. These objects should have a thermal expansion close to zero, be insensitive to humidity variations, chemically stable and opaque at the wavelength used by

the optical profilometer. For an optimal acquisition, the surface of the standard must have a reflectance value similar to the object analyzed and sufficiently high to allow measurement with a good signal-to-noise ratio. Highly specular materials require a special set-up to be acquired hence the standard must be also diffusive. In this work, I used a round cylinder with diameter of 8×100 mm of Invar 36 produced by Polymet Reine Metalle (Lüneburg, Germany). This material has a very low expansion coefficient[152] and can be found for a reasonable price (less than 20 euros). I cut the cylinder into three pieces with a length of 5 mm, 45 mm and 50 mm to be used depending on the height of the sample to be measured.

Furthermore, for assessing any vibration induced by the air inflow I built a cantilever using a piece feeler gauge tape with a thickness of $50 \mu\text{m}$ thermally treated at approximately 450°C for matting the surface.

5.3.2 Monitoring the effects of relative humidity change on the dimensional stability of hygroscopic artworks.

The most challenging artwork materials to model are the hygroscopic ones. These include wood panels and statues, ivory, canvas but also some plastics used in contemporary art. Besides, the effects on the repeatability of the measurement, the study of the dimensional stability of the artworks and its effect on the conservation have important implications on determining the best environmental conditions for the artwork[125, 10]. For assessing the dimensional stability different techniques can be used including Fiber Bragg grating sensors[46], 3D laser scanning[68], structured light scanner [134, 136], speckle imaging[177]. A review can be found in literature[45]. In our previous study[123] I develop different set-ups for evaluating the effects of variation of relative humidity on hygroscopic materials. In general, two approaches are used for testing the dimensional stability: a passive approach, monitoring the effects of environmental changes occurring naturally[134, 136] or an active approach[7], inducing changes of relative humidity (RH) and temperature using different methods and studying the response of the object. For studying artworks under specific RH levels previous studies[7, 177] have taken advantage of the variation of vapour pressure of different salt solutions for reaching a specific level of RH. The variation of environmental temperature might, however, influence the equilibrium of the dissolved salt and the environment. Another approach is to use climate chambers[117], which however might pose some limitations on the integration with other sensors and on the budget.

In our project I developed a humid chamber based on an ultrasonic humidifier and a micro-controller.



The instructions and the firmware for building and testing the humidity chamber control system can be found at <https://github.com/giacomomarchioro/humiditychambercontrol>.

As mentioned in the previous section, it is important to understand that controlling or recording the environmental parameters is only the first step for an

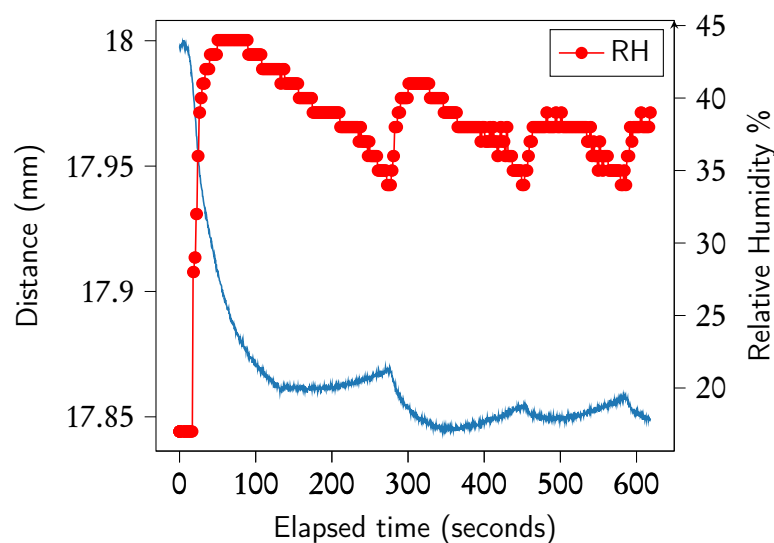


Figure 5.11: Displacement analysis of a piece of parchment at 25 °C inducing sudden variation of RH (circle marks).

accurate determination of the equilibrium inside the artwork. The moisture content can be determined experimentally[161] (and this is up to now one of the only methods for making real MC-coordinated measurement) or developing a model[44]. When the object reaches the equilibrium moisture content (EMC) it should also reach dimensional stability even though this might be affected also by other parameters[156]. A possible strategy is hence to keep the environmental parameters stable for a long time and, at the same time, keep assessing that the object shape is not changing by monitoring it with the technique chosen.

The responsivity of the artwork to the variation of RH can change depending on the material.

Due to my involvement in the digitization of the manuscripts of the Capitular Library of Verona I decided to study the dimensional stability of some samples of paper and parchment prepared using the traditional techniques. The dimensional stability of the manuscripts under digitization is very important when the exposure time is long (for instance for the acquisition of multi spectral images or induced fluorescence). Often the environmental conditions of the place where the objects are stored are different from the environmental conditions where the digitization takes place and it is hence very important to understand what displacement can be caused by the differences in relative humidity for acquiring sharp images.

Furthermore, the sheets of parchment and paper because of their limited volume theoretically reach the EMC more rapidly and hence are a good material for starting a study on the dimensional stability.

In figure 5.11 we can observe the swelling of a piece of lambskin parchment of 3×2 cm acquired using a ConoProbe-3HD (with a 25 mm lens) measuring the sample from the top in a small environmental chamber. We can notice that the piece of parchment responds very fast to the oscillations of relative humidity between 40 to 34 % that were induced artificially for testing the response. The latency of the humidity sensor used (a DHT-11 capacitive sensor, working at 1 Hz)

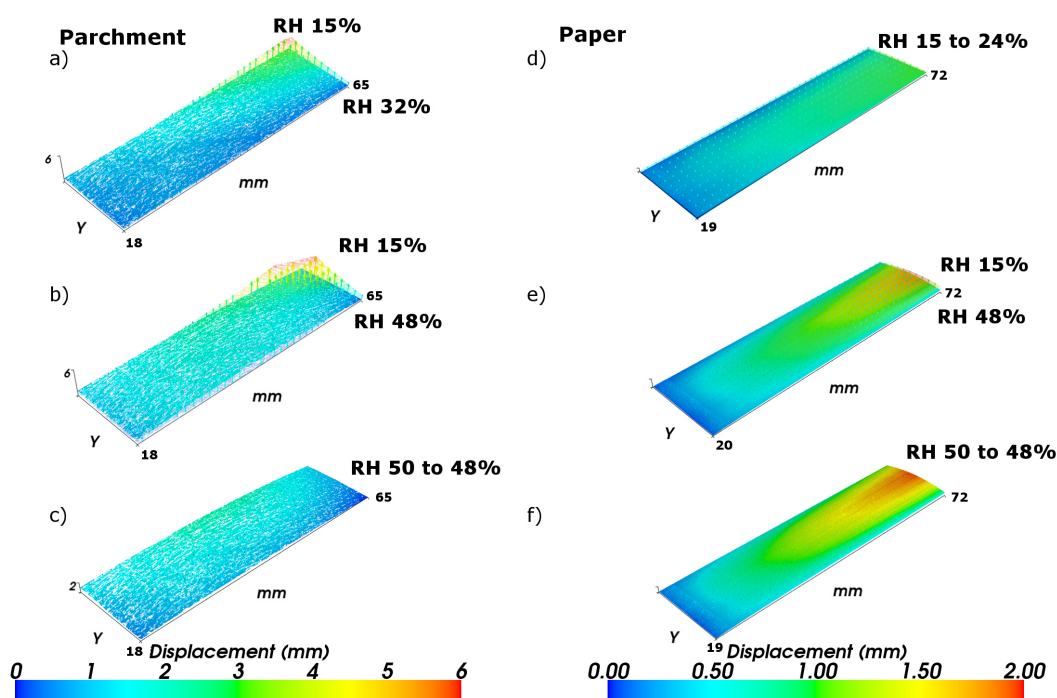


Figure 5.12: The analysis of sample of lambskin parchment deforming due to RH variation a) from 32% to 15%, b) from 48% to 15% c) 50 % to 48%. The same experiment is performed simultaneously to paper samples d), e), f). The samples are constrained using tape on the side indicated with the letter Y.

is probably greater compared to the response of the parchment. Of course, the entity of the displacement depends largely on the position where the measurement is performed. Measuring a single point as in figure 5.11 has several limitations on determining how the swelling of the material occurs. In figure 5.12 I performed a scan of paper and parchment samples enclosed in a small environmental chamber containing four 75×26 mm pieces of lambskin parchment prepared using the traditional technique and 40 g paper. Using some tape I blocked the short sides of the sample to the bottom of the humid chamber leaving the other sides unconstrained and free to move. In this way, I have tried to maximize the possibility of the parchment moving freely. For assuring that I was measuring the parchment at equilibrium I left the sample inside the humid chamber at the desired RH condition for approximately five hours.

In figure 5.12 we can observe the deformation of the parchment and paper samples. For each sample I analyzed a ROI of 18×65 mm. Because the measurements are performed using the same reference system it is possible to achieve an accuracy below the micron in the registration of the different acquisitions at different RH values. Each sample shows the surface at two different RH values. The transparent surface is linked with the surface below by means of arrows showing the displacement computed for each coordinate. We notice that the parchment, as expected, is more sensitive to RH variations showing out of plane bending of several millimetres on the unconstrained side. Lowering the RH to 15% the parchment tends to

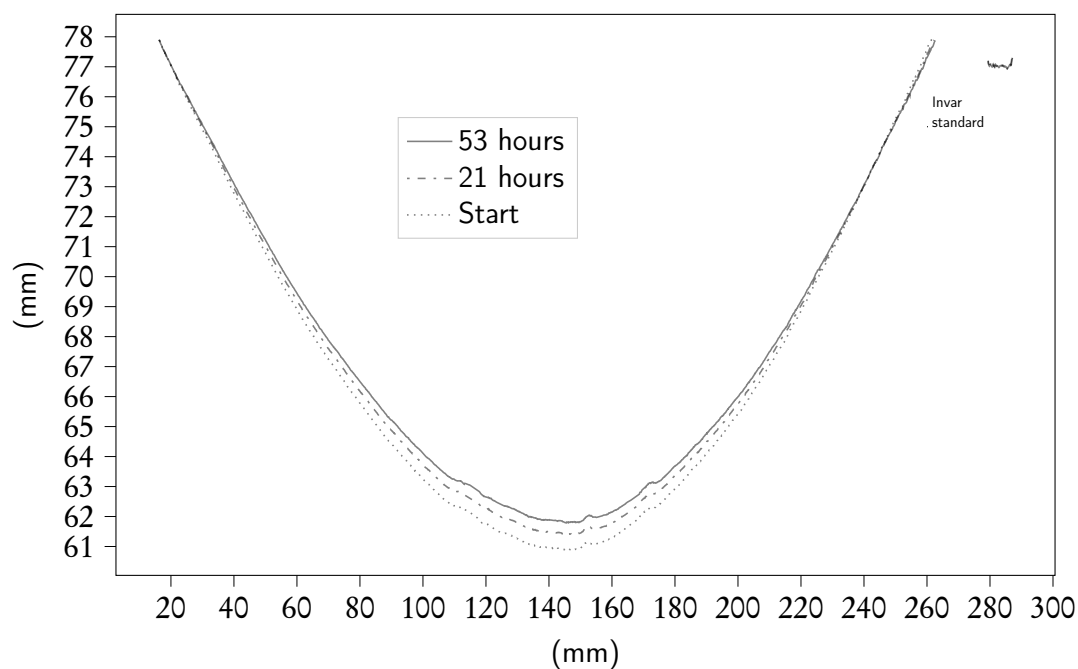


Figure 5.13: Three profiles measured along the curvature of the icons. We can see the deformation during a ramp to 50 % RH after 21 and 53 hours. On the top right corner the profile of the Invar reference cylinder.

deform, similar behaviours are reported in recent studies[104]. The deformation is not homogeneous affecting mostly the top right corner. The paper is less sensitive to the variation of RH and I recorded limited deformation on the order of 50-500 μm . Regarding the paper, the deformation is more uniform causing curvature parallel to the short side of the sample. A similar curvature was reported for composite paper samples[41].

This experiment can be extended to other hygroscopic materials and artworks adapting the humid chamber to contain larger objects. However, increasing the dimension of the humid chamber implies a harder control over the environmental condition that might not be homogeneous in all the volume.

I repeated the study on a 19th century wooden icon for assessing the usability of this technique for real artwork. The icon was stored at RH of 15% for several days. In this experiment, after exposing the artwork to a humid environment the curvature of the icon slowly decreases absorbing humidity. We can notice in figure 5.13 that after 53 hours the icon moved of approximately 1 mm that corresponds to an average rate of displacement of $18 \mu\text{m h}^{-1}$. Tornari et al.[180] found on wooden samples with a thickness 1 cm under RH variations from 45 to 80% a rate of displacement ranging from approximately 25 to $250 \mu\text{m h}^{-1}$. However, we must bear in mind that historical woods and complex artefacts such icons might behave differently compared to modern woods without any treatment and pictorial layer.

In groups of three scans, I measured the icon curvature at uneven time intervals with a time interval between each scan of ten minutes. The pattern of deformation

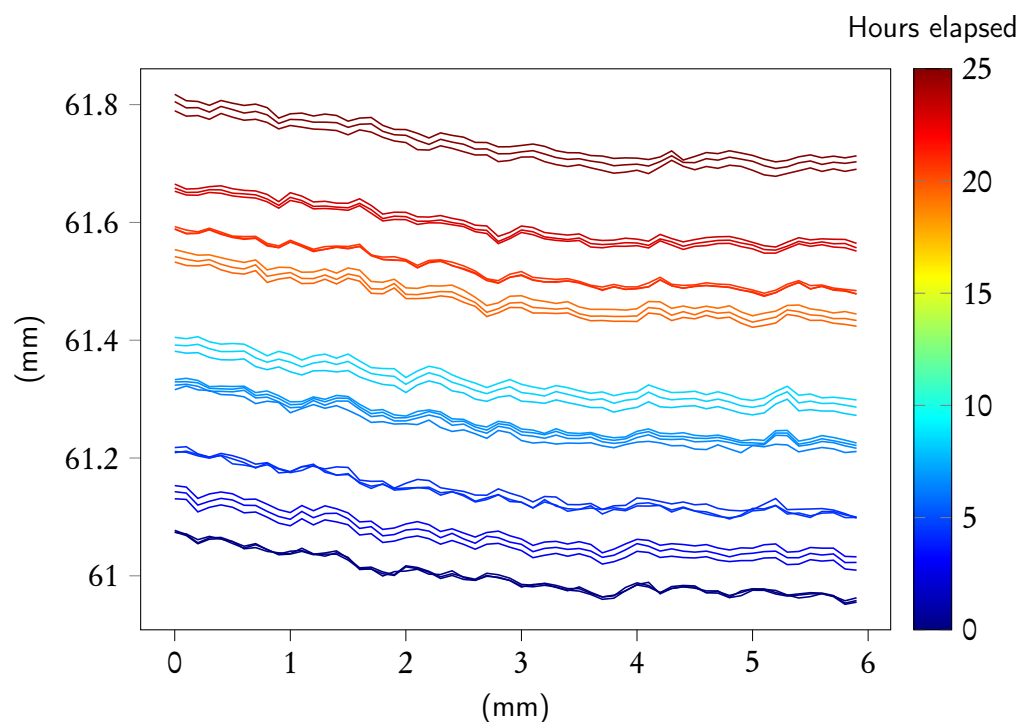


Figure 5.14: The series of profiles collected following the curvature of the icon transitioning from 15 % to 50 % RH.

on the portion of the profile is shown in figure 5.13. An average standard error uncertainty of $2.5 \mu\text{m}$ was determined on three consecutive scans before starting the humidification process: for each position was calculated the standard deviation of the three measurements and the standards deviations were averaged. The three initial scans are shown, overlapped, on the bottom of figure 5.14. We can notice that, before starting the humidification process, the object was in a steady state, at or closed to the dimensional stability. From this analysis we can estimate the velocity of the deformation of the object. In this case, because I worked with a real artwork I humidified the chamber gradually. From these series, it is possible to calculate an average velocity of displacement for each point of the profile. In this specific case, I estimated an average displacement velocity of 10 nm s^{-1} on the top of the curvature.

The rate of displacement could be an important parameter for assessing any deformation that might happen when scanning an object which has not reached the dimensional stability. Knowing the time needed for a single profile scan we can understand the entity of the displacement from the beginning to the end of the profile acquisition. In figure 5.14 I calculated a displacement of 170 nm at the end of the measurement of a profile scanned at 15 mm s^{-1} .

In this study, because I was working with a real artwork I limited the stress to the artwork, and the displacement is well below the repeatability of the instrument. However, special care must be taken when measuring hygroscopic artworks, in uncontrolled conditions or when the object was previously stored in an environment with different environmental conditions because the bias on the

scan might become noticeable, in particular during a long scan. The practice of performing scans during the night must be considered as well. This practice is widely adopted in the environments with visitors for avoiding the inconvenience of measuring during the opening hours but the excursions in RH might be considerable. These uncertainties highlight the importance of storing also information about the scanning pattern used as I mention in section 3.3.1. Knowing what was the starting and the end point of the scan and the pattern followed allows to better identify, and possibly correct, the resulting distortion on the surface mode due to the deformation of the object or the movements of the set-up.

5.4 The coastline paradox

“An embarrassing doubt arose as to whether actual frontiers were so intricate as to invalidate that otherwise promising theory”

—L.F. Richardson [150]

Solving —or mitigating— the coastline mapping problems gives us the confidence for assessing the survey of the interface under investigation. However, when we use the final survey for calculating parameters for describing the interface (e.g. length, area, roughness ...) we may find a strong dependence of these parameters with:

- the constraints we pose at the beginning of the measuring campaign (such as instrument, the resolution, and the scan step used).
- the processing procedure we use to calculate them.
- the part of the survey that we are analyzing.

The axial and lateral resolutions of the instrument and the scanning step determine, up to a certain point, the computed metrological parameters of the object.

In this section, I will use another concept introduced during the study of coastlines to highlight one important caveat when assessing the uncertainties and interpreting the results of complex and irregular surfaces. For this purpose, I will recall the historical background and perform the experiment that led to the discovery.

In a study published posthumously in 1960[150], Lewis F. Richardson tried to understand the relation between the length of the common boundary between two countries and their likeliness to start a war against each other. To measure the coastline Richardson used a divider on printed maps of the countries. The algorithm that follows (algorithm 1) describes in detail the manual procedure used

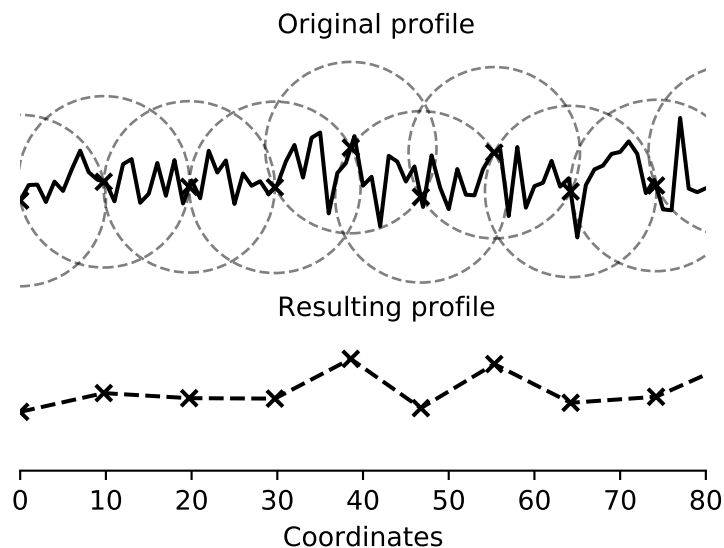


Figure 5.15: Example of the generalization of the procedure used by Richardson in his classical paper on a generic profile. Notice that some circles intersect the profile in many points, in this case the first intersection found following the profile along the direction of motion is used.

by Richardson.

Result: Length of the coastline or generic profile.
 Choose the distance between the divider spikes (the radius);
 Choose the direction of motion (clock-wise or counterclockwise);
 Choose a starting point on the coastline;
 Place one spike of the divider on the starting point;
while *Intersection do not overstep the starting point.* **do**
 Find the intersections of the other spike with the border;
 Position the spike on the first intersection found following the profile
 along the direction of motion;
 Record that you moved the divider;
end
 Multiply the times you moved the divider for distance between the
 divider spikes.

Algorithm 1: The procedure used by Richardson for determining the length of the coastline of the countries.

The procedure can be generalized for any polygonal chain, finding the intersections of circles with radius equal to the distances between the spikes of the divider instead of the intersections with the divider. The result of this procedure applied

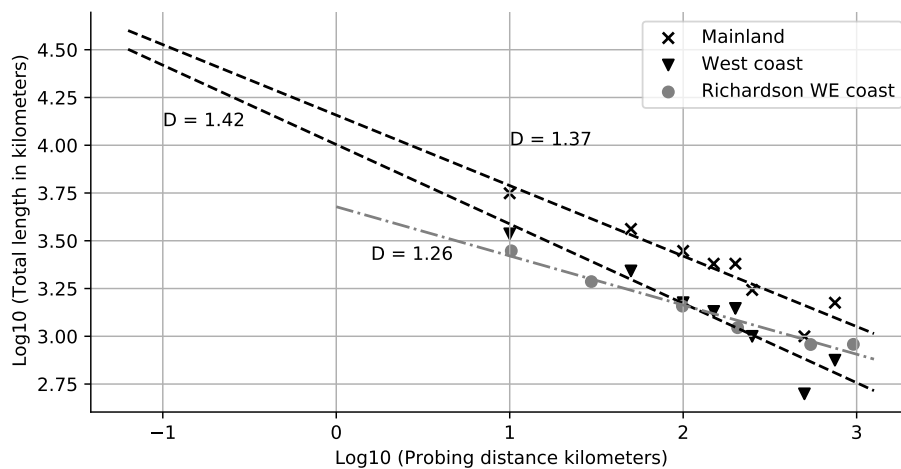



Figure 5.16: Log-Log plot of the total length of the whole coastline of the Great Britain (x) marker, the west coast of Great Britain and the original data computed by Richardson in his paper over the west coast of the Great Britain[150] against the probing distance.

to a profile is shown in figure 5.15.

I performed the experiment proposed by Richardson writing an algorithm in Python and using a survey of the coastline of Great Britain from a public data set available online[185].



The complete experiment can be reproduced at the following link: <https://colab.research.google.com/github/giacomomarchioro/phdthesis/blob/master/jupyter%20notebook/3%20-%20Introduction%20to%20fractal%20dimensions.ipynb>

Figure 5.16 reports in log-log scale the total length of the Great Britain coastline measured using different probing distances (in our case different circle's radii). The whole coastline of the mainland is measured with radii ranging from 80 meters to 160 kilometers. The results are compared with the computation applied only to the west coast (as the original paper) and the data retrieved by the corresponding publication [150]. In all the cases the total length of the coast decreases increasing the radius of the circle. This gave rise to what is called the **coastline paradox**: the apparent indeterminability of the length of the coastline due to its strong dependence on the method and resolution used to measure it. The reason for this behaviour is intuitive once understood how the method used for measuring the interface affects the final length of the coastline (see figure 5.15 and figure 5.17). In general, it can be proved starting from the axiom that the length of a line between two points is the minimum distance between them, resulting in every other path—especially if it is irregular—having a length greater than the line connecting the two sampled point. However, the implications and the corrections deserve special



Figure 5.17: Application of the algorithm proposed by Richardson using a radius (divider spacing) of: a) 80 m, b) 40 km, c) 100 km, d) 160 km. Superimposed to the coastline of Britain.

care and attention. The concept of the coastline paradox can be generalized to areas and to many computations involving the topography of the surface. Most of the metrological parameters shown in chapter 4 depend on the initial conditions: these include the resolution of the instrument, the cut-off filtering but also the sampling length and the sampling area. Hence, the standardization of the procedures and the precise description of the processing it is a crucial step for allowing the comparison between the results.

5.4.1 Richardson effect and fractal dimension

It is worth mentioning that another important aspect of the paper by Richardson was the fact that the results had an exponential trend. Thus we can linearize the data by computing the logarithm and fitting a line to the points as shown in the plot in figure 5.16 which is often called **Richardson plot**. Must be stressed that this result is not implied in the coastline paradox. Every measurement sampling a polyline different from a straight line will suffer from the coastline paradox but not every result of the measurement of a polyline will have a linear trend in the Richardson plot. Richardson proved this implicitly by applying the procedure he used to a circle and showing that in the log-log plot had a different trend.

The fact the coastline measurement follows a power law and can be linearized allow to retrieving what is known as a **fractal dimension**. In fact, this can be computed using the angular coefficient (m) of the linear fitting for determining a parameter D , defined as $1 + m$. Mandelbrot[121] used this parameter for introducing the concept of fractal geometry. There is often some confusion regarding the concepts, and the term **Richardson effect** is used sometimes as a synonym of the coastline paradox[188] sometimes as a synonym of the fractal properties of the coastline[128] or of generic materials[153].

The term fractal is often ambiguous and sometimes it is referred to any irregular surface as well as more formally to “*a set for which the Hausdorff-Besicovitch dimension strictly exceeds the topological dimension*”[120]. In general, the term **statistical self-similarity** [121] is used to indicate that the statistical properties of the object follow a power law when computed at different scales. The statistical self-similarity of some objects and the use of fractal dimensions are apparently one possible way to avoid the uncertainties linked to the measurement and give a scale-

independent characterization of the surface. However, we must consider that the fractal dimension can be computed in several ways the method that I used which is called “*yardstick method*”³ is only one of the possible methods that can be used for computing the fractal dimension and each one might return results with varying accuracy[116].

5.5 Summary

In this chapter, I gave an overview of the definitions of the surfaces across different fields aiming to offer a more precise interpretation of the meaning of the data collected and easing the possibility to compare it with data coming from other techniques at different scales.

Similarly to the problems related to the coastline mapping, also in our case, we have to consider: the uncertainties in determining the interface, the variations of the interface due to external forces and eventually the intrinsic uncertainties linked to the process we used for measuring the surface.

For the first problem, reference materials can be used for evaluating the response of the techniques and the artifacts.

I have studied how transparent materials influence the measurement retrieved using the conoscopic probes, showing that the linearity of the measurement is preserved even though an offset and a lowering of the signal quality is present in the final results.

I used an ISO 5436-1 type C reference specimen to evaluate the performance of the probe on reflective metallic objects. It proved useful for estimating the accuracy of the measurement with the certainty of a traceable standard. The properties of these standards are however similar only to a sub-set of the materials found in cultural heritage diagnostics, namely reflective metals.

Due to the lack of traceable reference specimens using materials with properties similar to the one used in cultural heritage diagnostics other strategies must be developed for assessing the performance for each measurement.

I compared the conoscopic holography scans performed on reference bronze e egg tempera samples with the acoustic microscopy scans provided by Ormylia Foundation.

I showed how the acoustic surface retrieved from the acoustic microscopy scan can be compared with the conoscopic holography scan for spotting artifacts. The acoustic surface, which is often neglected in surface metrology, can be effectively used on reflective metals samples. For taking advantage of the information of the two techniques a complete sensor-fusion process should be carried out. A multi-modal system is probably the best option for carrying out the data fusion of the two scans and easing the quantitative comparison.

The variations of the interfaces due to external forces (e.g. fluctuations of relative humidity (RH), temperature and vibrations) can compromise the metrological analysis. One of the possible solutions is to *coordinate* the various parameters (temperature, moisture content, vibrations ...) to the analysis or *predict* the pa-

³In fact Richardson used probably a nautical divider.

rameters knowing the environmental conditions (e.g. predict the moisture content from the RH trends).

Particularly, challenging is to assess and understand the influences of RH on hygroscopic materials. For this task, I built and presented an apparatus for carrying out dimensional metrology controlling the RH levels using an ultrasonic humidifier. I tested the response and the dimensional stability of parchment, paper samples and a wooden icon. The aim of this study was to test the usability of this apparatus based on conoscopic holography and to have some indications regarding the dimensional variations that we might expect when analyzing these materials. We must bear in mind that the scanning process can last many hours and hence a dimensional instability can lead to deformations and artifacts on the topological map.

Finally, I used the concept of the coastline paradox for highlighting the dependence of the results on the measuring condition. I performed, using a Python algorithm, the experiment used by Richardson in his publication, clarifying the concepts linked to the fractal analysis.

6

Case study

In this section I present and report some applications where I used the microprofilometer for specific tasks proposed by end-users (conservators and conservator scientists). Most of the data collected can be access and tested.

6.1 Introduction

The aim of this chapter is to illustrate practically the usage of the instrument in real scenarios. Hence, the case study will be centered on the usage of the instrument rather than on an extensive discussion of the case study results. The first section of each case study will contain a brief description of the case study and the materials under investigation. The second and the third section of each case study will deal respectively with the practical aspects for carrying out the analysis and on the data analysis. In fact, this important piece of information is often not reported in publications and texts but is relevant for the implementation of future researches using the instrument. The structure and the discussion of each case study try to give all these practical information and motivations supporting the choices made for each case study. A more detailed discussion on the topic of each case study can be found in the cited publications.

6.2 Effectiveness of monitoring aging process in metals and pictorial layers.

6.2.1 Aim and description of the study

The understanding of the ageing of the materials is one fundamental step for the conservation of Cultural Heritage. One of the goals of Scan4Reco project (Grant

	Metals	Pictorial layers	Protectives
Degradation phenomena	Deposition, Embrittlement, Allotropic transformation, Corrosion : (Pitting, Crevice corrosion, Filiform corrosion)	Deposition, flakes, detachments, losses	Deposition, flakes, detachments, losses
Ageing phenomena	Oxidation (related to patina formation)	Craquelure	(Craquelure)
Mechanical damage	Scratches, dents, fractures	Scratches, dents, fractures	Scratches

Table 6.1: Some of the processes that induce morphological variations of the surface.

agreement ID: 665091) was to create an aging model for silver, bronze and egg tempera materials.

The information retrieved using conoscopic holography systems aimed to understand the morphological variations on the surface of the artefacts.

In fact, depending on the material, the environmental conditions, and the conservation history several physicochemical phenomena modify the original surface at different scales.

Besides the physicochemical phenomena, during the conservation history of the material the morphological variations of the surface are also mechanical: related to the wear of the object caused by its fruition.

Table 6.1 summarizes the most common morphological variations of the surface during the conservation history of metals and organic layers. Effective monitoring of the conservation status of the surface must be carried on taking into account the contribution of each phenomenon which eventually determines the overall conservative status of the surface and it can be related or promoted by others. For an effective characterization, the morphological variation must be acquired at a scale that allows digitalization of an area representative of the alteration that took place. For instance, different information can be retrieved by analyzing a craquelure pattern on a canvas[22], in this case, large sampling areas are required to fully describe the alteration while for analyzing the morphological variation due to the formation of the patina is needed an instrument able to acquire smaller areas with higher accuracy. It is hence important to know at which scale alterations of the surface occur and so which instrument can be used for acquiring the information regarding the morphological variation. To address this question the following subsections describe the most common aging phenomena affecting the morphology of the surface of the selected materials.

Copper aging

Formation of cuprite round structures are reported with a diameter that goes from 65-70 nm (within 70 min. 80 % RH). SO₂ catalyzes the reaction forming structures with a diameter of 150 nm layers thickness goes from 35 to 40 nm depending on the relative humidity[103].

Silver aging

Alteration of the surface of silvers is due mostly to the formation of corrosion films, which are not uniform and can be composed of many different corrosion products (e.g. Ag₂O, Ag₂CO₃, Ag₂S, Ag₂SO₄, AgCl, AgNO₃). There is still an open debate regarding which of these corrosion products is most common. Capelo et al.[26], after leaving silver coupons for one year in the chapel and in the museum of Porto Cathedral, observed corrosion films with a thickness between 0.22 and 9.63 nm, mainly composed of silver oxides. Exposing silver coated quartz crystals to humidity and 250 ppm of SO₂ [103] results in the formation of round structures of Ag₂O with a diameter of 50-70 nm and heights of 5 nm that contributes to the increase of the overall roughness of the samples from 2 to 4 nanometers. For these samples, the corrosion layer goes asymptotic to a limit value of 1.1 nm. Silvers sulphide is another possible corrosion product found in museum artifacts. Layers of silver sulphide with a thickness of 250 Angstrom, change the appearance of the sample causing a yellowing of the sample [73], although it has been shown that weathering in SO₂ enriched atmosphere cause the formation of silver oxides, must be taken into account that COS, carbonyl sulphide, is actually the most abundant sulfur compound in the atmosphere.

Bronze aging

Aging of bronze varies depending on the type of alloy used. After 13 days of treatments in a salt cabinet (5% solution NaCl (pH 6.5) ASTM B117-03) Gallese et al.[54] found a thickness loss ranging from 0.1 a 3.5 micron while leaving the sample in a climate chamber for 30 days (R.H. up to 85% 1ppm of SO₂) found a thickness loss ranging 0.3 to 0.8 micron. Corrosion products of the bronze include: cuprite, leadchloride, couprous chloride and the four isomers of copper trihydroxide[158].

Pictorial layers and varnishes aging

The alteration of organic films such as pictorial layers and varnishes is driven by many mechanisms involved in the polymerization and formation of the film. A comprehensive treatment of these mechanisms involved in artificial ageing can be found in literature [47]. Most of the topological effects of the ageing of the pictorial layers and varnishes are related to stress caused by tensions due to the polymerization or the deformation of the support where the film is applied. This stress can cause the formation of cracks or cracquelure[22] that eventually lead to the detachment and the loss of the film.

Average scan time...	... for one sample	... for the samples collection	... for the study
Egg tempera	1h. 10 min.	87 h.	350 h.
Bronze	3 h. 10 min.	31 h. 30 min.	126 h.
Silver	2 h. 40 min	47 h.	188 h.

Table 6.2: Average scan times for each sample typology.

6.2.2 Materials and methods

Opificio delle Pietre Dure (OPD) prepared a sample collection containing 10 silver samples and 10 bronze samples with different varnishes. Ormylia foundation prepared a set of egg tempera patches on a wood panel, containing 60 different pigments mixtures. All the samples were aged in three steps, and they were acquired before and after the aging process. A complete description of the preparation of the samples and the artificial ageing applied to them can be accessed online¹.

For acquiring the samples I used the conoscopic system mounted in its vertical configuration placed on an optical table for isolating the system from environmental vibrations. A ConoPoint-3HD conoscopic probe was equipped with a 50H lens with a measurement range of 2 millimetres and an accuracy of 2.5 microns. The scan was performed while the horizontal axis was moving at a constant speed of 10 mm/sec. The scanning step was set to 50 microns for the egg tempera and for bronze samples, while it was set to 25 microns for the silver samples.

6.2.3 Acquisition times

Table 6.2 reports the average time for scanning each sample typology. For acquiring some samples with multiple materials, it might be necessary to perform more than one scan optimizing the scanning parameters (i.e. laser power) for each material. The time requirements for acquisition at this resolution are on the order of hours for sample. Besides the actual scanning time must be considered that table 6.2 does not include the time required for positioning the sample and setting the system, which usually requires approximately 15 minutes for each sample. Furthermore, it must be taken into account that often the scan must be repeated to find the best acquisition parameters or to correct any acquisition error.

6.2.4 Data analysis

A complete analysis of the results on bronze and silver samples can be found in literature[32], the data collected on the bronze samples has been used in other studies highlighting the possibilities to use neural networks for investigating the surface topography[43]. Hence, here I focus on the topological features of the egg tempera data set.

Figure 6.1 shows a 3D rendering of a scan of the sample 6 composed of hematite and a white pigment dispersed in egg yolk and water. We can observe the cre-

¹<https://ec.europa.eu/research/participants/documents/downloadPublic?documentIds=080166e5abb21b68&appId=PPGMS>

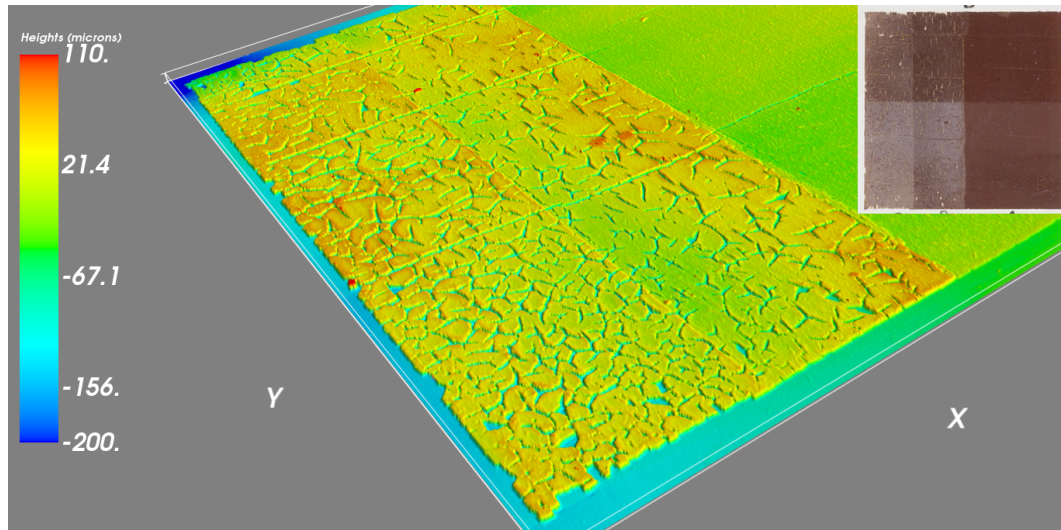


Figure 6.1: 3D rendering of a egg tempera patch after the aging process.

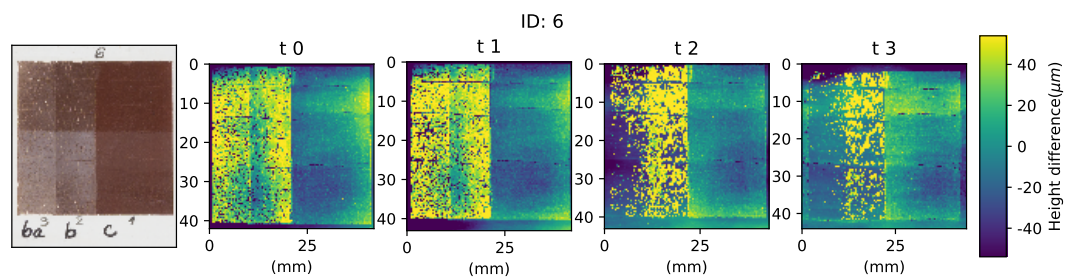


Figure 6.2: Height difference from the reference plane of the egg tempera sample (6) after three aging steps.

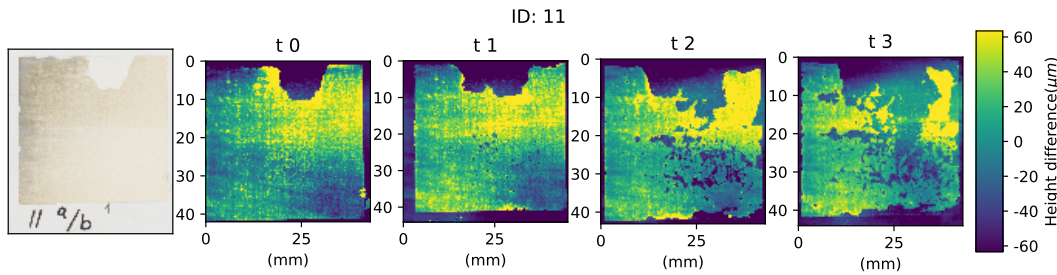


Figure 6.3: Height difference from the reference plane of the egg tempera sample (11) after three aging steps.

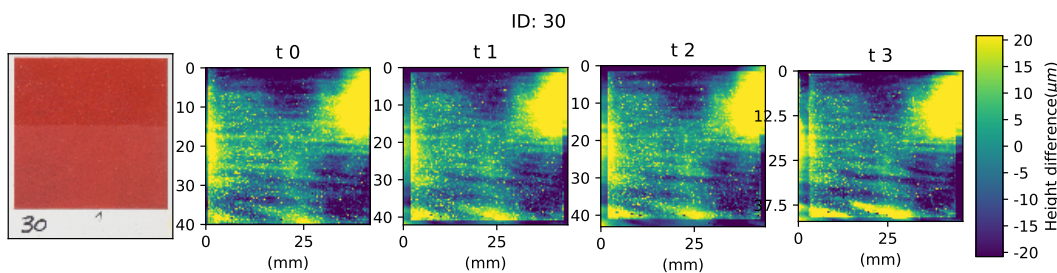


Figure 6.4: Height difference from the reference plane of the egg tempera sample (30) after three aging steps.

quelure on the layers due to the desiccation of the egg tempera and three horizontal cracks across the sample. These three cracks are due to the deformation of the support caused by natural aging. These are already present before the artificial aging in the scan performed in October 2016 (t_0), and appear to be stable during the three aging steps and the successive scans performed in May 2017 (t_1), October 2017 (t_2) and May 2018 (t_3) (figure 6.2). Most of the pictorial layer of the stripe *a* and *b* of figure 6.2 is lost at the end of the third aging step.

From the analysis of the ageing sequence, it seems that before the layer detached it raises some tens of microns. This phenomenon can be observed also on the sample 11 (figure 6.3). In this sample some of the pictorial layer areas that are lost rise of some tens of microns from the initial step. This can be observed for instance on the top of the sample from t_0 to t_1 and also on the bottom from t_1 to t_2 and from from t_2 to t_3 . The capability of detecting the detachments of the pictorial layers in the early stages seems a promising application of these analyses for the preventive consolidation of the pictorial layers.

Some of the patches resist to artificial ageing without any evident loss of materials (figure 6.4). In the sample 30 we can also observe some granules on the surface and how the pictorial layer reproduces the surface morphology of the wood panel underneath the pictorial layer.

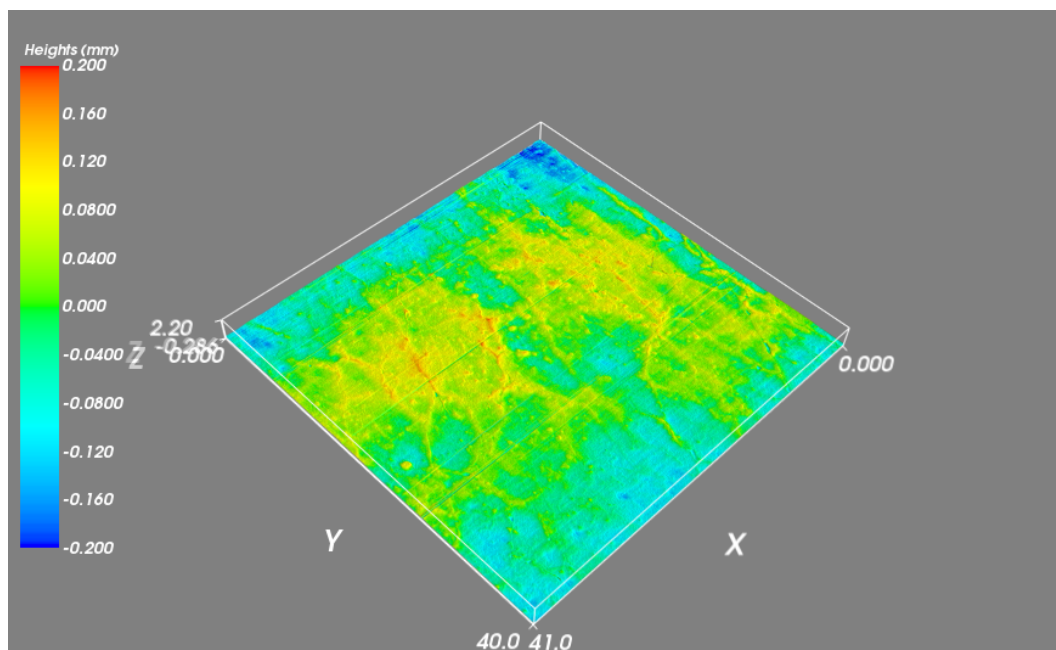



Figure 6.5: 3D rendering of conoscopic holography scan of the wrinkling on the Pala Pesaro.

	<p>The results on the other 57 samples can be accessed at the following link: https://colab.research.google.com/github/giacomomarchioro/phdthesis/blob/master/jupyter%20notebook/Analysis_eggtempera_dataset.ipynb</p>
---	---

6.2.5 Discussions and conclusion

The analysis of bronze and silver samples did not highlight identifiable topological features after the aging steps. At statistical level some differences can be observed using the standard ISO parameters for calculating the properties of the surface[32] these could be linked with the alteration of the varnishes combined with the corrosion process. In general, must be considered that as shown in chapter 5 when semi-transparent layers are present some uncertainties may interfere with the results.

The modifications of the topology of egg-tempera pictorial layers influence the surface also at a bigger scale. Granules, craquelure and other surface feature can be monitored during the aging. A particularly interesting use of the microprofilometric analysis could be the early detection of the detachments.

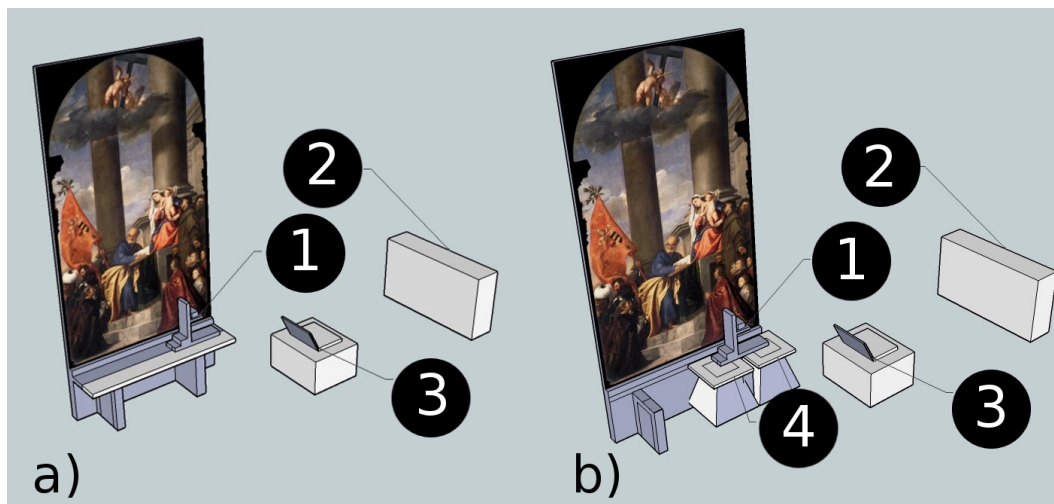


Figure 6.6: 3D reconstruction of the set-up and the environment during the acquisitions a) with the microprofilometer on the same structure of the canvas b) with the microprofilometer on a separate structure. 1. microprofilometer 2. heating system 3. terminal 4. stools for maintaining the profilometer separated from the metal structure.

6.3 Microprofilometric analyses of crack pattern on Pesaro Madonna (Venice)

6.3.1 Aim and description of the study

The restorer working on Pesaro Madonna—a large canvas (*telero*) painted by Titian between 1519 and 1526— wanted to assess how the cleaning was affecting some wrinkling present on the canvas. The crack pattern, as shown in figure 6.5, have positive peaks and can be compared to the crack pattern obtained by Mecklenburg[125] due to deformation of the canvas caused by environmental fluctuations. High temperature and relative humidity fluctuations are very likely to happen during the conservation history of the painting in the Fari church where it is still conserved. Another possible hypothesis on the origin of the crack pattern is linked to the ageing process of the varnish that could have created some strain on the areas.

6.3.2 Timeline and report of the measurements

The measurements started on Wednesday the first of February 2017, for acquiring the uncleaned surface, the surface was cleaned and hence a second measurement was performed on the third of February. The first set of measurements present several artifacts and so the scan of the canvas was repeated during the following week from the sixth to the eleventh.

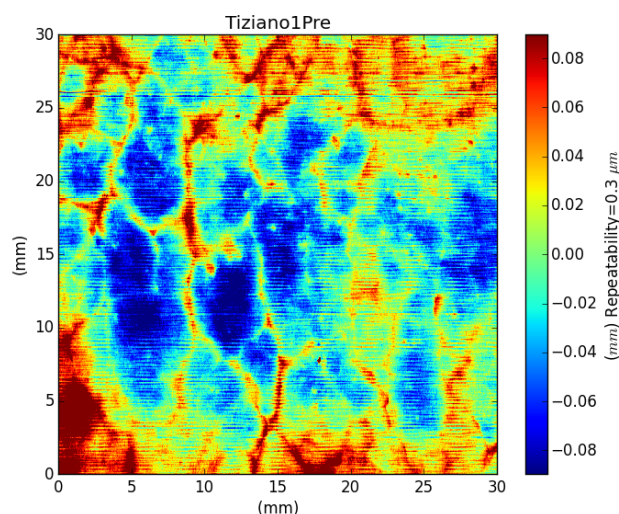


Figure 6.7: A ROI of the initial measurement performed on the painting.

The first set of measurements process

Initially the set-up was installed as depicted in figure 6.6 *a*, the microprofilometer was built in its vertical configuration with a ConoPoint-3 equipped with a 50 mm lens. It was placed on two wooden boards over the iron structure that supported the painting. The first measurements had a scan step of $25\ \mu\text{m}$ acquiring an area of $45\ \text{mm} \times 80\ \text{mm}$ in 3 hours and 15 minutes. This produced array with a size of about 10.5 millions of points, due to the large size was difficult to handle with the tools developed and the PC of the microprofilometer. Furthermore as shown in figure 6.7 the acquisition had several artifacts.

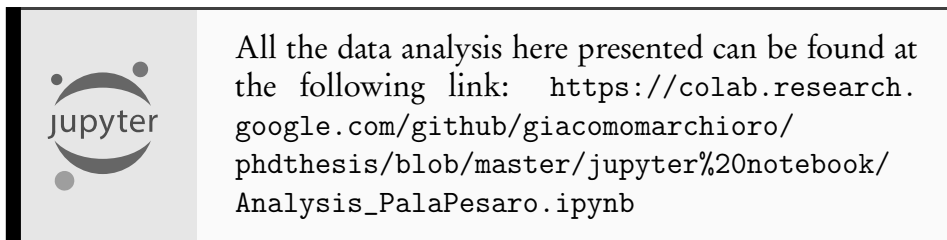
The second set of measurements

To solve the problems of the first set of measurements several parameters have been changed and tested. The first attempt was to reduce the axis speed from $25\ \text{mm s}^{-1}$ to $10\ \text{mm s}^{-1}$. This velocity has been chosen because it is a good trade off between vibrations reduction and velocity. The axis speed has been set to $10\ \text{mm s}^{-1}$ nevertheless, the acquisition still had the artifacts. The test has been repeated using $15\ \text{mm s}^{-1}$ with similar results.

At this point was clear that some source of error was external to the microprofilometer itself. The first hypothesis was that the painting was moving micro-metrically and this caused the acquisition artifacts. The microprofilometer could be the source of vibrations that moved the painting. The microprofilometer has been removed from the wooden boards and placed on two stools (as shown in figure 6.6 *b*), in this way the vibrations transfer between the two systems (the canvas and the microprofilometer) was limited. The first measurement with this new set-up showed improvements. Other sources of interference have been evaluated, the more probable source of interference was the heating system which using fans could create air flows able to move the canvas. The air conditioner has been switched off.

For acquiring these measurements I used the same configuration of the previous set of measurements changing the scan step to $50\ \mu\text{m}$ and acquiring an area of $40\ \text{mm} \times 41\ \text{mm}$ hence reducing the acquisition time to 47 minutes maintaining the velocity to $15\ \text{mm s}^{-1}$.

6.3.3 Data analysis



Evaluation of the artifacts

Before starting evaluating the differences between the scans before and after the cleaning, I performed a quality control step and an exploratory analysis of the data using the Hierarchical Peak-Valley analysis (HPVA) (that was developed in section 4.11.1). Figure 6.8 shows clearly that the vertical levels are still dominated by artifacts, that appear as horizontal lines. The left part of the acquisition is less affected.

These artifacts are probably due to periodic fluctuations of the canvas but further studies should be performed for assessing the precise cause.

Estimation of the difference before and after the cleaning

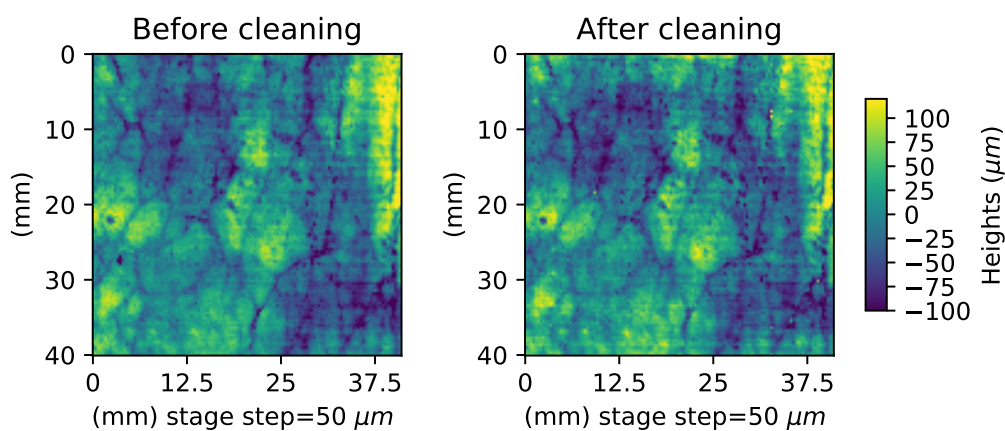


Figure 6.9: The acquisition of the cleaned area before and after the cleaning process.

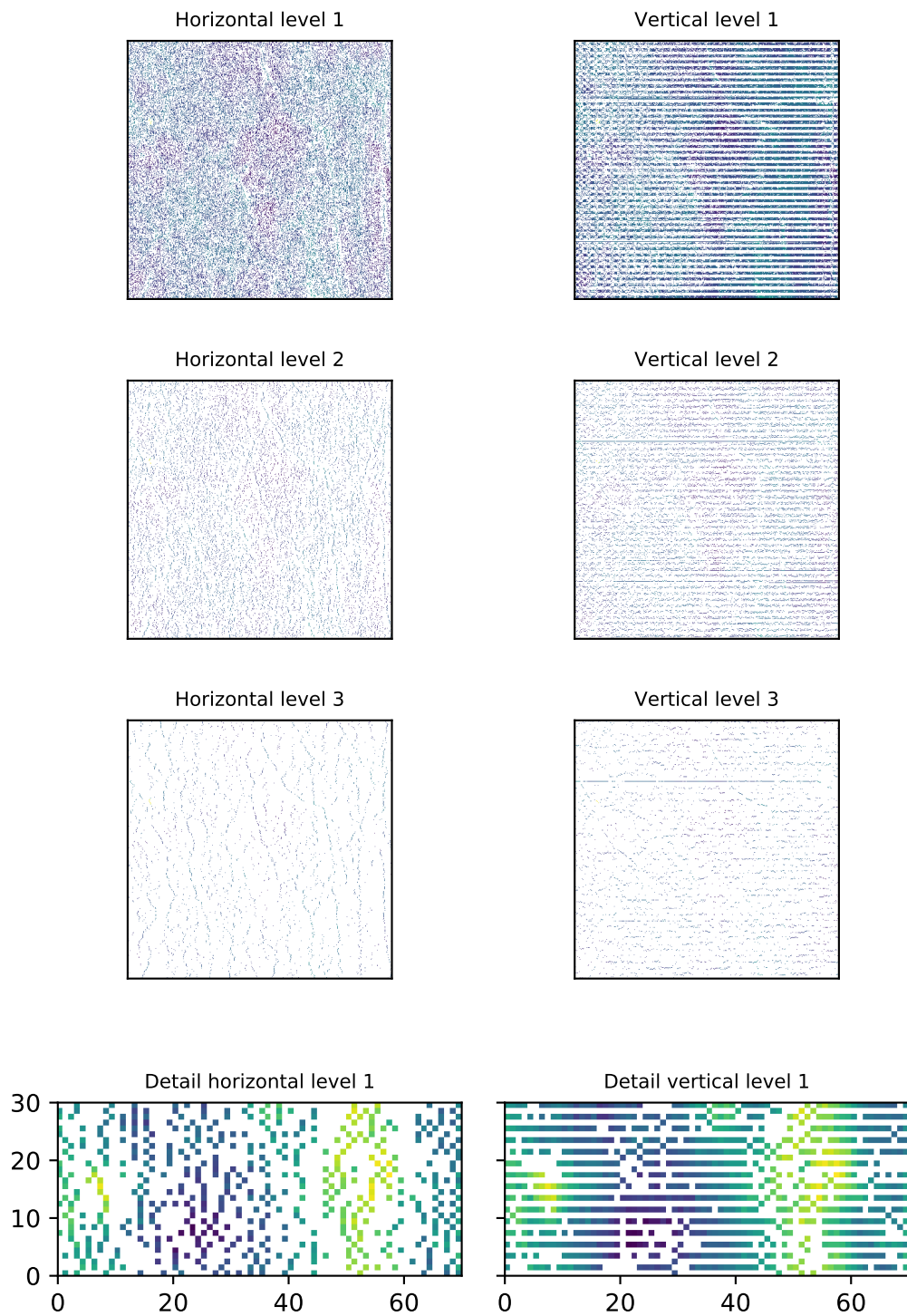


Figure 6.8: The peaks found using HPVA on a region of the Peasaro Madonna.

The instrument was kept with the stages fixed in the same position before and after the cleaning to ensure accurate registration of the acquisitions. When the restorer was cleaning the area the probe was moved outside the working area of the restorer but the linear stages were left in position.

Ideally, this will result in a perfect registration of the acquisition on the plane of the painting surface as well as on the perpendicular to the plane of the painting. The re-positioning of the probe on the plane of the painting did not cause any noticeable errors. However, the canvas moved and produced an offset of around one millimeter on the distance measurement from the probe to the canvas. Hence for retrieving the difference between the two scans I fitted a plane and performed a levelling subtracting the fitted planes to the original data. This process may introduce some uncertainties in the calculation of the differences. Figure 6.9 shows the resulting levelled scan before and after the cleaning process. We can observe that the cleaning did not affect visibly the crack pattern. For calculating the heights difference (D) between the scans, I subtracted the levelled scan acquired before the cleaning (B) to the levelled scan acquired after the cleaning (A).

$$D = A - B$$

In this way, the negative values mean that material has been removed and the positive values mean that material has been added. This interpretation, however, is limited due to the fact that the difference is computed on the levelled surface so any distortions introduced by the levelling process can be counted as positive or negative variations. The result is shown in figure 6.10.

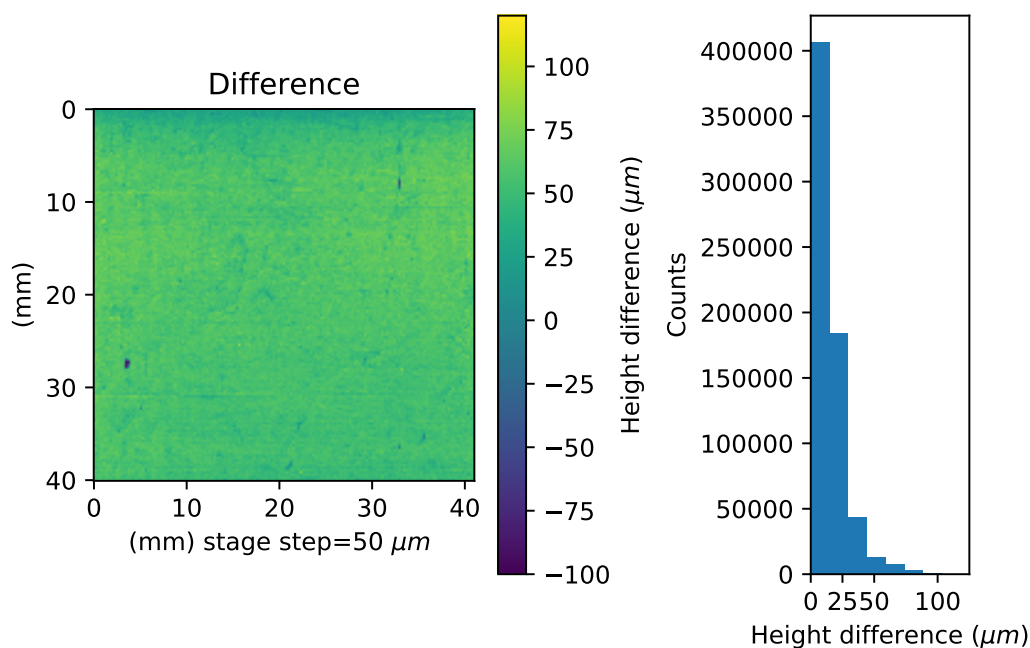


Figure 6.10: The difference between the levelled scan after the cleaning and the levelled scan before the cleaning.

We can notice that a small lump has been removed on the left side of the area. A mean absolute difference of 14 μm has been calculated as follows:

$$\left(\frac{1}{n}\right) \sum_{i=1}^n |D_i|$$

On the histogram of figure 6.10 we can observe the distribution of the height difference. These are usually always less than 100 μm . Some of the highest values are registered on the lump and others on the peaks of the crack pattern.

Some uncertainties are however linked to these results. One factor that might raise some uncertainty is linked to the aforementioned errors introduced by the levelling process, another is due to the fact the cleaning was removing a semi-transparent varnish that could have introduced some offset on the measured values.

6.3.4 Discussions and conclusion

For monitoring the effects of cleaning procedure on surface morphology directly on-site the environmental inferences must be taken into account.

The interference due to air flows (e.g. conditioning systems, open windows ...) can be critical for the measurements mostly when the object has a very large surface (i.e. ten squared meters).

The possibility to re-position the system to acquire exactly the same area before and after the cleaning is crucial for this type of analyses. In this study, we were able to acquire the same area but with a distance offset.

The crack pattern was analyzed before and after the cleaning qualitatively and quantitatively levelling the surface and showing height differences lower than 100 μm . The accuracy of these results is always linked with the uncertainties introduced by the scanning patterns, transparency of the materials and processing. However, it is still an important tool for assessing the scales at which the cleaning effects is affecting the surface.

6.4 Testing an innovative cleaning procedure for tarnished silver samples

6.4.1 Aim and description of the study

The Opificio delle Pietre Dure (OPD) is one of the main institutions working on the conservation of Cultural Heritage in Italy. They asked our lab to assess the effect of an innovative procedure for cleaning tarnished silver on a silver test sample (see figure 6.11). The test sample was prepared by OPD using a silver coupon polished with sandpaper in a predominant direction. This gave a lay to the sample easily identifiable to the naked eye. The samples were tarnished artificially. Seven different squared patches (areas labelled from A1 to G1) with a side of about 5 mm were treated with different cleaning methodologies. The restorer cleaned the patch with a motion perpendicularly to the lay direction. Next to each patch, an untreated patch was left as reference (areas labelled from A2 to G2).



Figure 6.11: Part of the silver sample reconstructed using the data from the conoscopic holography scan and a texture obtained fusing multiple photos taken with a Nikon D810.

Here I report the activity that I carried out, that consisted in acquiring the samples with conoscopic holography scanning system and comparing the results with the results I obtained scanning the samples using Atomic Force Microscopy (AFM). Furthermore, I have tested some of the algorithms that I have shown in the previous sections. Further analysis and explanations can be found in the open-access proceedings[39].

6.4.2 Methods

Due to the small scales at which these modifications happen, I used the conoscopic holography set-up that allowed to reach the highest performance on the sample. The ConoPoint-3R with a 25 mm lens has laser spot size of $5\ \mu\text{m}$ and a repeatability of $0.06\ \mu\text{m}$. To take advantage of the small laser spot size, the stage step was set to $5\ \mu\text{m}$ and an axis velocity of $5\ \text{mm s}^{-1}$ this determined a scan duration for each patch of about half an hour.

To identify and avoid the effects of the scanning artifacts along the direction of motion, I scanned the samples in different orientations: parallel to the direction of motion and with an inclination of 45 degrees.

We decided to compare the measurements obtained using our scanning system with the scan obtained using Atomic Force Microscopy (AFM). In collaboration with LAPS laboratory at the University of Verona. I scanned in semi-contact mode five times each patch of the sample using a NT-MDT -SMENA A AFM. The scan length of each scan was of $60\ \mu\text{m}$, each row containing 256 measurements.

6.4.3 Data analysis

After the assessment of the quality of the measurements, I examined visually the conoscopic holography scans to find any trace of the cleaning process left by the cleaning tools. Some traces perpendicular to the original lay seems visible in the

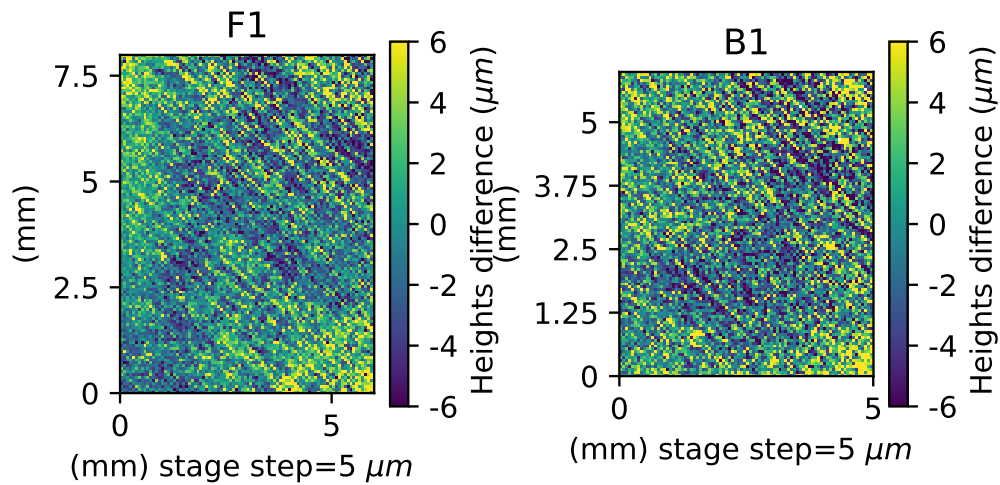


Figure 6.12: Conoscopic Holography heights difference map of two areas of the sampled cleaned using different methods.

area F1 as shown in figure 6.12. In general, the inside of the area seems lower compared to the borders (see figure 6.12 area B1) and this could be due to the cleaning process. I have tested the homogeneity of the roughness on the different patches dividing the areas into sub-patches of different size. Figure 6.13 shows the results dividing the sample B1, after leveling the surface, in squared patches with a side of $750\ \mu\text{m}$. For each patch, I computed the roughness parameter S_q . The roughness has values around $2\ \mu\text{m}$ for most of the patches except for some areas where the computed roughness is greater than $5\ \mu\text{m}$.

The arrays with the computed S_q values can be used for characterizing the surface. In figure 6.14, for each pair of cleaned and reference area, I have plotted the distribution of the roughness retrieved by applying the algorithm to each cleaned and uncleaned area. However, the average roughness of the cleaned area (left boxplot of the pair) does not appear significantly different from the average roughness of the uncleaned area used as reference (right boxplot of the pair). Some differences between the cleaning methods can be extracted as shown in our publication [39].

Analysis using the Atomic Force Microscope

Figure 6.15a shows the scan of a portion of the cleaned sample (C1). Even in this case, the samples were tilted of 45 degrees for easing the identification of artifacts due to the scanning process. On the figure the scale bar represents the width of the laser spot of the conoscopic holography system. We can observe that the widths of the pattern of the surface are on the order of 15 to $50\ \mu\text{m}$. The height difference between the maximum and the minimum of this small portion is only of $452\ \text{nm}$. Some scratches perpendicular to the main lay of the surface are visible in figure 6.15b. These scratches can be attributed to the rubber used for cleaning the area. However, these traces have a width of a few microns and depth below the micron,

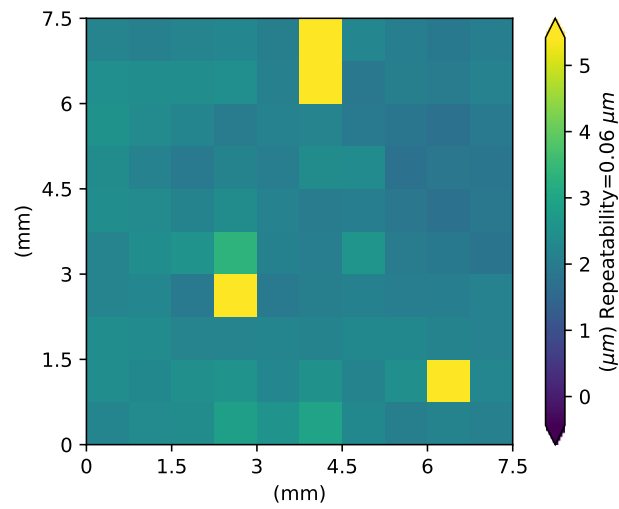


Figure 6.13: Subdivision of the sample B1, after levelling, in squared patches with side 750 µm and computation of Sq parameter for each patch.

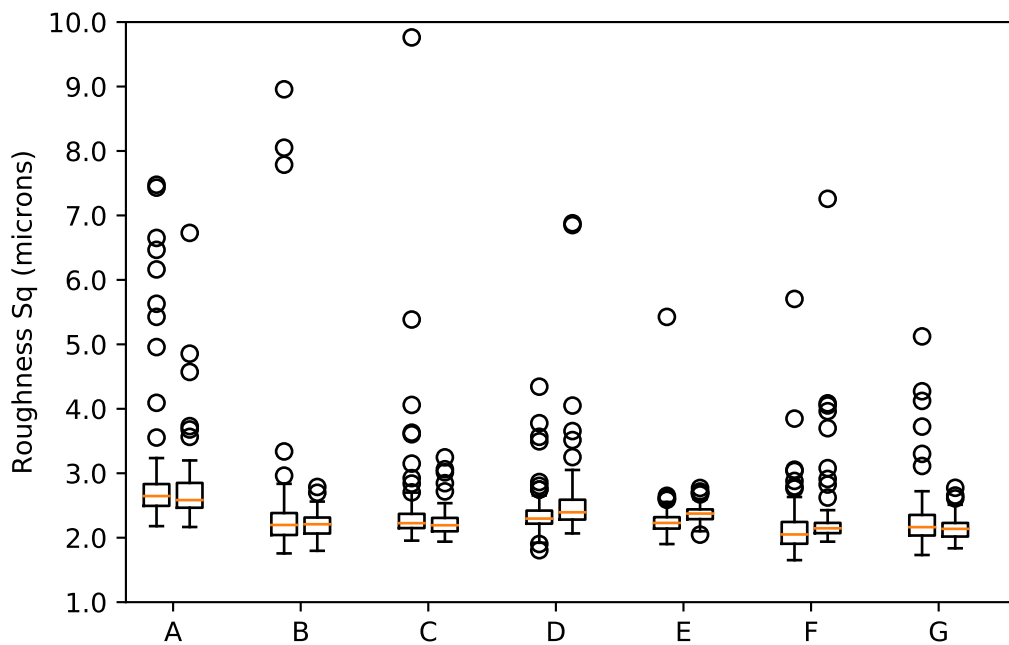


Figure 6.14: Boxplot of the Sq values recorded on each sample after the leveling and subdivision of the area in patch with a side 750 µm. For each pair of box, on the left side the cleaned area on the right the reference uncleaned area.

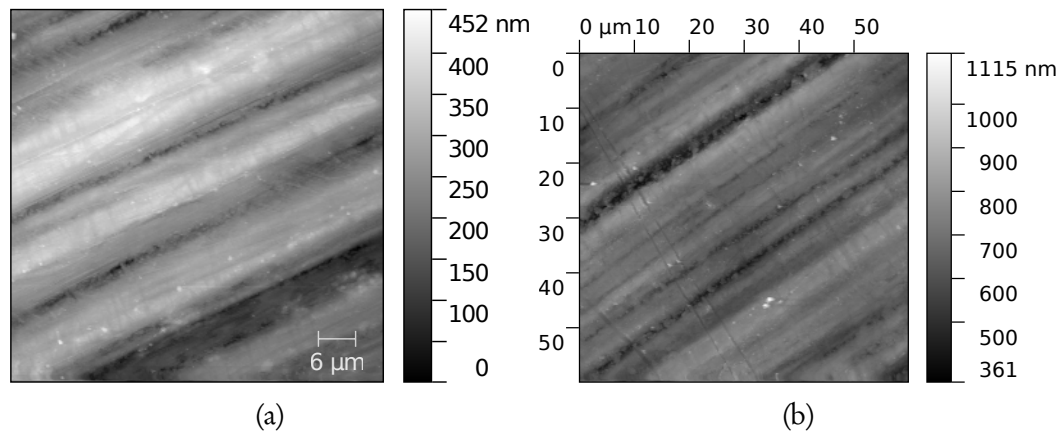


Figure 6.15: a) AFM scan of a portion of the cleaned sample C1 tilted of 45 degrees. b) AFM scan of the cleaned sample D1 tilted of 45 degrees.

and hence can not be detected by the conoscopic holography system.

For each of the five measurements taken on the areas was computed the S_q roughness parameters. Figure 6.16 reports the average of the S_q value for the cleaned area and the reference uncleaned area. Despite the high uncertainties, the cleaned area shows always a lower S_q roughness compared to the uncleaned area.

6.4.4 Discussions and conclusion

The method of giving a predominant lay to the surface and using the cleaning tool perpendicular to the lay used by OPD is promising combined with the AFM. The AFM is able to identify and record the topological feature and the traces left by the cleaning instruments. The conoscopic holography set-up did not reach the resolution needed for identifying precisely the effects at nanometer scale of the cleaning but gave a wider understanding on the area where the tool was used for longer or with more force, eventually consuming more of the surface. Comparing the same area before and after the cleaning would be probably an easier solution for assessing the effects of the cleaning on micro and millimeter scale using the conoscopic holography system. The chaotic behaviour of the surface due to the combination of manufacturing and cleaning procedures produces regions of the sample with very high roughness difference (see 6.13 at page 128). The sampling with the AFM could be hence guided or combined with the information coming from scans at lower resolution.

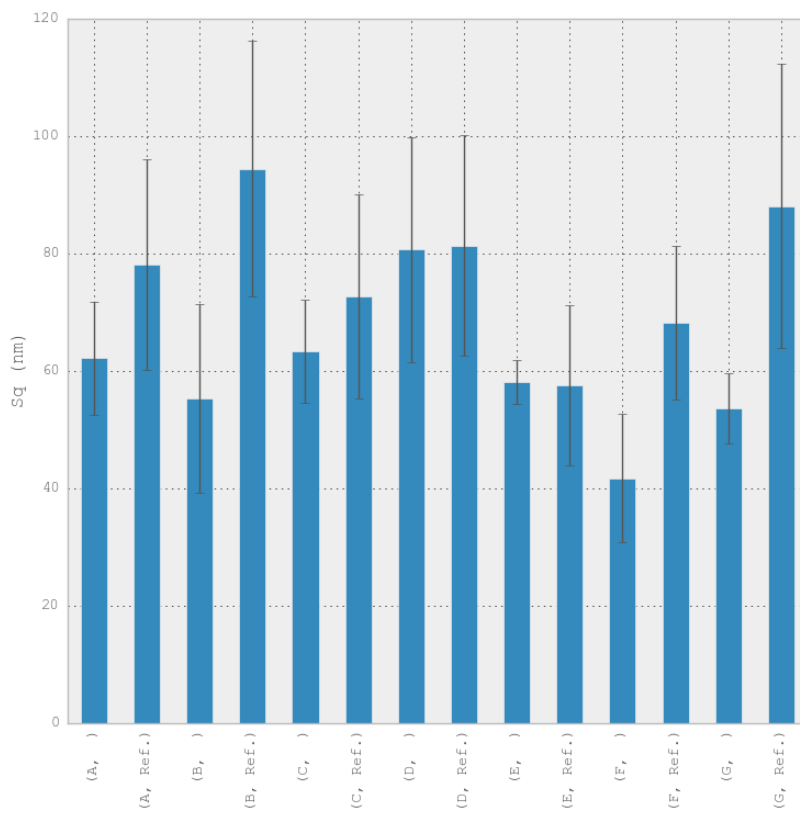


Figure 6.16: Averaged Sq roughness computed on cleaned and uncleaned patches on five scan for each patch.

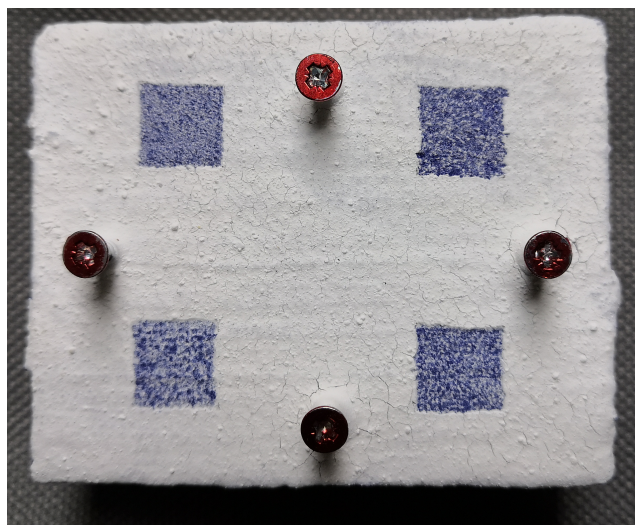


Figure 6.17: Mock-up of the smalt-blue mural painting samples with limewash layer and cleaning tests. From the top left clockwise: dry ultrasonic, wet precision engraver, wet scalpel, dry scalpel.

6.5 Testing the effects of laser cleaning methodology for removing limewash layers from a mural painting

6.5.1 Aim and description of the study

A research group of *Scuola universitaria professionale della Svizzera italiana* (SUPSI) contacted our laboratory for assessing the effectiveness of laser cleaning methods. The research aimed to find the most effective method for revealing the blue pictorial layers of a 16th-century wall painting that was covered with a lime layer during its conservation history.

The study was conducted on mock-up samples and eventually the knowledge acquired was used for the cleaning of the mural painting.

6.5.2 Methods

The restorer (Francesco M. Wiesner), at the time student at SUPSI, prepared a sample collection of 20 mural painting mock-ups. Each mock-up consisted of a layer of concrete foam followed by lime and sand layers for mimicking the original mural paintings. Above a preparatory layer with a brown pigment was added a smalt-blue layer. The mock-ups were artificially carbonated and eventually part of them was covered with a final limewash layer to cover the original blue pigment.

Figure 6.17 shows the final result of this process. As emerged from the previous case study, the most effective way of investigating this kind of processes was to compare the same surface before and after the modification. For this purpose, some reference must be placed on the samples to retrieve the controls points needed for registering the data. Leaving two opposite edges of the sample without

the lime layer could be one possible solution, however these samples are usually brittle so their morphology might modify during the ageing and cleaning affecting the registration.

I proposed to use at least three screws in-built on the samples. Due to the fragility of the samples, the screws could not be inserted for the whole length obliging us to use lenses with a longer focal length to be able to acquire at the same time the screw and the surface. The screws were eventually painted using a red dye for increasing their reflectance at the wavelength of the laser of the conoscopic probe and increasing the signal to noise ratio.

The microprofilometer was used in its vertical configuration and with a ConoPoint-3 equipped with a 75 mm lens. The measurements were performed setting a scan step of 100 μm and an axis speed of 25 mm s^{-1} allowing to acquire an area of 5 cm \times 6 cm in approximately half an hour. For most of the samples, I collected acquisition before applying the limewash layer, after the application and after the removing of the limewash layer.

6.5.3 Data analysis

I scanned the same samples different times and I computed an average standard deviation per pixel of 3 μm . The thickness of the limewash layer measured with the microprofilometer ranged from tens of microns to more than one millimeter.

For a first characterization of the surface I measured a 1 cm^2 in the middle of the samples before and after applying the limewash. In the original surface I computed an Sa roughness of 34.6 μm with a standard deviation (STD) of 4.6 μm and an Sq roughness of 43.7 μm with a STD of 5.8 μm . After applying the limewash the roughness lowered to a value of Sa of 28.1 μm (STD 3.9 μm) and a value of Sq of 36.1 μm (STD 4.1 μm). The limewash is hence filling the valleys on the surface of the sample, flattening the overall surface topography.

The 3D renderings of the surface in figure 6.18 show a region of the original surface, the same region after the application of the limewash and eventually the same region after a square patch of the limewash has been removed. We can notice the lay due to the painting of the smalt layer using the brush, and some granules that are visible after applying the limewash layer.

The various cleaning procedure can be studied monitoring the effects on the metrological parameters: Sp, Sv, Sz, Sq, Sa. For this study, I have used the following definition of these parameters, after levelling the surface, and producing an array of heights difference S .

Sp is the maximum peak height:

$$Sp = \arg \max(S) \quad (6.1)$$

Sv is the max valley height:

$$Sv = |\arg \min(S)| \quad (6.2)$$

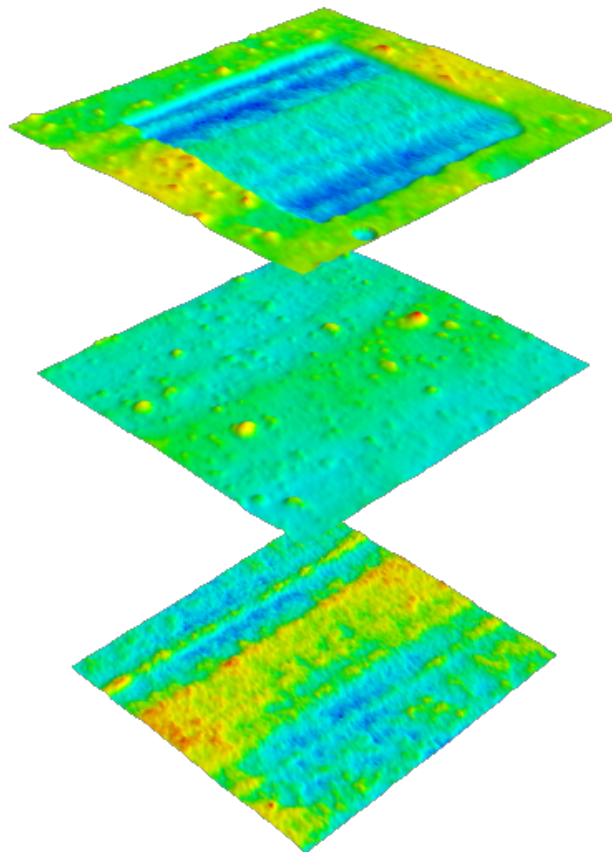


Figure 6.18: 3D rendering of a part of the conoscopic holography acquisition of the mock-up samples. From the bottom to the top: after the application of blue-smalt, after the application of the limewash layer and after the removing of the limewash layer.

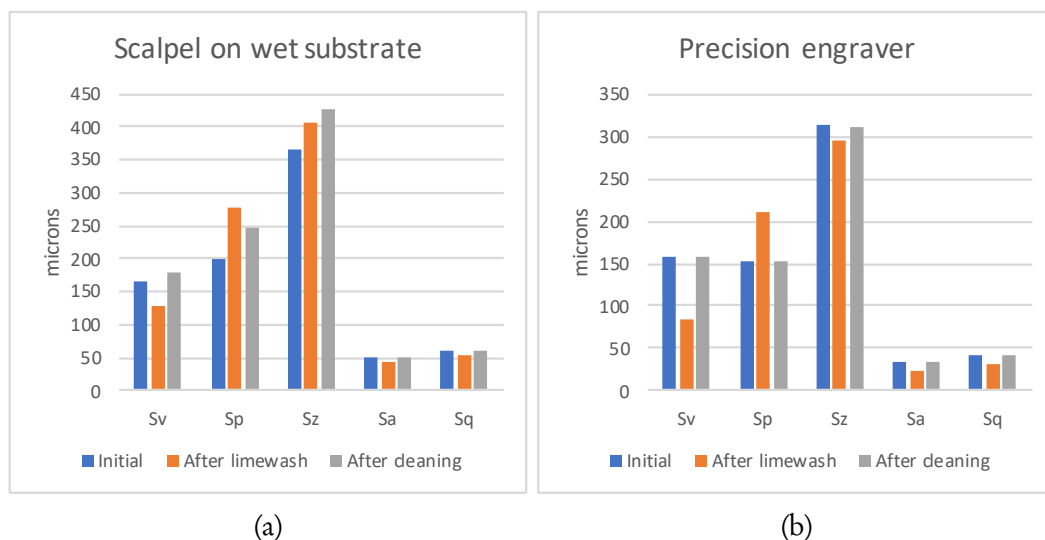


Figure 6.19: The analysis of S_p , S_v , S_z , S_q , S_a variation after applying the limewash and the consecutive removal using a) a scalpel on wet substrate and b) a precision engraver.

Eventually, S_z is defined as:

$$S_z = S_p - S_v \quad (6.3)$$

S_a and S_q are defined as the average and the root mean square of the heights. Figure 6.19 shows the comparison between the results obtained using a scalpel and the results using a precision engraver for removing the wet limewash layer. As explained before, the application of the limewash fill the valleys, this is evident from the decreasing of the value S_v after the application. The increasing of the max peak height (S_p) can be attributed to the granules present on the limewash. The peaks due to the granules are sporadic, these can be inferred by the fact the S_a and S_q parameters are still lower compared to the original values. Hence the filling of the valleys is predominant.

After the removing of the limewash the parameters get closer to the original values, in particular using the precision engraver where the differences between the original values and the values obtained on the cleaned surface are limited to few microns.

6.5.4 Discussions and conclusion

I briefly reported part of the study performed for assessing the removal of limewash from mural paintings samples.

In this case, the thickness of the limewash layer and the effects of its application can be monitored using the conoscopic holography set-up. The surface metrology analysis can give important insight into the variation of metrological parameters at micrometre level. Of course, the decision of the cleaning process can not be driven only by the metrological parameters but helps the restorer and the conservation

scientists to perform an informed choice and reason on the effects of the cleaning on the morphology of the surface.

6.6 End-user feedback

For each case study, I collected the end-user feedback, after they accepted the informed consent form, using the following anonymous questionnaire <https://forms.gle/N3b3JWwnnpAb9zpL6>. The results are presented in the deliverable of the Scan4Reco project *D7.4 - End-User based Evaluation Report* available online ².

The questionnaire was compiled by six experts working on cultural heritage that used the results of the system but were not related to its development. Three of them were conservators and the remaining conservation scientists. On a scale from 1 (Not important) to 5 (Very important) 80% of the respondents consider very important to measure accurately the surface of the artwork. In particular, all the respondents consider dents and physical damage and effects of cleaning treatments an important aspect to monitor in cultural heritage. 80% of the respondents consider important also to monitor craquelure, cracks propagation and deformation of the supports. Two of the respondents were able to use the data from the microprofilometer to monitor the effects of cleaning treatments and dents and damage to the objects.

Eventually, more than 80% consider important to present the results after monitoring the same area during a period of time or after sequential events (e.g. cleaning treatments) not only using the standard metrological parameters but also showing the differences in the surface reconstruction on the same area before and after.

6.7 Summary

The inspection of the cleaning effects has received much attention by the conservation scientist community [25, 170], the end-users questioned confirmed the importance of acquiring an accurate reconstruction of the surface and all agree that monitoring of cleaning is one of the main application. Here I presented the results obtained using the conoscopic holography system developed in this dissertation.

The analysis of the artificially aged reference samples (sec. 6.2) did not highlight particular topological features for bronze and silver samples which however show a statistical difference in the distribution of the heights amongst the ageing steps. For the egg tempera panel the conoscopic analysis was able to record different morphological features (craquelure, cracks, granules ...) some promising results were obtained on the prediction of the detachments of the pictorial layers.

In the microprofilometric analyses of the crack pattern on Pesaro Madonna (sec. 6.3), the canvas wrinkles were characterized and compared before and after

²<https://ec.europa.eu/research/participants/documents/downloadPublic?documentIds=080166e5be67895f&appId=PPGMS>

the cleaning. The results show the preservation of the original pattern and differences lower than 100 microns after the removing of the varnish layer. Some uncertainties must be taken into account due to the effects of environmental influences and the presence of transparent layers.

When testing innovative cleaning procedures (sec. 6.4) the possibility of acquiring large areas allows getting an insight on the inhomogeneities of the cleaning procedure at a wider level compared to other techniques with a limited field of view.

However, the micrometer resolution allows only to monitor a subset of morphological features and effects and the combination with other techniques with higher resolution is often necessary.

For the analysis of the removal of thick layers (sec. 6.5) the accuracy seems sufficient to get an insight on the effects of the cleaning on the surface before and after the removal of the layer, helping to choose the best methodology for preserving the original surface.

In general, an accurate re-positioning and registration of the scan is an important step for the analysis because this allows better monitoring of the effects under study.

Conclusion

Surface and dimensional metrology should not be the preserve of industrial sectors and mechanical engineers but are important tools for every researcher analyzing objects as they are. In particular, for the scientist involved in the conservation of the ancient manufacturing products, such as Cultural Heritage objects, the benefits that these disciplines can add are manifold. However, the challenges for extracting meaningful data from surface topography are many. To have a complete understanding of all the problems and uncertainties linked to this area of study in this thesis I implemented a whole framework based on conoscopic holography sensor starting from the hardware up to the software. The scanning system is based on micrometric linear stages that are common choice for developing scanning applications for Cultural Heritage, however the implementation of the systems often lack of an appropriate description, due to a poor standardization of the terms used for describing the scanning modalities. The usage of conoscopic holography sensors for surface metrology could deserve particular attention for their ability to scan object at different scales. In the last decades, some promising results have been obtained applying custom systems based on these probes on artworks. However, the uncertainties are many: the probe surface interactions are not always clear. Thus I proposed different strategies to understand the accuracy and the performance of the instruments under different conditions. Acoustic microscopy is potentially a supplementary technique that can address some uncertainties and artefacts acquired during the analysis. Reference standard materials are another important tool for assessing the performance of the instrument, but there is currently a lack of reference standards with surface properties similar to the one encountered on artwork's surface. The application of surface metrology to Cultural Heritage objects presents characteristic challenges because some artworks materials are unconventional for surface metrology, and are often hygroscopic and unstable. Thus, we have to take into account that these materials are more susceptible to environmental variations, the dimensional stability of the object must be hence assessed. For this task, I implemented different custom systems able to monitor dimensional changes of the materials under controlled relative humidity conditions. The next challenge is the analysis of the data collected. Due to the complexity of the data, the replicability of the results is granted only if the workflow used for analyzing the data is adequately standardized and described. In the last century, the procedures have been standardized in hundreds of proprietary standards that cannot easily be transposed to academia. Even if the research group had the resources to buy all these standards, many directives are based on empirical knowledge gained analyzing millions of samples of specific industrial production (often metal parts).

Hence, are not applicable to many Cultural Heritage objects. It is not possible that a single research institution has the access and the resources to carry out an extensive metrological analysis of artworks to gain the knowledge necessary to perform correctly the analysis as the industrial sector did in the last century. One possible solution is to study samples of artworks materials aged under controlled conditions. However, to get consistent results a large number of samples must be analyzed and, due to the time requirements of scanning techniques, is not feasible to perform this task without a high level of automation. Furthermore, due to the heterogeneity of the materials that arise from the ageing, further analytical analysis must be performed to assign the surface topography data to specific processes and materials. For addressing this issue I implemented a file format for producing, describing and analyzing flat sample collections. This format is based on a particular definition of the scalable vector graphic format (SVG), an open image vector file format that has been modified for visualizing and describing flat sample collections. The data contained can be visualized with any browser but also read by positioning system and hence can be used for automating the creation and the analysis of the samples facilitating the sharing and the reuse of the samples collections. Eventually, data collected must be stored in an accessible file format and hence I test and implemented different libraries for exporting the results in open-source file formats.

The route of inferring information on artworks using reference artworks materials has some well-known limitations. Thus, in parallel is important to implement other strategies for analyzing heterogeneous surfaces and understanding the most suitable processing for extracting the information. I implemented different algorithms for the analysis of the surface subdividing the surface in the sampling area of varying size and computing metrological field parameters for each area. Furthermore, I tested segmentation algorithms normally used in image processing. These algorithms have shown some promising results on test materials. Eventually, I proposed an algorithm to explore and analyze areal topography maps, based on the identification of a hierarchy of peaks and valleys. This method helps to identify artefacts and the multi-scale signals to extract with other signal processing techniques. All the functions and the procedure implemented during the project have been integrated into a Python module that is available on a public repository.

Concluding, surface and dimensional metrology can potentially be a crucial tool in the future developments of the diagnostic and conservation of Cultural Heritage. They can provide complementary important information for characterizing the object but also accurate 3D models that can be used for positioning other analytical instruments on specific areas. For taking full advantage of the benefits of surface metrology a large amount of data must be collected and this trend is often required by current state-of-the-art data analysis approaches such as Neural Networks. It is clear that the acquisition of these data set will not be performed by a single research group but by the whole community. However, for being able to efficiently share data set the quality of the data must be controlled and any bias or uncontrolled factors taken into account. It is eventually, important to agree in a common lexicon and in a detailed understanding of the scanning strategies used during the acquisition of the data, so that the results must be eventually stored

in a standard open-source file format with all the relevant meta-data. These stimulating challenges can become an excellent exercise in the cooperation between institutions across the world in a joint cause for protecting the cultural heritage of humanity.

Future works

The possibility to scan large areas with high accuracy can be exploited for creating multi-modal system where probes are positioned using the data coming from the conoscopic holography. Adding techniques with higher resolution is crucial to overcome the limitation of the conoscopic probe in retrieving topological information in the nanoscale. This seems particularly important for the monitoring of the cleaning process where nanometric variations of the surface can result in a variation of the appearance of the object. Particularly, interesting seems the usage of micro-electrical mechanical atomic force microscope systems[11] that could be positioned using the information retrieved by the conoscopic holography adapting the positioning system. In this way, would be possible to reach a multi-scale analysis from millimetres to nanometers. The capabilities of the conoscopic probe as it is, are more suitable for dimensional metrology, the dimensional stability of the object under different environmental conditions might be an important field of study for determining the most appropriate conditions for storing the object and the interference of these variations on other analyses. Thermal dilatation and deformations due to moisture absorption should be studied in a wide range of case study for retrieving a better understanding of these phenomena.

Bibliography

- [1] C. 40. *Etats geometriques de surface calcul des parametres de profil*. fr. Standard. Vélizy-Villacoublay Cedex,FR: Comite de normalisation des moyens de production, Mar. 1993. URL: http://www.cnomo.com/fichiers/4/9938/E0014015n_1993.pdf.
- [2] M. Aceto, A. Agostino, G. Fenoglio, A. Idone, M. Gulmini, M. Picollo, P. Ricciardi, and J. K. Delaney. "Characterisation of colourants on illuminated manuscripts by portable fibre optic UV-visible-NIR reflectance spectrophotometry". In: *Anal. Methods* 6 (5 2014), pp. 1488–1500. DOI: 10 . 1039 / C3AY41904E. URL: <http://dx.doi.org/10.1039/C3AY41904E>.
- [3] R. Achanta, A. Shaji, K. Smith, A. Lucchi, P. Fua, and S. Süsstrunk. "SLIC Superpixels". In: (2010), p. 15. URL: <http://infoscience.epfl.ch/record/149300>.
- [4] I. Aicardi, F. Chiabrando, A. M. Lingua, and F. Noardo. "Recent trends in cultural heritage 3D survey: The photogrammetric computer vision approach". In: *Journal of Cultural Heritage* 32 (2018), pp. 257–266. ISSN: 1296-2074. DOI: <https://doi.org/10.1016/j.culher.2017.11.006>. URL: <http://www.sciencedirect.com/science/article/pii/S129620741630423X>.
- [5] A. Aldrovandi, M. Galeotti, A. Cagnini, A. Casini, M. Picollo, B. Radicati, M. L. Altamura, M. T. Cianfanelli, and P. Riitano. *Fiber Optics Reflectance Spectra (FORS) of Pictorial Materials in the 270-1700 nm range*. <http://fors.ifac.cnr.it/index.php>. (Accessed on 03/12/2020). May 2011.
- [6] M. Alfeld, J. V. Pedroso, M. van Eikema Hommes, G. Van der Snickt, G. Tauber, J. Blaas, M. Haschke, K. Erler, J. Dik, and K. Janssens. "A mobile instrument for in situ scanning macro-XRF investigation of historical paintings". In: *J. Anal. At. Spectrom.* 28 (5 2013), pp. 760–767. DOI: 10 . 1039 / C3JA30341A. URL: <http://dx.doi.org/10.1039/C3JA30341A>.
- [7] O. Allegretti, M. Fioravanti, P. Dionisi-Vici, and L. Uzielli. "The influence of dovetailed cross beams on the dimensional stability of a panel painting from the Middle Ages". In: *Studies in Conservation* 59.4 (2014), pp. 233–240.
- [8] I. Alvarez, J. M. Enguita, J. Marina, and C. F. Bobis. "On-line submicron profile measurements from safe distances with conoscopic holography: feasibility and potential problems". In: *Optical Engineering* 47.2 (2008), p. 023602.
- [9] S. Amanatiadis, G. Apostolidis, and G. Karagiannis. "Infrared Hyperspectral Spectroscopic Mapping Imaging from 800 to 5000 nm. A Step Forward in the Field of Infrared "Imaging"". In: *International Conference on Transdisciplinary Multispectral Modeling and Cooperation for the Preservation of Cultural Heritage*. Springer. 2018, pp. 462–471.
- [10] A. Aurand, C. Gauvin, D. Jullien, and C. Young. "Understanding the Moisture Induce Fatigue Damage in Panel Paintings: A Methodological Approach for Quantifying the Role of Preparatory Layers in the Overall Response". In: *ICOM-CC Joint Interim Meeting on Physical Issues in the Conservation of Paintings: Monitoring, Documenting and Mitigating*. May 2016. URL: <http://eprints.gla.ac.uk/162875/>.
- [11] M. Azizi, N. Sarkar, and R. R. Mansour. "Single-Chip CMOS-MEMS Dual Mode Scanning Microwave Microscope". In: *IEEE Transactions on Microwave Theory and Techniques* 61.12 (2013), pp. 4621–4629.
- [12] W. Bates. "A wavefront shearing interferometer". In: *Proceedings of the Physical Society* 59.6 (1947), p. 940.
- [13] G. Berkovic and E. Shafir. "Optical methods for distance and displacement measurements". In: *Adv. Opt. Photon.* 4.4 (Dec. 2012), pp. 441–471. DOI: 10 . 1364 / AOP . 4 . 000441. URL:

- <http://aop.osa.org/abstract.cfm?URI=aop-4-4-441>.
- [14] A. K. Bewoor and V. A. Kulkarni. *Metrology and measurement*. McGraw-Hill Education, 2009.
- [15] M. Bigerelle, T. Mathia, and S. Bouvier. “The multi-scale roughness analyses and modeling of abrasion with the grit size effect on ground surfaces”. In: *Wear* 286-287 (2012). Tribology in Manufacturing Processes, pp. 124–135. ISSN: 0043-1648. DOI: <https://doi.org/10.1016/j.wear.2011.08.006>. URL: <http://www.sciencedirect.com/science/article/pii/S0043164811005503>.
- [16] F. Blateyron. “Good practices for the use of areal filters”. In: *Proc. 3rd Seminar on Surface Metrology of the Americas*. 2014.
- [17] F. Blateyron. “The Areal Feature Parameters”. In: *Characterisation of Areal Surface Texture*. Ed. by R. Leach. Berlin, Heidelberg: Springer Berlin Heidelberg, 2013, pp. 45–65. ISBN: 978-3-642-36458-7. DOI: 10.1007/978-3-642-36458-7_3. URL: https://doi.org/10.1007/978-3-642-36458-7_3.
- [18] F. Blateyron. “The Areal Feature Parameters”. In: *Characterisation of Areal Surface Texture*. Ed. by R. Leach. Berlin, Heidelberg: Springer Berlin Heidelberg, 2013, pp. 45–65. ISBN: 978-3-642-36458-7. DOI: 10.1007/978-3-642-36458-7_3. URL: https://doi.org/10.1007/978-3-642-36458-7_3.
- [19] G. Bradski. “The OpenCV Library”. In: *Dr. Dobb’s Journal of Software Tools* (2000).
- [20] A. Brambilla, I. Osticioli, A. Nevin, D. Comelli, C. D’Andrea, C. Lofrumento, G. Valentini, and R. Cubeddu. “A remote scanning Raman spectrometer for in situ measurements of works of art”. In: *Review of Scientific Instruments* 82.6 (2011), p. 063109.
- [21] Bruker. *Dektak XTL - Technical Details | Stylus Profiler - Stylus Profilers | Dektak | Bruker*. <https://web.archive.org/web/20200630072110/https://www.bruker.com/products/surface-and-dimensional-analysis/stylus-profilometers/dektak-xtl/technical-details.html>. (Accessed on 06/30/2020).
- [22] S. Bucklow. “The Description of Craquelure Patterns”. In: *Studies in Conservation* 42.3 (1997), pp. 129–140. ISSN: 00393630. URL: <http://www.jstor.org/stable/1506709>.
- [23] S. H. Bui and T. V. Vorburger. “Surface metrology algorithm testing system”. In: *Precision Engineering* 31.3 (2007), pp. 218–225. ISSN: 0141-6359. DOI: <https://doi.org/10.1016/j.precisioneng.2007.01.002>. URL: <http://www.sciencedirect.com/science/article/pii/S0141635907000323>.
- [24] T. S. BV. *index | TIOBE - The Software Quality Company*. <https://web.archive.org/web/20200811134830/https://www.tiobe.com/tiobe-index/>. (Accessed on 08/15/2020). Aug. 2020.
- [25] I. Cacciari, D. Ciofini, M. Mascalchi, A. Mencaglia, and S. Siano. “Novel approach to the microscopic inspection during laser cleaning treatments of artworks”. In: *Analytical and Bioanalytical Chemistry* 402.4 (Feb. 2012), pp. 1585–1591. ISSN: 1618-2650. DOI: 10.1007/s00216-011-5292-9. URL: <https://doi.org/10.1007/s00216-011-5292-9>.
- [26] S. Capelo, P. M. Homem, J. Cavalheiro, and I. T. E. Fonseca. “Linear sweep voltammetry: a cheap and powerful technique for the identification of the silver tarnish layer constituents”. In: *Journal of Solid State Electrochemistry* 17.1 (Jan. 2013), pp. 223–234. ISSN: 1432-8488, 1433-0768. DOI: 10.1007/s10008-012-1884-3. URL: <https://link.springer.com/article/10.1007/s10008-012-1884-3> (visited on 08/04/2017).
- [27] E. Cappelletto, P. Zanuttigh, and G. M. Cortelazzo. “3D Scanning of Cultural Heritage with Consumer Depth Cameras”. In: *Multimedia Tools Appl.* 75.7 (Apr. 2016), pp. 3631–3654. ISSN: 1380-7501. DOI: 10.1007/s11042-014-2065-4. URL: <https://doi.org/10.1007/s11042-014-2065-4>.

- [28] S. Cass. *The Top Programming Languages 2019 - IEEE Spectrum*. https://web.archive.org/web/20200813045851if_/https://spectrum.ieee.org/computing/software/the-top-programming-languages-2019. (Accessed on 08/15/2020). Sept. 2019.
- [29] A. Cayley. “XL. On contour and slope lines”. In: *The London, Edinburgh, and Dublin Philosophical Magazine and Journal of Science* 18.120 (1859), pp. 264–268. DOI: 10.1080/14786445908642760. eprint: <https://doi.org/10.1080/14786445908642760>. URL: <https://doi.org/10.1080/14786445908642760>.
- [30] D. Charlot, L. M. Mugnier, and G. Y. Sirat. “3-D camera based on conoscopic holography”. In: *Industrial Inspection II*. Vol. 1265. International Society for Optics and Photonics. 1990, pp. 52–62.
- [31] P. E. Ciddor. “Refractive index of air: new equations for the visible and near infrared”. In: *Appl. Opt.* 35.9 (Mar. 1996), pp. 1566–1573. DOI: 10.1364/AO.35.001566. URL: <http://ao.osa.org/abstract.cfm?URI=ao-35-9-1566>.
- [32] I. M. Ciortan, G. Marchioro, C. Daffara, R. Pintus, E. Gobetti, and A. Giachetti. “Aging Prediction of Cultural Heritage Samples Based on Surface Microgeometry”. In: *Eurographics Workshop on Graphics and Cultural Heritage*. The Eurographics Association; 2018, pp. 147–154. ISBN: 978-3-03868-057-4. DOI: 10.2312/gch.20181352. URL: <https://www.tib.eu/de/suchen/id/eurographics%3Adoi%7E10.2312%252Fgch.20181352%22%7D>.
- [33] J. Clerk-Maxwell. “L. On hills and dales”. In: *The London, Edinburgh, and Dublin Philosophical Magazine and Journal of Science* 40.269 (1870), pp. 421–427. DOI: 10.1080/14786447008640422. eprint: <https://doi.org/10.1080/14786447008640422>. URL: <https://doi.org/10.1080/14786447008640422>.
- [34] L. of Congress. *Center for the Library’s Analytical Scientific Samples (CLASS)*. <https://web.archive.org/web/20200402235947/https://www.loc.gov/preservation/scientists/projects/class.html>. (Accessed on 04/07/2020). 2019.
- [35] *ConoPoint series User Manual Rev 8*. http://www.optimet.com/register_files/OPTIMET-Point-Sensors-Manual.pdf#page=23. (Accessed on 12/02/2019).
- [36] *Conoscope Lenses - Eckhardt Optics LLC*. <https://web.archive.org/web/20190326011513/https://eckop.com/optics/opticsadvanced-lenses/how-conoscope-lenses-work/>. (Accessed on 07/24/2019).
- [37] openGPS® Consortium. *openGPS® - open source software for 3D surface characterisation*. <https://web.archive.org/web/20180527145644/http://open-gps.sourceforge.net/>. (Accessed on 07/27/2020). Aug. 2014.
- [38] A. Cosentino. “FORS Spectral Database of Historical Pigments in Different Binders”. In: *e-conservation Journal* 2 (2014), pp. 53–65. DOI: <http://dx.doi.org/10.18236/econs2.201410>.
- [39] C. Daffara, N. Gaburro, G. Marchioro, A. Romeo, G. Basilissi, A. Cagnini, and M. Galeotti. “Surface micro-profilometry for the assessment of the effects of traditional and innovative cleaning treatments of silver”. In: *Lasers in the Conservation of Artworks XI (Proceedings of International Conference LACONA XI)*. Nicolaus Copernicus University Scientific Publishing House. 2017, pp. 3875–4. URL: https://wydawnictwo.umk.pl/upload/files/OPEN%5C%20ACCESS/Lasers%5C%20in%5C%20the%5C%20Conservation/LaCona_11-12.pdf%7D.
- [40] C. Daffara, E. Pampaloni, L. Pezzati, M. Barucci, and R. Fontana. “Scanning multispectral IR reflectography SMIRR: an advanced tool for art diagnostics”. In: *Accounts of chemical research* 43.6 (2010), pp. 847–856.

- [41] M.-L. Dano and J.-P. Bourque. “Deformation behaviour of paper and board subjected to moisture diffusion”. In: *International Journal of Solids and Structures* 46.6 (2009), pp. 1305–1316. ISSN: 0020-7683. DOI: <https://doi.org/10.1016/j.ijsolstr.2008.10.035>. URL: <http://www.sciencedirect.com/science/article/pii/S0020768308004666>.
- [42] *DCMI: Home*. <https://web.archive.org/web/20200716171657/https://www.dublincore.org/>. (Accessed on 07/19/2020). July 2020.
- [43] N. Dimitriou, S. Papadopoulos, A. Drosou, and D. Tzovaras. “A 3D-CNN Approach for the Spatio-Temporal Modeling of Surface Deterioration Phenomena”. In: *2018 IEEE 13th Image, Video, and Multidimensional Signal Processing Workshop (IVMSP)*. 2018, pp. 1–5.
- [44] P. Dionisi-Vici, M. De Vincenzi, and L. Uzielli. “An analytical method for the characterization of microclimates for the conservation of wooden Cultural Heritage objects”. In: *Art2005: Proceedings of the 8th International Conference on Non-Destructive Investigations and Microanalysis for the Diagnostics and Conservation of the Cultural and Environmental Heritage, Lecce (Italy) 15–19 May 2005*. 2005.
- [45] J. M. Dullieu-Barton, L. Dokos, D. Eastop, F. Lennard, A. R. Chambers, and M. Sahin. “Deformation and strain measurement techniques for the inspection of damage in works of art”. In: *Studies in Conservation* 50.sup1 (2005), pp. 63–73.
- [46] R. Falciai, C. Trono, G. Lanterna, and C. Castelli. “Continuous monitoring of wooden works of art using fiber Bragg grating sensors”. In: *Journal of Cultural Heritage* 4.4 (2003), pp. 285–290.
- [47] R. L. Feller. *Accelerated aging: photochemical and thermal aspects*. Getty Publications, 1995.
- [48] D. Flack and J. Hannaford. “Fundamental good practice in dimensional metrology.” In: *NP Laboratory, Ed* (2006). URL: <http://eprintspublications.npl.co.uk/3360/>.
- [49] R. Fontana, M. Barucci, P. Carcagnì, C. Daffara, E. Pampaloni, and L. Pezzati. “Autofocus laser system for multi-NIR scanning imaging of painting surfaces”. In: *O3A: Optics for Arts, Architecture, and Archaeology III*. Ed. by L. Pezzati and R. Salimbeni. Vol. 8084. International Society for Optics and Photonics. SPIE, 2011, pp. 26–34. DOI: 10.1117/12.889487. URL: <https://doi.org/10.1117/12.889487>.
- [50] R. Fontana, M. C. Gambino, M. Greco, L. Marras, M. Materazzi, E. Pampaloni, and L. Pezzati. “High-precision surface analysis of the roughness of Michelangelo’s David”. In: *Optical Metrology for Arts and Multimedia*. Vol. 5146. 2003, pp. 236–243. URL: <http://proceedings.spiedigitallibrary.org/proceeding.aspx?articleid=767730> (visited on 02/13/2016).
- [51] R. Fontana, M. C. Gambino, M. Greco, L. Marras, M. Materazzi, E. Pampaloni, L. Pezzati, and P. Poggi. “Integrating 2D and 3D data for diagnostics of panel paintings”. In: *Optical Metrology for Arts and Multimedia*. Vol. 5146. International Society for Optics and Photonics. 2003, pp. 88–98.
- [52] R. Fontana, M. C. Gambino, C. Mazzotta, M. Greco, E. Pampaloni, and L. Pezzati. “High-resolution 3D survey of artworks”. In: *Optical Metrology in Production Engineering*. Vol. 5457. International Society for Optics and Photonics. 2004, pp. 719–726.
- [53] N. Gaburro, G. Marchioro, and C. Daffara. “A versatile optical profilometer based on conoscopic holography sensors for acquisition of specular and diffusive surfaces in artworks”. In: *Optics for Arts, Architecture, and Archaeology VI*. Ed. by L. Pezzati and P. Targowski. Vol. 10331. International Society for Optics and Photonics. SPIE, 2017, pp. 48–56. DOI: 10.1117/12.2270307. URL: <https://doi.org/10.1117/12.2270307>.
- [54] F. Gallese, G. Laguzzi, L. Luvidi, V. Ferrari, S. Takacs, and G. Venturi Pagani Cesa. “Comparative investigation into the corrosion of different bronze alloys suitable for outdoor sculptures”. In: *Corrosion Science* 50.4 (Apr.

- 2008), pp. 954–961. ISSN: 0010-938X. DOI: 10.1016/j.corsci.2007.11.015. URL: <http://www.sciencedirect.com/science/article/pii/S0010938X0700323X>.
- [55] *GCI Reference Collection | Getty Conservation Institute*. https://web.archive.org/web/20190717154734/https://www.getty.edu/conservation/publications_resources/reference_collection/index.html. (Accessed on 09/17/2019).
- [56] S. Gillies et al. *Shapely: manipulation and analysis of geometric objects*. toblerity.org, 2007–. URL: <https://github.com/Toblerity/Shapely>.
- [57] J. A. Golby, M. J. Padgett, and S. P. Woodall. “Inspection interferometer with scanning autofocus, and phase angle control features”. US Patent 5,469,259. 1995.
- [58] R. Gothandaraman and S. Muthuswamy. “Robot-assisted 3D digital reconstruction of heritage artifacts: area similarity approach”. In: *Industrial Robot: the international journal of robotics research and application* (2020).
- [59] D. Graham, M. Sault, and C. J. Bailey. “National ocean service shoreline—Past, present, and future”. In: *Journal of Coastal Research* (2003), pp. 14–32.
- [60] N. Grassi, L. Giuntini, P. Mandò, and M. Massi. “Advantages of scanning-mode ion beam analysis for the study of Cultural Heritage”. In: *Nuclear Instruments and Methods in Physics Research Section B: Beam Interactions with Materials and Atoms* 256.2 (2007), pp. 712–718. ISSN: 0168-583X. DOI: <https://doi.org/10.1016/j.nimb.2006.12.196>. URL: <http://www.sciencedirect.com/science/article/pii/S0168583X0700170X>.
- [61] P. de Groot and D. Fitzgerald. “Measurement, certification and use of step-height calibration specimens in optical metrology”. In: *Optical Measurement Systems for Industrial Inspection X*. Ed. by P. Lehmann, W. Osten, and A. A. G. Jr. Vol. 10329. International Society for Optics and Photonics. SPIE, 2017, pp. 328–336. DOI: 10.1117/12.2269800. URL: <https://doi.org/10.1117/12.2269800>.
- [62] R. M. Groves. “Prognosis of Structural and Materials Health in Heritage Conservation”. In: *3rd European Conference of the PHM Society 2016*. 2016. URL: http://pure.tudelft.nl/ws/files/10206407/Paper_Groves_PHME16_v3_FINAL.pdf.
- [63] R. M. Groves, J. Caballero, I. Quinzan, and E. Ribes-Gómez. “Damage and deterioration monitoring of artwork by data fusion of 3D surface and hyperspectral measurements”. In: *Optical Sensing and Detection III*. Ed. by F. Berghmans, A. G. Mignani, and P. D. Moor. Vol. 9141. International Society for Optics and Photonics. SPIE, 2014, pp. 296–304. DOI: 10.1117/12.2051898. URL: <https://doi.org/10.1117/12.2051898>.
- [64] D. L. Hall and J. Llinas. “An introduction to multisensor data fusion”. In: *Proceedings of the IEEE* 85.1 (1997), pp. 6–23.
- [65] G. Häusler and J. M. Herrmann. “Range sensing by shearing interferometry: influence of speckle”. In: *Applied optics* 27.22 (1988), pp. 4631–4637.
- [66] G. Häusler, J. Hutfless, M. Maul, and H. Weissmann. “Range sensing based on shearing interferometry”. In: *Applied optics* 27.22 (1988), pp. 4638–4644.
- [67] M. Hess. “A metric test object informed by user requirements for better 3D recording of cultural heritage artefacts”. PhD thesis. UCL (University College London), 2015. URL: http://discovery.ucl.ac.uk/1471114/7/2015-09-14Mona%20Hess%20PhD_FinalVersion_highresRPS.pdf.
- [68] M. Hess, C. Korenberg, C. Ward, S. Robson, and C. Entwistle. “Use of 3D laser scanning for monitoring the dimensional stability of a Byzantine ivory panel”. In: *Studies in Conservation* 60.sup1 (2015), S126–S133. DOI: 10.1117/0039363015Z.000000000217. eprint: <https://doi.org/10.1117/0039363015Z.000000000217>. URL: <https://doi.org/10.1117/0039363015Z.000000000217>.

- [69] H. P. Ho, M. G. Somekh, M. Liu, and C. See. “Direct and indirect dual-probe interferometers for accurate surface wave measurements”. In: *Measurement Science and Technology* 5.12 (1994), p. 1480.
- [70] F.-P. Hocquet, H. Calvo del Castillo, A. Cervera Xicotencatl, C. Bourgeois, C. Oger, A. Marchal, M. Clar, S. Rakkaa, E. Micha, and D. Strivay. “Elemental 2D imaging of paintings with a mobile EDXRF system”. In: *Analytical and Bioanalytical Chemistry* 399.9 (Mar. 2011), pp. 3109–3116. ISSN: 1618-2650. DOI: 10.1007/s00216-010-4281-8. URL: <https://doi.org/10.1007/s00216-010-4281-8>.
- [71] J. D. Hunter. “Matplotlib: A 2D graphics environment”. In: *Computing in Science & Engineering* 9.3 (2007), pp. 90–95. DOI: 10.1109/MCSE.2007.55.
- [72] *Integrating Imaging and Analytical Technologies for Conservation Practice*. https://web.archive.org/web/20190307050122/https://www.getty.edu/conservation/our_projects/imaging_experts_mtg_rep.pdf. (Accessed on 09/04/2019). Sept. 2013.
- [73] P. Iou. “Ancient silver artefacts: corrosion processes and preservation strategies”. In: *Corrosion and Conservation of Cultural Heritage Metallic Artefacts* 39 (2013), pp. 213–235.
- [74] *Geometrical product specifications (GPS) – Extraction*. en. Standard. Geneva, CH: International Organization for Standardization, 2010. URL: <https://www.iso.org/standard/24235.html>.
- [75] *Geometrical product specifications (GPS) – Filtration – Part 1: Overview and basic concepts*. en. Standard. Geneva, CH: International Organization for Standardization, 2015. URL: <https://www.iso.org/standard/61375.html>.
- [76] *Geometrical product specifications (GPS) – Filtration – Part 21: Linear profile filters: Gaussian filters*. en. Standard. Geneva, CH: International Organization for Standardization, 2011. URL: <https://www.iso.org/standard/50176.html>.
- [77] *Geometrical product specifications (GPS) – Filtration – Part 22: Linear profile filters: Spline filters*. en. Standard. Geneva, CH: International Organization for Standardization, 2015. URL: <https://www.iso.org/standard/61377.html>.
- [78] *Geometrical product specifications (GPS) – Filtration – Part 29: Linear profile filters: Spline wavelets*. en. Standard. Geneva, CH: International Organization for Standardization, 2015. URL: <https://www.iso.org/standard/61378.html>.
- [79] *Geometrical product specifications (GPS) – Filtration – Part 30: Robust profile filters: Basic concepts*. en. Standard. Geneva, CH: International Organization for Standardization, 2015. URL: <https://www.iso.org/standard/62881.html>.
- [80] *Geometrical product specifications (GPS) – Filtration – Part 31: Robust profile filters: Gaussian regression filters*. en. Standard. Geneva, CH: International Organization for Standardization, 2016. URL: <https://www.iso.org/standard/66242.html>.
- [81] *Geometrical product specifications (GPS) – Filtration – Part 40: Morphological profile filters: Basic concepts*. en. Standard. Geneva, CH: International Organization for Standardization, n.a. URL: <https://www.iso.org/standard/61379.html>.
- [82] *Geometrical product specifications (GPS) – Filtration – Part 41: Morphological profile filters: Disk and horizontal line-segment filters*. en. Standard. Geneva, CH: International Organization for Standardization, 2015. URL: <https://www.iso.org/standard/61380.html>.
- [83] *Geometrical product specification (GPS) – Filtration – Part 61: Linear areal filters – Gaussian filters*. en. Standard. Geneva, CH: International Organization for Standardization, 2015. URL: <https://www.iso.org/standard/60813.html>.
- [84] *Geometrical product specifications (GPS) – Filtration – Part 71: Robust areal filters: Gaussian regression filters*. en. Standard. Geneva,

- CH: International Organization for Standardization, 2014. URL: <https://www.iso.org/standard/60159.html>.
- [85] *Geometrical product specifications (GPS) – Filtration – Part 85: Morphological areal filters: Segmentation*. en. Standard. Geneva, CH: International Organization for Standardization, 2013. URL: <https://www.iso.org/standard/60158.html>.
- [86] *Geometrical product specifications (GPS) – Surface texture: Areal – Part 1: Indication of surface texture*. en. Standard. Geneva, CH: International Organization for Standardization, 2016. URL: <https://www.iso.org/standard/46065.html>.
- [87] *Geometrical product specifications (GPS) – Surface texture: Areal – Part 2: Terms, definitions and surface texture parameters*. en. Standard. Geneva, CH: International Organization for Standardization, 2012. URL: <https://www.iso.org/standard/42785.html>.
- [88] *Geometrical product specifications (GPS) – Surface texture: Areal – Part 3: Specification operators*. en. Standard. Geneva, CH: International Organization for Standardization, 2012. URL: <https://www.iso.org/standard/42895.html>.
- [89] *Geometrical product specifications (GPS) – Surface texture: Areal – Part 72: XML file format x3p*. en. Standard. Geneva, CH: International Organization for Standardization, 2017. URL: <https://www.iso.org/standard/62310.html>.
- [90] *Geometrical Product Specifications (GPS) – Surface texture: Profile method – Nominal characteristics of contact (stylus) instruments*. en. Standard. Geneva, CH: International Organization for Standardization, 1996. URL: <https://www.iso.org/standard/1916.html>.
- [91] *Geometrical Product Specifications (GPS) – Surface texture: Profile method – Terms, definitions and surface texture parameters – Amendment 1: Peak count number*. en. Standard. Geneva, CH: International Organization for Standardization, 2009. URL: <https://www.iso.org/standard/44475.html>.
- [92] *Geometrical Product Specifications (GPS) – Surface texture: Profile method – Rules and procedures for the assessment of surface texture – Technical Corrigendum 1*. en. Standard. Geneva, CH: International Organization for Standardization, 1998. URL: <https://www.iso.org/standard/29875.html>.
- [93] *Geometrical Product Specifications (GPS) – Surface texture: Profile method; Measurement standards – Part 1: Material measures*. en. Standard. Geneva, CH: International Organization for Standardization, 2000. URL: <https://www.iso.org/standard/21978.html>.
- [94] *Corrosion tests in artificial atmospheres – Salt spray tests*. en. Standard. Geneva, CH: International Organization for Standardization, 2017. URL: <https://www.iso.org/standard/63543.html>.
- [95] *Geometrical product specifications (GPS) – Surface texture: Profile – Part 1: Indication of surface texture*. en. Standard. Geneva, CH: International Organization for Standardization, n.a. URL: <https://www.iso.org/standard/72196.html>.
- [96] *Geometrical product specifications (GPS) – Surface texture: Profile – Part 2: Terms, definitions and surface texture parameters*. en. Standard. Geneva, CH: International Organization for Standardization, n.a. URL: <https://www.iso.org/standard/72226.html>.
- [97] *Geometrical product specifications (GPS) – Surface texture: Profile – Part 3: Specification operators*. en. Standard. Geneva, CH: International Organization for Standardization, n.a. URL: <https://www.iso.org/standard/72228.html>.
- [98] IUPAC. *surface (S06154)*. Compendium of Chemical Terminology, 2nd ed. (the "Gold Book"). Compiled by A. D. McNaught and A. Wilkinson. Blackwell Scientific Publications, Oxford (1997). Online version <https://goldbook.iupac.org/terms/view/S06154>. (Accessed on 10/24/2019). 2019.

- [99] S. Jaturunruangsri. “Evaluation of material surface profiling methods: contact versus non-contact”. Accepted: 2015-03-18T10:35:20Z. Thesis. Brunel University London, 2015. URL: <http://bura.brunel.ac.uk/handle/2438/10431> (visited on 06/06/2020).
- [100] *JSON Schema | The home of JSON Schema*. <https://web.archive.org/web/20200717074839/https://json-schema.org/>. (Accessed on 07/19/2020). Sept. 2019.
- [101] G. T. Karagiannis. “High resolution spectroscopic mapping imaging applied in situ to multilayer structures for stratigraphic identification of painted art objects”. In: *Optics, Photonics and Digital Technologies for Imaging Applications IV*. Vol. 9896. International Society for Optics and Photonics. 2016, 98961F.
- [102] G. Karagiannis, D. Alexiadis, A. Damtsios, G. Sergiadis, and C. Salpistis. “3D non destructive “sampling” of art objects”. In: *IEEE instrumentation and measurements* 60.9 (2011), pp. 1–28.
- [103] C. Kleber, U. Hilfrich, and M. Schreiner. “In situ QCM and TM-AFM investigations of the early stages of degradation of silver and copper surfaces”. In: *Applied Surface Science* 253.7 (Jan. 2007), pp. 3712–3721. ISSN: 0169-4332. DOI: 10.1016/j.apsusc.2006.08.005. URL: <http://www.sciencedirect.com/science/article/pii/S0169433206010695>.
- [104] L. Krzemień, A. Czyżewska, M. Soboń, R. Kozłowski, and Ł. Bratasz. “Risk of climate-induced damage in historic parchment”. In: *Heritage Science* 8.1 (2020), p. 17. DOI: 10.1186/s40494-020-0360-0. URL: <https://doi.org/10.1186/s40494-020-0360-0>.
- [105] R. Kumar, K. K. Saini, and S. Chand. “A New Steganography Technique Using Snake Scan Ordering Strategy.” In: *International Journal of Image, Graphics & Signal Processing* 5.6 (2013).
- [106] E. Laso, F. Obeso, Y. Malet, C. Nerriec, V. Patera, and I. Alvarez. “OMEGA: novel optical sensor 3D measuring system for complex geometry in adverse environment”. In: *Practical Holography IX*. Vol. 2406. International Society for Optics and Photonics. 1995, pp. 235–245.
- [107] S. Lawman and H. Liang. “High precision dynamic multi-interface profilometry with optical coherence tomography”. In: *Applied Optics* 50.32 (2011), pp. 6039–6048. DOI: 10.1364/AO.50.006039. URL: <http://ieop.nyu.ac.uk/id/eprint/9583/>.
- [108] R. Leach. “Measurement Good Practice Guide No. 37, The Measurement of Surface Texture using Stylus Instruments”. In: *NP Laboratory, Ed* (2001).
- [109] R. Leach, ed. Berlin, Heidelberg: Springer Berlin Heidelberg, 2011. ISBN: 978-3-642-12012-1. DOI: 10.1007/978-3-642-12012-1. URL: <https://doi.org/10.1007/978-3-642-12012-1>.
- [110] R. Leach. “Some Common Terms and Definitions”. In: *Optical Measurement of Surface Topography*. Ed. by R. Leach. Berlin, Heidelberg: Springer Berlin Heidelberg, 2011, pp. 15–22. ISBN: 978-3-642-12012-1. DOI: 10.1007/978-3-642-12012-1_2. URL: https://doi.org/10.1007/978-3-642-12012-1_2.
- [111] R. K. Leach and P. M. Harris. “Ambiguities in the definition of spacing parameters for surface-texture characterization”. In: *Measurement Science and Technology* 13.12 (Nov. 2002), pp. 1924–1930. DOI: 10.1088/0957-0233/13/12/316. URL: <https://doi.org/10.1088/0957-0233/13/12/316>.
- [112] R. Leach, A. Weckenmann, J. Coupland, and W. Hartmann. “Interpreting the probe-surface interaction of surface measuring instruments, or what is a surface?” In: *Surface Topography: Metrology and Properties* 2.3 (2014), p. 035001.
- [113] R. Leach and A. Hart. “A comparison of stylus and optical methods for measuring 2D surface textures.” In: (2002).
- [114] S. Legrand, M. Alfeld, F. Vanmeert, W. De Nolf, and K. Janssens. “Macroscopic Fourier transform infrared scanning in reflection mode (MA-rFTIR), a new tool for chemical imaging of cultural heritage artefacts in the mid-infrared range”. In: *Analyst* 139.10 (2014), pp. 2489–2498.

- [115] J. P. Lesso, A. J. Duncan, W. Sibbett, and M. J. Padgett. “Surface profilometry based on polarization analysis”. In: *Optics letters* 23.23 (1998), pp. 1800–1802.
- [116] Z. Liang, Z. Feng, and X. Guangxiang. “Comparison of Fractal Dimension Calculation Methods for Channel Bed Profiles”. In: *Procedia Engineering* 28 (2012). 2012 International Conference on Modern Hydraulic Engineering, pp. 252–257. ISSN: 1877-7058. DOI: <https://doi.org/10.1016/j.proeng.2012.01.715>. URL: <http://www.sciencedirect.com/science/article/pii/S1877705812007254>.
- [117] R. Luimes, A. Suiker, A. Jorissen, P. van Duin, and H. Schellen. “Hygro-mechanical response of oak wood cabinet door panels under relative humidity fluctuations”. In: *Heritage Science* 6.1 (2018), p. 72.
- [118] *M6 JETSTREAM - Overview, large sample Micro-XRF analysis - M6 JETSTREAM | Bruker*. <https://web.archive.org/web/20190203091259/https://www.bruker.com/products/x-ray-diffraction-and-elemental-analysis/micro-xrf-and-txrf/m6-jetstream/overview.html>. (Accessed on 10/09/2019).
- [119] I. D. MacLeod. “Modern Metals in Cultural Heritage: understanding and characterization”. In: *AICCM Bulletin* 40.2 (2019), pp. 122–122. DOI: 10.1080/10344233.2019.1710969. eprint: <https://doi.org/10.1080/10344233.2019.1710969>. URL: <https://doi.org/10.1080/10344233.2019.1710969>.
- [120] B. Mandelbrot, W. Freeman, and Company. *The Fractal Geometry of Nature*. Einaudi paperbacks. Henry Holt and Company, 1983. ISBN: 9780716711865. URL: <https://books.google.it/books?id=0R2LkE3N7-oC>.
- [121] B. Mandelbrot. “How Long Is the Coast of Britain? Statistical Self-Similarity and Fractional Dimension”. In: *Science* 156.3775 (1967), pp. 636–638. ISSN: 0036-8075. DOI: 10.1126/science.156.3775.636. eprint: <https://science.sciencemag.org/content/156/3775/636.full.pdf>. URL: <https://science.sciencemag.org/content/156/3775/636>.
- [122] G. Marchioro, G. Apostolidis, G. Karagianis, M. Galeotti, and C. Daffara. “Surface and subsurface layers characterization in artworks using conoscopic laser holography and acoustic microscopy”. In: *Optics for Arts, Architecture, and Archaeology VI*. Vol. 10331. International Society for Optics and Photonics. 2017, p. 103310L.
- [123] G. Marchioro, L. Perlini, and C. Daffara. “Monitoring microclimate-induced deformations on hygroscopic materials using conoscopic holography sensors”. In: *Optics for Arts, Architecture, and Archaeology VII*. Vol. 11058. International Society for Optics and Photonics. 2019, p. 1105812.
- [124] S. Mazzocato and C. Daffara. “Experiencing the Untouchable: A Method for Scientific Exploration and Haptic Fruition of Artworks Microsurface Based on Optical Scanning Profilometry”. In: *Sensors* 21.13 (2021). ISSN: 1424-8220. DOI: 10.3390/s21134311. URL: <https://www.mdpi.com/1424-8220/21/13/4311>.
- [125] M. F. Mecklenburg. *Determining the acceptable ranges of relative humidity and temperature in museums and galleries, part 1, structural response to relative humidity*. 2007.
- [126] A. Migliori, P. Bonanni, L. Carraresi, N. Grassi, and P. Mando. “A novel portable XRF spectrometer with range of detection extended to low-Z elements”. In: *X-Ray Spectrometry* 40.2 (2011), pp. 107–112.
- [127] L. M. Mugnier and G. Y. Sirat. “Reconstruction of a three-dimensional object from its conoscopic hologram”. In: *Inverse Problems in Scattering and Imaging*. Vol. 1767. International Society for Optics and Photonics. 1992, pp. 287–298.
- [128] J.-C. Muller. “Fractal Dimension and Inconsistencies in Cartographic Line Representations”. In: *The Cartographic Journal* 23.2 (1986), pp. 123–130. DOI: 10.1179/caj.1986.23.2.123. eprint: <https://doi.org/10.1179/>

- caj . 1986 . 23 . 2 . 123. URL: <https://doi.org/10.1179/caj.1986.23.2.123>.
- [129] B. Muralikrishnan and J. Raja. *Computational surface and roundness metrology*. Springer Science & Business Media, 2008.
- [130] D. Nečas and P. Klapetek. “Gwyddion: an open-source software for SPM data analysis”. In: *Central European Journal of Physics* 10 (1 2012), pp. 181–188. ISSN: 1895-1082. DOI: 10.2478/s11534-011-0096-2.
- [131] P. Neubert and P. Protzel. “Compact Watershed and Preemptive SLIC: On Improving Trade-offs of Superpixel Segmentation Algorithms”. In: *2014 22nd International Conference on Pattern Recognition*. Aug. 2014, pp. 996–1001. DOI: 10.1109/ICPR.2014.181.
- [132] T. E. Oliphant. *A guide to NumPy*. Vol. 1. Trelgol Publishing USA, 2006.
- [133] L. Ou, J. Wang, Q. Xu, J. Kang, and Y. Huang. “Faraday Rotation Angle Measurement Based on Conoscopic Interference Pattern in Optical Current Transducer”. In: *Energy Procedia* 14 (2012). 2011 2nd International Conference on Advances in Energy Engineering (ICAEE), pp. 1060–1066. ISSN: 1876-6102. DOI: <https://doi.org/10.1016/j.egypro.2011.12.1055>. URL: <http://www.sciencedirect.com/science/article/pii/S1876610211044754>.
- [134] G. Palma, P. Pingi, E. Siotto, R. Bellucci, G. Guidi, and R. Scopigno. “Deformation analysis of Leonardo da Vinci’s “Adorazione dei Magi” through temporal unrelated 3D digitization”. In: *Journal of Cultural Heritage* 38 (2019). DOI 10.1016/j.culher.2018.11.001, pp. 174–185. URL: <http://vcg.isti.cnr.it/Publications/2019/PPSBGS19a>.
- [135] S. Pancharatnam. “Generalized theory of interference and its applications”. In: *Proceedings of the Indian Academy of Sciences-Section A*. Vol. 44. 6. Springer. 1956, pp. 398–417.
- [136] A. Pelagotti, F. Uccheddu, E. Massa, and M. Carfagni. “Comparing two 3D measurement techniques for documenting painted wooden panels surface deformations on a real test case: “Mystical Marriage of Saint Catherine” by Renaissance artist Piero di Cosimo”. In: vol. 364. 1. 2018, p. 012090.
- [137] *Pick and Place | Pick, place, measure and sort components | Alicona*. <https://web.archive.org/web/20190427224956/https://www.alicon.com/products/pick-and-place/>. (Accessed on 09/17/2019).
- [138] C. Y. Poon and B. Bhushan. “Comparison of surface roughness measurements by stylus profiler, AFM and non-contact optical profiler”. In: *Wear* 190.1 (1995). Macro and Micro-Tribology and Mechanics of Magnetic Storage Systems, pp. 76–88. ISSN: 0043-1648. DOI: [https://doi.org/10.1016/0043-1648\(95\)06697-7](https://doi.org/10.1016/0043-1648(95)06697-7). URL: <http://www.sciencedirect.com/science/article/pii/S0043164895066977>.
- [139] *Portable ED-XRF Spectrometer (PXRF) - ELIO - XGLAB*. <https://web.archive.org/web/20161208153400/https://www.xglab.it/combined-xrf-spectrometer-raman-analyzer-xraman.shtml>. (Accessed on 07/28/2020).
- [140] D. Pradhan, G. S. Mahobia, K. Chattopadhyay, and V. Singh. “Effect of surface roughness on corrosion behavior of the superalloy IN718 in simulated marine environment”. In: *Journal of Alloys and Compounds* 740 (2018), pp. 250–263. ISSN: 0925-8388. DOI: <https://doi.org/10.1016/j.jallcom.2018.01.042>. URL: <http://www.sciencedirect.com/science/article/pii/S0925838818300434>.
- [141] D. Pritchard, J. Sperner, S. Hoepner, and R. Tenschert. “Terrestrial laser scanning for heritage conservation: the Cologne Cathedral documentation project”. English. In: *ISPRS Annals of the Photogrammetry, Remote Sensing and Spatial Information Sciences* 4 (Aug. 2017). 26th International CIPA Symposium 2017, CIPA 2017 ; Conference date: 28-08-2017 Through 01-09-2017, pp. 213–220. ISSN: 2194-9042. DOI: 10.5194/isprs-annals-IV-2-W2-213-2017. URL: <http://sc.isprs.org/events/details/id-26th-international-cipa-symposium.html>.

- [142] R. Proksch, J. Cleveland, and D. Bocek. “Linear variable differential transformers for high precision position measurements”. US Patent 2,002,0159. Nov. 2000.
- [143] J. Raja, B. Muralikrishnan, and S. Fu. “Recent advances in separation of roughness, waviness and form”. In: *Precision Engineering* 26.2 (2002), pp. 222–235. ISSN: 0141-6359. DOI: [https://doi.org/10.1016/S0141-6359\(02\)00103-4](https://doi.org/10.1016/S0141-6359(02)00103-4). URL: <http://www.sciencedirect.com/science/article/pii/S0141635902001034>.
- [144] P. Ramachandran and G. Varoquaux. “Mayavi: 3D Visualization of Scientific Data”. In: *Computing in Science & Engineering* 13.2 (2011), pp. 40–51. ISSN: 1521-9615.
- [145] M. M. Ramos and F. Remondino. “Data fusion in Cultural Heritage - A Review”. In: *ISPRS - International Archives of the Photogrammetry, Remote Sensing and Spatial Information Sciences* XL5 (Aug. 2015), pp. 359–363. DOI: 10.5194/isprsarchives-XL-5-W7-359-2015.
- [146] S. Rana and J. Morley. “Surface networks”. In: (2002). URL: <https://discovery.ucl.ac.uk/id/eprint/183/1/working-paper43.pdf>.
- [147] E. Ravaioni and L. Giuntini. “Sviluppo hardware e software di un sistema a multirivelatore per spettroscopia a raggi x finalizzata allo studio di beni culturali”. PhD thesis. Università di Bologna, 2015.
- [148] *RDF - Semantic Web Standards*. <https://web.archive.org/web/20200714055728/https://www.w3.org/RDF/>. (Accessed on 07/19/2020). Mar. 2014.
- [149] *Reconfigurable MACRO-XRF Scanner for cultural heritage applications - CRONO - XGLAB*. <https://web.archive.org/web/20161208153639/https://www.xglab.it/reconfigurable-MACRO-XRF-Scanner-for-cultural-heritage-applications-crono.shtml>. (Accessed on 07/28/2020).
- [150] L. F. Richardson. “The problem of contiguity: an appendix to statistics of deadly quarrels”. In: *General systems yearbook* 6 (1961), pp. 139–187.
- [151] M. F. Rodríguez. “Técnicas avanzadas de perfilometría óptica in-situ basada en interferometría de desplazamiento lateral para medidas submicrométricas”. PhD thesis. Universidad de Oviedo, 2012. URL: <http://digibuo.uniovi.es/dspace/handle/10651/13419>.
- [152] R. Roy, D. K. Agrawal, and H. A. McKinstry. “Very low thermal expansion coefficient materials”. In: *Annual Review of Materials Science* 19.1 (1989), pp. 59–81.
- [153] T. SAKAI, M. FUJIKAWA, S. LAURICH-MCINTYRE, and R. C. BRADT. “Quantitative analysis for shape irregularity of ceramic particles based on Richardson effect”. In: *Journal of the Society of Materials Science, Japan* 45.12Appendix (1996), pp. 235–241.
- [154] P. Sanmartín, B. Silva, and B. Prieto. “Effect of Surface Finish on Roughness, Color, and Gloss of Ornamental Granites”. In: *Journal of Materials in Civil Engineering* 23.8 (2011), pp. 1239–1248. DOI: 10.1061/(ASCE)MT.1943-5533.0000285.
- [155] P. Santos, M. Ritz, R. Tausch, H. Schmedt, R. Monroy, A. De Stefano, O. Posniak, C. Fuhrmann, and D. W. Fellner. “CultLab3D: On the Verge of 3D Mass Digitization”. In: *Proceedings of the Eurographics Workshop on Graphics and Cultural Heritage*. GCH '14. Darmstadt, Germany: Eurographics Association, 2014, pp. 65–73. ISBN: 9783905674637.
- [156] R. Sargent. “Evaluating dimensional stability in solid wood: a review of current practice”. In: *Journal of Wood Science* 65.1 (2019), p. 36. DOI: 10.1186/s10086-019-1817-1. URL: <https://doi.org/10.1186/s10086-019-1817-1>.
- [157] R. Schmitt, M. Peterek, E. Morse, W. Knapp, M. Galetto, F. Härtig, G. Goch, B. Hughes, A. Forbes, and W. Estler. “Advances in Large-Scale Metrology – Review and future trends”. In: *CIRP Annals* 65.2 (2016), pp. 643–665. ISSN: 0007-8506. DOI: <https://doi.org/10.1016/j.cirp.2016.05.002>. URL: <http://www.sciencedirect.com/science/article/pii/S0007850616301895>.

- [158] D. A. Scott. “A Review of Copper Chlorides and Related Salts in Bronze Corrosion and as Painting Pigments”. In: *Studies in Conservation* 45.1 (2000), pp. 39–53. ISSN: 00393630. URL: <http://www.jstor.org/stable/1506682>.
- [159] J. Seewig. “Linear and robust Gaussian regression filters”. In: *Journal of Physics: Conference Series* 13 (Jan. 2005), pp. 254–257. DOI: 10.1088/1742-6596/13/1/059. URL: <https://doi.org/10.1088%2F1742-6596%2F13%2F1%2F059>.
- [160] N. Senin, L. A. Blunt, R. K. Leach, and S. Pini. “Morphologic segmentation algorithms for extracting individual surface features from areal surface topography maps”. In: *Surface Topography: Metrology and Properties* 1.1 (Oct. 2013), p. 015005. DOI: 10.1088/2051-672x/1/1/015005. URL: <https://doi.org/10.1088%2F2051-672x%2F1%2F1%2F015005>.
- [161] L. Senni, C. Casieri, A. Bovino, M. C. Gaetani, and F. De Luca. “A portable NMR sensor for moisture monitoring of wooden works of art, particularly of paintings on wood”. In: *Wood Science and Technology* 43.1 (Feb. 2009), pp. 167–180. ISSN: 1432-5225. DOI: 10.1007/s00226-008-0200-y. URL: <https://doi.org/10.1007/s00226-008-0200-y>.
- [162] G. Y. Sirat. *Illumination techniques for overcoming speckle artifacts in metrology applications*. US Patent 6,169,634. Jan. 1999.
- [163] G. Y. Sirat. “Conoscopic holography. I. Basic principles and physical basis”. In: *JOSA A* 9.1 (1992), pp. 70–83. URL: <https://www.osapublishing.org/abstract.cfm?uri=josaa-9-1-70> (visited on 02/15/2016).
- [164] G. Y. Sirat, J. Vecht, and Y. Malet. “Linear conoscopic holography”. US Patent 5,953,137. Sept. 1999.
- [165] G. Y. Sirat, F. Paz, M. Kleinman, and M. Doherty. “ConoProbe and ConoLine: two new three-dimensional measurement systems”. In: *Third International Symposium on Laser Precision Microfabrication*. Vol. 4830. International Society for Optics and Photonics. 2003, pp. 319–324.
- [166] G. S. Spagnolo, R. Majo, M. Carli, D. Ambrosini, and D. Paoletti. “Virtual gallery of ancient coins through conoscopic holography”. In: *Optical Metrology for Arts and Multimedia*. Vol. 5146. International Society for Optics and Photonics. 2003, pp. 202–209.
- [167] “Part V - Applications of three-dimensional surface metrology”. In: *Three Dimensional Surface Topography*. Ed. by K. Stout and L. Blunt. Oxford: Butterworth-Heinemann, 2000, pp. 175–213. ISBN: 978-1-85718-026-8. DOI: <https://doi.org/10.1016/B978-185718026-8/50120-X>. URL: <http://www.sciencedirect.com/science/article/pii/B978185718026850120X>.
- [168] K. J. Stout, P. J. Sullivan, E. Dong W. P. Main-sah, N. Lou, T. Mathia, and H. Zahouani. *The development of methods for the characterisation of roughness in three dimensions*. Tech. rep. EUR 15178 EN. Commission of the european communities. Luxembourg, 1993. URL: <https://publications.europa.eu/s/mFz6>.
- [169] *Streaming measurements | Articles | TiePie - USB oscilloscopes, spectrum analyzers, data loggers, multimeters, Arbitrary Waveform Generators*. <https://web.archive.org/web/20200606104931/https://www.tiepie.com/en/articles/streaming-measurements>. (Accessed on 07/23/2020).
- [170] J. Striova, R. Fontana, M. Barucci, A. Felici, E. Marconi, E. Pampaloni, M. Raffaelli, and C. Riminesi. “Optical devices provide unprecedented insights into the laser cleaning of calcium oxalate layers”. In: *Microchemical Journal* 124 (2016), pp. 331–337. ISSN: 0026-265X. DOI: <https://doi.org/10.1016/j.microc.2015.09.005>. URL: <http://www.sciencedirect.com/science/article/pii/S0026265X15002064>.
- [171] *Surface Texture Parameters - SoftGauges*. https://web.archive.org/web/20190504005713/http://resource.npl.co.uk/softgauges/SP_Surf_Para.htm. (Accessed on 12/03/2019).

- [172] Y. R. Teo, Y. Yong, and A. J. Fleming. “A comparison of scanning methods and the vertical control implications for scanning probe microscopy”. In: *Asian Journal of Control* 20.4 (2018), pp. 1352–1366.
- [173] P. TePla. *Transducer | PVA TePla SAM*. <https://web.archive.org/web/20200817105237/https://www.pvatepla-sam.com/en/products/transducer/>. (Accessed on 08/17/2020). 2020.
- [174] The HDF Group. *Hierarchical Data Format, version 5*. <http://www.hdfgroup.org/HDF5/1997-NNNN>.
- [175] *The numpy.ma module — NumPy v1.15 Manual*. <https://web.archive.org/web/20190111082546/https://docs.scipy.org/doc/numpy/reference/maskedarray.generic.html>. (Accessed on 11/06/2019).
- [176] L. Todhunter, R. Leach, S. Lawes, F. Blateyron, and P. Harris. “Development of mathematical reference standards for the validation of surface texture parameter calculation software”. In: *Journal of Physics: Conference Series* 1065 (Aug. 2018), p. 082004. DOI: 10.1088/1742-6596/1065/8/082004. URL: <https://doi.org/10.1088%5C%2F1742-6596%5C%2F1065%5C%2F8%5C%2F082004>.
- [177] V. Tornari, E. Bernikola, N. Tsigarida, M. Andrianakis, K. Hatzigiannakis, and J. Leissner. “Preventive deformation measurements on cultural heritage materials based on non-contact surface response of model samples”. In: *Studies in Conservation* 60.sup1 (2015), S143–S158. DOI: 10.1179/0039363015Z.000000000219. eprint: <https://doi.org/10.1179/0039363015Z.000000000219>. URL: <https://doi.org/10.1179/0039363015Z.000000000219>.
- [178] F. Vanmeert, E. Hendriks, G. Van der Snickt, L. Monico, J. Dik, and K. Janssens. “Chemical Mapping by Macroscopic X-ray Powder Diffraction (MA-XRPD) of Van Gogh’s Sunflowers: Identification of Areas with Higher Degradation Risk”. In: *Angewandte Chemie International Edition* 57.25 (2018), pp. 7418–7422.
- [179] P. Virtanen, R. Gommers, T. E. Oliphant, M. Haberland, T. Reddy, D. Cournapeau, E. Burovski, P. Peterson, W. Weckesser, J. Bright, S. J. van der Walt, M. Brett, J. Wilson, K. Jarrod Millman, N. Mayorov, A. R. J. Nelson, E. Jones, R. Kern, E. Larson, C. Carey, Í. Polat, Y. Feng, E. W. Moore, J. VanderPlas, D. Laxalde, J. Perktold, R. Cimrman, I. Henriksen, E. A. Quintero, C. R. Harris, A. M. Archibald, A. H. Ribeiro, F. Pedregosa, P. van Mulbregt, and S. 1. O. Contributors. “SciPy 1.0—Fundamental Algorithms for Scientific Computing in Python”. In: *arXiv e-prints*, arXiv:1907.10121 (July 2019), arXiv:1907.10121. arXiv: 1907.10121 [cs.MS].
- [180] T. Vivi, T. Basset, M. Andrianakis, and K. Kosma. “Impact of Relative Humidity on Wood Sample: A Climate Chamber Experimental Simulation Monitored by Digital Holographic Speckle Pattern Interferometry”. In: *Journal of Imaging* 5 (July 2019), p. 65. DOI: 10.3390/jimaging5070065.
- [181] G. Vogg, T. Heidmann, and S. Brand. “Scanning acoustic GHz-microscopy versus conventional SAM for advanced assessment of ball bond and metal interfaces in microelectronic devices”. In: *Microelectronics Reliability* 55.9 (2015). Proceedings of the 26th European Symposium on Reliability of Electron Devices, Failure Physics and Analysis, pp. 1554–1558. ISSN: 0026-2714. DOI: <https://doi.org/10.1016/j.microrel.2015.06.066>. URL: <http://www.sciencedirect.com/science/article/pii/S0026271415001584>.
- [182] A. Wang, C. Y. Gao, J. Xu, H. Zhang, and S. Q. Sun. “Conoscopic interferometry for probing electro-optic coefficients of strontium calcium barium niobate crystal”. In: *Optics and Lasers in Engineering* 49.7 (2011), pp. 870–873.
- [183] W. Wei. “Surface micro-roughness, cleaning and perception”. In: *Proceedings of the ICOM-CC 16th Triennial Meeting (CD format)*. Lisbon, Portugal. 2011, pp. 19–23. URL: <https://www.icom-cc-publications-online.org/publicationDetail.aspx?cid=c1119e3b-3cd1-49cf-a2e6-c2824a97c390>.

- [184] X. Wen, O. C. Au, J. Xu, L. Fang, R. Cha, and J. Li. “Novel RD-optimized VBSME with matching highly data re-usable hardware architecture”. In: *IEEE Transactions on Circuits and Systems for Video Technology* 21.2 (2011), pp. 206–219.
- [185] P. Wessel and W. H. F. Smith. “A global, self-consistent, hierarchical, high-resolution shoreline database”. In: *Journal of Geophysical Research: Solid Earth* 101.B4 (1996), pp. 8741–8743. DOI: 10.1029/96JB00104. eprint: <https://agupubs.onlinelibrary.wiley.com/doi/pdf/10.1029/96JB00104>. URL: <https://agupubs.onlinelibrary.wiley.com/doi/abs/10.1029/96JB00104>.
- [186] D. Whitehouse. *Handbook of Surface and Nanometrology*. CRC Press, 2010. ISBN: 9781420082029.
- [187] G. W. Wolf. “A FORTRAN subroutine for cartographic generalization”. In: *Computers & Geosciences* 17.10 (1991), pp. 1359–1381. ISSN: 0098-3004. DOI: [https://doi.org/10.1016/0098-3004\(91\)90002-U](https://doi.org/10.1016/0098-3004(91)90002-U). URL: <http://www.sciencedirect.com/science/article/pii/009830049190002U>.
- [188] I. Wolfram Research. *Richardson Effect – from Wolfram MathWorld*. <https://web.archive.org/web/20190915184256/https://mathworld.wolfram.com/RichardsonEffect.html>. (Accessed on 08/26/2020). 1999-2020.
- [189] H. Yang, J. Lu, W. P. Brown, I. Daubechies, and L. Ying. “Quantitative Canvas Weave Analysis Using 2-D Synchrosqueezed Transforms: Application of time-frequency analysis to art investigation”. In: *IEEE Signal Processing Magazine* 32.4 (July 2015), pp. 55–63. ISSN: 1558-0792. DOI: 10.1109/MSP.2015.2406882.
- [190] X. Yang and J. Li. *Advances in mapping from remote sensor imagery: techniques and applications*. CRC Press, 2012.
- [191] P. Zapico, P. Fernández, D. Blanco, G. Valiño, and J. C. Rico. “A comparison between discrete and continuous scanning with conoscopic holography”. In: *Procedia engineering* 132 (2015), pp. 840–847.